Characterization of SKAP/Kinastrin isoforms

Dissertation

in partial fulfilment of the requirements for the degree of

doctor rerum naturalium (Dr. rer. nat.)

submitted to the Faculty Council of the School of Medicine

at Friedrich Schiller University of Jena

by M.Sc.

Anita Cindrić Vranešić

born on 18.03.1988 in Karlovac/Croatia

June, 2016

Reviewers:

1. Prof. Dr. Otmar Huber
   Institute of Biochemistry II
   University Hospital Jena

2. Apl. Prof. Dr. Regine Heller
   Center for Molecular Biomedicine
   University Hospital Jena

3. PD Dr. Cagatay Günes
   Department of Urology
   University Hospital Ulm

Date of the public disputation: 06.12.2016

Table of contents

Abbreviations

(v/v)	Volume/volume
(w/v)	Weight/volume
A40E	Substitution of alanine for glutamic acid at codon 40
AAA+ ATPases	ATPases associated with diverse cellular activities
APS	Ammonium persulfate
ATP	Adenosine 5′-triphosphate
BCC	Basal cell carcinoma
bp	Base pair
CC	Coiled-coil
CCAN	Constitutive centromere-associated network
cDNA	Complementary DNA
CENP	Centromere protein
DABCO	1,4-Diazabicyclo-(2.2.2)-octane solution
DAPI	4',6-diamidino-2-phenylindole
DMEM	*Dulbecco´s Modified Eagle´s Medium*
DMSO	Dimethyl sulfoxide
DNA	Deoxyribonucleic acid
dNTPs	Deoxynucleotide triphosphates
DYNLL	Dynein light chain
E. coli	*Escherichia coli*
EB1	End binding 1
EDTA	Ethylenediaminetetraacetic acid
E_{FRET}	FRET efficiency
EGFP	Enhanced green fluorescent protein
EGTA	Ethylene glycol-bis(2-aminoethylether)-N,N,N′,N′-tetraacetic acid
ELISA	Enzyme-linked immunosorbent assay
FCCS	Fluorescence cross-correlation spectroscopy
FCS	Fluorescence correlation spectroscopy
FCS	Fetal calf serum
FPLC	Fast protein liquid chromatography
FRET	Förster resonance energy transfer
g	Gravitational acceleration
GAPDH	Glyceraldehyde 3-phosphate dehydrogenase
GSH	Glutathione
GST	Glutathione S-transferase
HRP	Horseradish peroxidase
HT	Hypoxanthine/thymidine
hTERT	Telomerase reverse transcriptase

IF	Immunofluorescence
IgG	Immunoglobulin G
IL-6	Interleukin 6
IP	Immunoprecipitation
IPBA	4-iodophenylboronic acid
IPTG	Isopropylβ-D-1-thiogalactopyranoside
IQGAP1	IQ motif containing GTPase activating protein 1
kb	Kilobase
kDa	Kilodalton
KMN	Super-complex composed of KNL1, Mis12 and Ndc80 complexes
MBP	Maltose-binding protein
OD	Optical density
ODF	Outer dense fiber
PBS	Phosphate-buffered saline
PCR	Polymerase chain reaction
PDS	Pleomorphic dermal sarcoma
PEG	Polyethylene-glycol
PEI	Polyethileneimine
RACE	Rapid amplification of cDNA ends
RFP	Red fluorescent protein
RNA	Ribonucleic acid
ROI	Region of interest
RPMI	*Roswell Park Memorial Institute*
RT	Reverse transcription
S24F	Substitution of phenylalanine for serine at codon 24
SAC	Spindle assembly checkpoint
SAP	Shrimp alkaline phosphatase
SCC	Squamous cell carcinoma
SCOS	Sertoli-cell-only syndrome
SDS	Sodium dodecyl sulphate
SDS-PAGE	SDS-polyacrylamide gel electrophoresis
shRNA	Short hairpin RNA
SKAP	Small kinetochore-associated protein
TBS	Tris-buffered saline
TEMED	Tetramethylethylenediamine
TIP60	Tat-interactive protein 60 kDa
UTR	Untranslated region
UV	Ultra violet
WB	Western blot

Units

sec	second
min	minute
h	hour
ng	nanogram
µg	microgram
mg	milligram
ml	millilitre
µM	micromolar (micromole/liter)
mM	millimolar (millimole/liter)
M	molar (mole/liter)
µm	micrometer
cm^2	square centimeter
U	unit
V	Volt
%	percent

Summary

SKAP (Small Kinetochore-Associated Protein/Kinastrin) is a multifunctional protein involved in mitotic regulation, apoptosis and directional cell migration. Additionally, it is suggested to act as an oncogene in human skin cancers. Despite being associated with important cellular processes, mechanisms underlying SKAP´s roles in these processes are not yet fully understood. SKAP is predicted to be expressed in different isoforms, however, studies reported in the literature did not differentiate between them. With the aim to better understand the roles of SKAP, in this work I studied the expression profile and functional differences between SKAP isoforms in human and mouse.

In the first set of experiments, various human tissues and cells of different origin were analyzed by RT-PCR, Western blotting and immunocytochemistry. Newly generated anti-SKAP monoclonal antibodies revealed that human SKAP exists in only two protein isoforms although 4 protein-coding transcripts are reported in the databases. SKAP16 represents the ubiquitously expressed isoform whereas SKAP1 revealed only testis/sperm-specific expression. Similarly, in mouse two isoforms were found whereby SKAP1 is expressed in testes at 4 weeks postnatally, after completion of the first wave of spermatogenesis when elongated spermatids can be detected in the testes. These findings pointed to a sperm-specialized function of SKAP1. To get further insight into the function of SKAP1, biochemical analyses aimed at identifying novel SKAP1-specific interaction partners. Pull-down and co-immunoprecipitation experiments discovered that Pontin, Reptin, β-catenin and TIP60 bind to SKAP1. Particularly interesting is the interaction between SKAP1 and Pontin, a member of AAA+ ATPases. Co-localization of SKAP1 and Pontin in the flagellar region of human sperm suggests a function for SKAP1-Pontin interaction in sperm motility.

Additionally, homo-oligomerization of both SKAP1 and SKAP16 was revealed by FRET and FCCS, showing that SKAP proteins *in vivo* function as homomeric complexes. Finally, qPCR analyses showed a significant overexpression of SKAP in colon cancer compared to healthy colon tissue, suggesting that SKAP indeed is a potential oncogene.

In conclusion, since most previous studies on SKAP in somatic cells were performed with isoforms I could not detect in any of the human cells analyzed, this work presents a completely new basis for further studies on the role of SKAP in human somatic and germ cells and in male fertility.

Zusammenfassung

SKAP (Small Kinetochore-Associated Protein/Kinastrin) ist ein multifunktionelles Protein, das an der Regulation der Mitose, Apoptose und an der gerichteten Zellmigration beteiligt ist. Darüber hinaus wird vermutet, dass SKAP eine onkogene Funktion bei Hautkrebs ausübt. Obwohl SKAP mit vielen wichtigen zellulären Funktionen assoziiert ist, sind die molekularen Mechanismen bisher unklar. SKAP wird in verschiedenen Isoformen exprimiert, jedoch berücksichtigen bisherige Studien diese nicht. Ziel dieser Arbeit war es die Funktion der SKAP-Isoformen hinsichtlich Expressionsmuster und funktioneller Unterschiede im Menschen und in der Maus besser zu verstehen.

Die Analyse von verschiedenen humanen Geweben und Zelllinien mittels RT-PCR, Western Blot und Immunhistochemie zeigt, dass SKAP im Menschen hauptsächlich in 2 Isoformen exprimiert wird: I) als ubiquitär vorkommendes SKAP16 und II) als Hoden- bzw. Spermien-spezifisches SKAP1. Vergleichbar ist die Situation in der Maus, wo die Expression von SKAP1 im Hoden 4 Wochen nach der Geburt nachweisbar ist. Dieser Zeitpunkt korreliert mit dem Abschluss der Spermatogenese und der Existenz elongierter Spermatiden im Hoden der Maus. Diese Ergebnisse lassen eine Spermien-spezifische Funktion von SKAP1 vermuten. Um die Funktion von SKAP1 besser zu charakterisieren, wurden mittels biochemischer Analysen neue SKAP1-spezifische Interaktionspartner identifiziert. Anhand von Pull-down und Co-Immunpräzipitationsexperimenten konnte gezeigt werden, dass Pontin, Reptin, β-Catenin und TIP60 mit SKAP1 interagieren. Von besonderem Interesse dabei ist die Interaktion zwischen SKAP1 und Pontin, einer AAA+ ATPase. Es ließ sich beobachten, dass SKAP1 und Pontin im Flagellum humaner Spermien co-lokalisieren. Diese Daten legen eine funktionelle Rolle der SKAP1/Pontin-Interaktion für die Motilität von Spermien nahe.

Darüber hinaus, konnte mittels FRET und FCCS gezeigt werden, dass sowohl SKAP1 als auch SKAP16 homo-oligomere Komplexe *in vivo* bilden. qPCR-Studien in Kolonkarzinomproben untermauern die Hypothese einer onkogenen Funktion von SKAP. Hier wurde eine signifikant erhöhte SKAP-Expression in Karzinomproben in Vergleich zu Proben aus gesundem Kolon beobachtet.

Da bisherige Studien über SKAP im Wesentlichen Isoformen verwendeten, die in keinen der hier analysierten Zellen nachgewiesen werden konnten, stellt diese Arbeit eine neue Basis für weitere Studien über SKAP in somatischen Zellen und

Keimzellen dar. Ebenfalls von großem Interesse sind meine Ergebnisse für zukünftige Studien zu SKAP im Hoden/Spermien infertiler Patienten.

1 Introduction

1.1 Mitosis

In eukaryotes, processes like development, cell replacement and regeneration occur via mitotic division. A critical requirement during mitosis is preserving genetic integrity of the cells by faithful distribution of their genetic material between the two daughter cells. Mitosis is comprised out of five sequential steps: prophase, prometaphase, metaphase, anaphase and telophase (Fig. 1). In prophase, duplicated chromosomes condense and microtubule spindle apparatus starts to polymerize from the centrosomes. In parallel, kinetochores assemble at the centromeres. During prometaphase, nuclear envelope disintegrates, allowing spindle microtubules to enter the nuclear space and to begin to search and attach to kinetochores. Subsequently, in metaphase, chromosomes attached to the spindle microtubules are aligned at the metaphase plate. When all kinetochores are attached to the spindle microtubules and all chromosomes are properly aligned, the cell continues with the anaphase. During anaphase, sister chromatids of the aligned chromosomes separate and move to the opposite poles of the cell. Finally, at telophase, the cell elongates, chromosomes start to decondense and the nuclear envelope is formed around each set of daughter chromosomes. After mitosis is complete, cell cytoplasm is divided and daughter cells are separated in a process called cytokinesis. All the stages of mitosis are highly regulated, especially the kinetochore attachment and chromosome segregation, as they are crucial to conserve the genetic integrity (Cheeseman and Desai 2008).

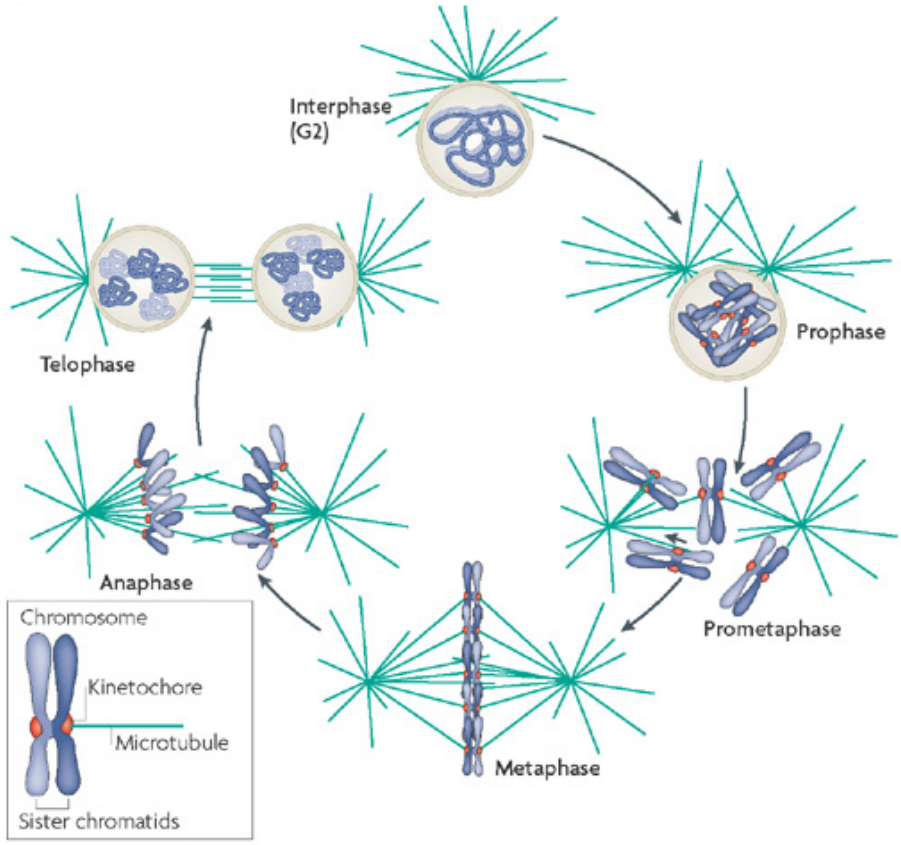

Figure 1. Scheme of the mitotic division (from (Cheeseman and Desai 2008)).

1.1.1 Kinetochore-microtubule interface

One of the central players in mitosis is the kinetochore, a large protein complex composed of more than hundred different proteins. It plays a key role in attachment of spindle microtubules and regulation of chromosome segregation during mitosis. The kinetochore assembles around the centromeric chromosomal DNA (Fig. 2). Centromeric regions are defined epigenetically mainly by the presence of a specialized histone H3 variant CENP-A (centromere protein-A). In addition to CENP-A, a CENP-T-W-S-X complex also localizes to centromeric chromatin and forms nucleosome-like structures. Kinetochore proteins that assemble directly at centromeres form a constitutive centromere-associated network (CCAN). CCAN is comprised of 16 proteins that are associated with the centromere throughout the cell cycle and primarily play a structural role in forming a stable base that allows the rapid accumulation of the outer kinetochore proteins as the cell enters mitosis. Among the outer kinetochore proteins, the KMN network (a super-complex composed of KNL1, Mis12 and Ndc80 complexes) has a central role in forming a microtubule-binding interface.

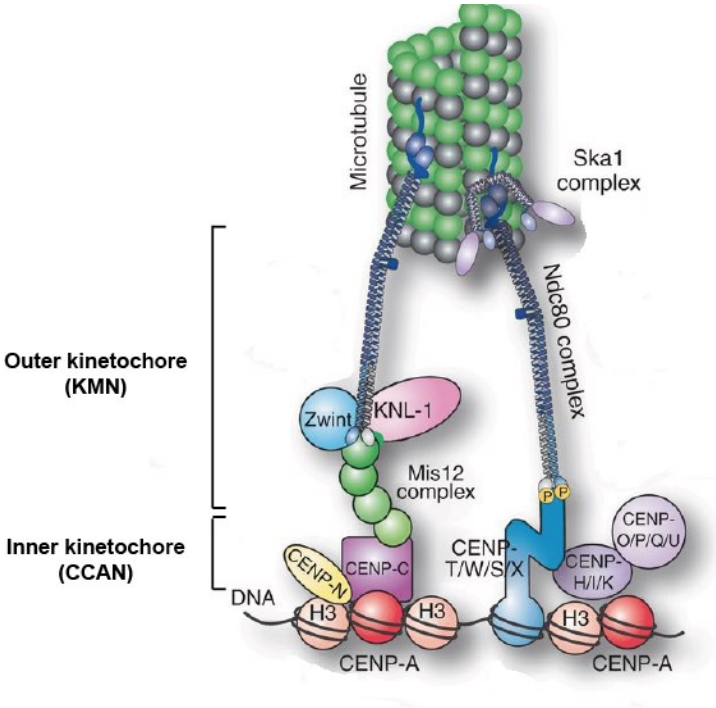

Figure 2. Simplified diagram of the human kinetochore structure in mitosis (modified from (Cheeseman 2014)).

Kinetochore-microtubule interaction is a dynamic process. Initially, kinetochore proteins bind to the lateral surface of microtubules. These attachments are facilitated by motor proteins including CENP-E kinesin and cytoplasmic dynein. Afterwards, lateral attachments are converted to robust end-on attachments, where the microtubule ends are embedded in the kinetochore. The movement of chromosomes/sister chromatids is driven by microtubule polymerization and depolymerization.

The kinetochore function is highly coordinated by numerous regulatory proteins to connect the kinetochore activity with the cell cycle and to correct any potential errors. Main regulators of kinetochore function are protein kinases that localize to kinetochore and phosphorylate kinetochore-bound substrates. The most important task of eliminating inappropriate microtubule attachments is performed by Aurora B kinase. It phosphorylates KMN network components in case of errors where only one of the kinetochores is attached to microtubules, both kinetochores attach to microtubules from the same spindle pole or one kinetochore attaches to microtubule from both spindle poles. Phosphorylated KMN components detach from microtubules and allow the formation of correct bi-oriented attachments (each kinetochore is attached to microtubules from opposite spindle poles). If errors still persist, a second line of control is mediated by spindle assembly checkpoint (SAC) proteins. Proteins

of the SAC are able to sense errors in kinetochore-microtubule attachments and to generate a signal which arrests the cell cycle (Cheeseman and Desai 2008, Takeuchi and Fukagawa 2012, Tanaka 2013, Cheeseman 2014, Pesenti et al. 2016). Even though many studies have contributed to the understanding of the kinetochore structure and underlying mechanistic details, the fundamental principles of kinetochore function are still not completely understood.

1.2 Small Kinetochore-Associated Protein (SKAP)/Kinastrin

SKAP is originally described as an essential component of the vertebrate mitotic spindle and kinetochore (Fang et al. 2009). It plays important roles in faithful chromosome segregation, progression into anaphase and maintenance of centrosome integrity. Cells lacking SKAP show severe chromosome segregation defects that result in aneuploidy (Fang et al. 2009, Dunsch et al. 2011, Huang et al. 2012, Wang et al. 2012).

1.2.1 SKAP in mitosis

Mechanistic aspects of the function of SKAP in mitosis have been partly elucidated through identification of different interaction partners of SKAP. Several studies have described an Astrin-SKAP complex (Schmidt et al. 2010, Dunsch et al. 2011, Friese et al. 2016). Astrin is also an important mitotic spindle- and kinetochore-associated protein required for proper chromosome alignment and mitotic progression (Chang et al. 2001, Mack and Compton 2001, Thein et al. 2007). In mitotic cells, Astrin and SKAP form a complex that localizes to spindle microtubules and to bi-oriented kinetochores. The Astrin-SKAP complex is essential for maintaining the spindle structure and stabilizing kinetochore-microtubule attachments (Schmidt et al. 2010, Dunsch et al. 2011, Friese et al. 2016). Huang et al. reported a direct interaction of SKAP with the mitotic motor CENP-E, which is critical for achieving accurate chromosome alignment at the spindle equator during mitosis (Huang et al. 2012). Another SKAP interaction partner is Mis13, an outer kinetochore core complex protein that functions with SKAP in facilitating a stable spindle-kinetochore attachment (Wang et al. 2012). Binding of SKAP to microtubules is at least in part mediated by its interaction with EB1 (end binding 1), a microtubule plus end-tracking protein. Together with EB1, SKAP binds to microtubule plus ends and acts as a regulator of microtubule plus end dynamics (Dunsch et al. 2011, Wang et al. 2012). SKAP is also able to bind microtubules directly and it displays a plus end-tracking

activity, which is necessary for proper mitotic spindle positioning (Friese et al. 2016, Kern et al. 2016). A model of SKAP interactions in mitosis according to data provided by current studies is depicted in Fig. 3.

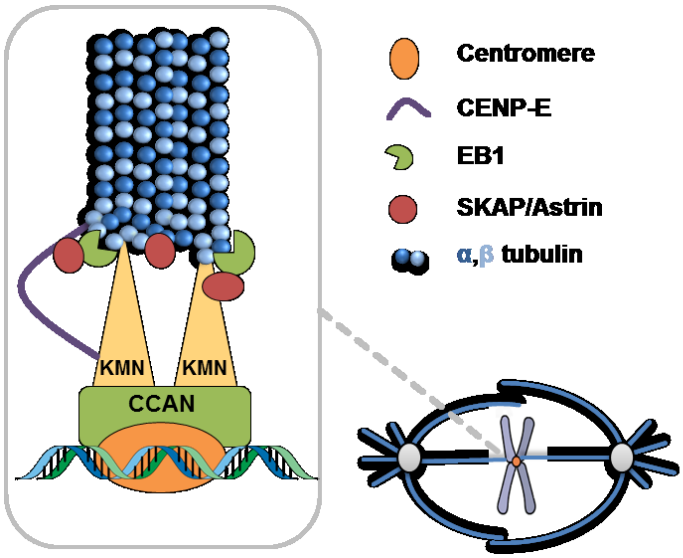

Figure 3. Model of SKAP interactions in mitosis. The SKAP/Astrin complex localizes at the interface of spindle microtubules and outer kinetochore. The C-terminal part of SKAP interacts with Mis13 (a part of the KMN network; an outer kinetochore super-complex composed of KNL1, Mis12 and Ndc80 complexes) and the mitotic motor protein CENP-E, while the N-terminal side mediates the interaction with EB1 (microtubule plus end-tracking protein). The SKAP/Astrin complex also binds to microtubule plus ends directly. These interactions assure a stable spindle-kinetochore attachment during mitosis.

1.2.2 Mitosis-unrelated roles of SKAP

Besides its mainly investigated roles in mitosis, SKAP has also been implicated in biological processes that are not directly related to mitosis. For instance, Lu et al. have shown that SKAP promotes UV-induced cell apoptosis (Lu et al. 2014). Overexpression of SKAP increased the sensitivity of HeLa cells to UV apoptotic stimuli, while the knockdown of SKAP decreased the portion of apoptotic cells after UV exposure. The mechanism of SKAP´s pro-apoptotic activity seems to involve the negative regulation of the anti-apoptotic protein Prp19. Another study revealed that SKAP plays a role in directional cell migration (Cao et al. 2015). SKAP was found to form a complex with IQGAP1 (IQ motif containing GTPase activating protein 1). IQGAP1 is a scaffold protein with a role in orchestrating directional cell migration. Disruption of SKAP-IQGAP1 interaction resulted in inhibition of directional cell migration, suggesting that the interaction with SKAP is necessary to link IQGAP1 to the microtubule plus ends.

1.2.3 SKAP as an oncogene

SKAP was recently classified as a human oncogene. Lee et al. found a melanoma and cutaneous squamous cell carcinoma (SCC)-associated mutation in the SKAP encoding gene (S24F) (Lee et al. 2014). Overexpression of SKAP3 isoform carrying the S24F substitution disrupted sister chromatid cohesion in primary human keratinocytes, increased aneuploidy in primary tumors and enhanced tumorigenesis *in vivo*. These findings imply that SKAP3 mutagenesis probably plays a role in SCC development. The same mutation was reported to be present in basal cell carcinoma (BCC) (Jaju et al. 2015, Bonilla et al. 2016) and pleomorphic dermal sarcoma (PDS) (Helbig et al. 2016). SCC, BCC and PDS-associated SKAP mutation was not found in a variety of other human cancers (Lee et al. 2016), suggesting that this mutation is probably specifically connected to skin cancers. However, it is not yet clear how exactly the observed mutation contributes to disease development.

1.2.4 SKAP isoforms

Processes such as alternative splicing and alternative transcription/translation start site usage give rise to different protein isoforms. The human SKAP encoding gene, KNSTRN, localizes to chromosome 15 (15q15.1) and has 16 transcript variants listed in the Ensembl database (www.ensembl.org; Ensembl ID: ENSG00000128944). Putative protein-coding transcripts are depicted in Fig. 4. KNSTRN1 encodes the longest protein isoform (SKAP1), which is predicted to have 2 coiled-coil domains in its C-terminal part. Another isoform, SKAP16, is encoded by KNSTRN16 which uses an alternative downstream start codon in the same reading frame as KNSTRN1. As a result, SKAP16 lacks the 78 N-terminal amino acids when compared to SKAP1. KNSTRN5 and KNSTRN3 transcripts are produced by alternative splicing in the 3´-coding region and give rise to shorter isoforms that differ from SKAP1 in their C-terminal parts. In further text, the gene and its transcripts will be referred to as KNSTRN and the protein as SKAP.

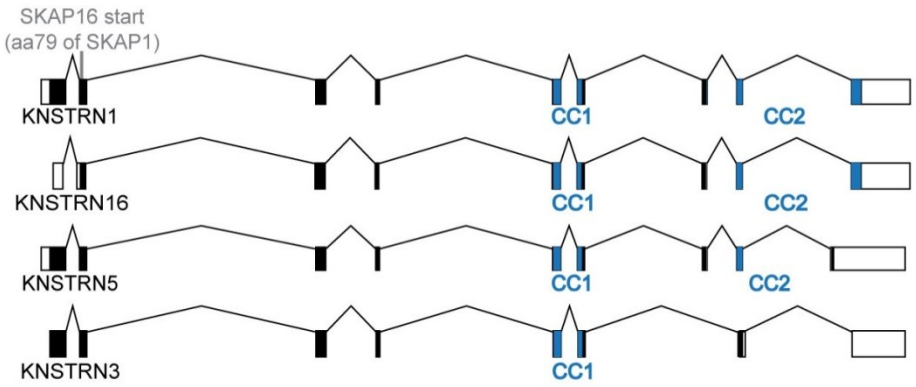

Figure 4. Scheme of the predicted protein-coding KNSTRN transcripts. The scheme was made according to data from Ensembl database using wormweb software (http://wormweb.org/exonintron). Black boxes represent exons of the transcripts, 5´-UTR and 3´-UTR are depicted as white boxes. Blue exon parts mark the regions coding for the two coiled-coil domains (CC1 and CC2) (from (Cindric Vranesic et al. 2016)).

1.2.5 Murine SKAP

According to the Ensembl database, the murine SKAP encoding gene, Knstrn (Ensembl ID: ENSMUSG00000027331), gives rise to 9 transcript variants, whereby Knstrn1 and Knstrn4 (Fig. 5) code for proteins similar to human SKAP1 and SKAP16, respectively. Knstrn1 codes for the longest protein isoform, while Knstrn4 encodes a protein lacking a stretch of 78 N-terminal amino acids.

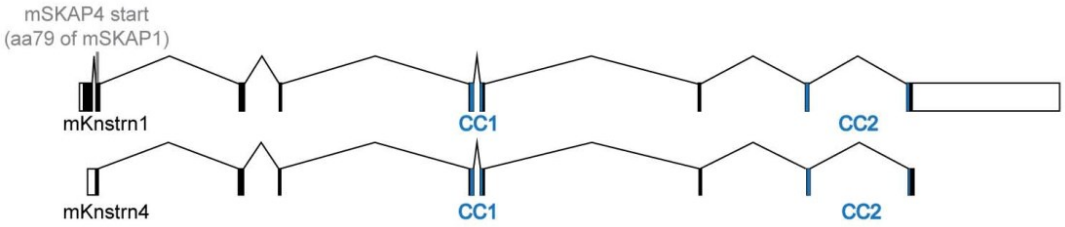

Figure 5. Schematic representation of mouse Knstrn1 and Knstrn4 transcripts. The scheme was made according to data from Ensembl database using wormweb software (http://wormweb.org/exonintron). Black boxes represent exons of the transcripts, 5´-UTR and 3´-UTR are depicted as white boxes. Blue exon parts mark the regions coding for the two coiled-coil domains (CC1 and CC2) (from (Cindric Vranesic et al. 2016)).

1.3 AAA+ ATPases Pontin and Reptin

Pontin and Reptin are highly conserved members of the AAA+ ATPases (ATPases associated with diverse cellular activities) superfamily which includes DNA-helicases and chaperones. These proteins are characterized by conserved Walker A and Walker B domains (for binding and hydrolysis of ATP, respectively), an arginine finger and sensor domains (for sensing whether the protein is bound to di- or trinucleotide). Both Pontin and Reptin are capable of forming homohexameric and

heterohexameric ring structures, as well as heterododecamers. They often function within the same macromolecular complexes and have many roles in diverse cellular processes (Huber et al. 2008, Jha and Dutta 2009, Nano and Houry 2013). Pontin and Reptin are, for instance, well-known to regulate gene transcription. For example, Pontin and Reptin both interact with β-catenin and have opposing effects on β-catenin-mediated transcriptional activity. Pontin increases the activation of the downstream genes, while Reptin inhibits it (Bauer et al. 1998, Bauer et al. 2000). β-catenin is a major player in canonical Wnt signaling which is involved in many cellular processes such as embryonic development and cell proliferation. Wnt signaling is activated in many human cancers and therefore, Pontin and Reptin, through regulating Wnt signaling, are also involved in cellular transformation. Additionally, in context of transcriptional regulation, Pontin and Reptin are associated with several chromatin-remodeling complexes, such as TIP60 (Tat-interactive protein 60 kDa) (Jha et al. 2013), INO80 (Jonsson et al. 2004, Tosi et al. 2013) and SWR1 (Nguyen et al. 2013). It is speculated that Pontin and Reptin act as chaperones necessary for the optimal assembly of these complexes (Jha et al. 2013). Indeed, Pontin and Reptin are often suggested to have the chaperone function in various complexes. By now, they are shown to participate in the R2TP complex (Nano and Houry 2013). R2TP is a chaperone complex including HSP90 (heat shock protein 90). This complex is involved in snoRNPs assembly, pre-ribosomal RNA processing, apoptosis and RNA polymerase II assembly. Furthermore, Pontin and Reptin have been reported to associate with microtubular structures, not only during mitosis (Gartner et al. 2003, Sigala et al. 2005, Ducat et al. 2008), but also in cilia (Stolc et al. 2005). They also function in DNA damage response, cancer metastasis and apoptosis (Jha and Dutta 2009).

1.4 Spermatogenesis

Spermatogenesis is a process of spermatozoa production from primordial germ cells within seminiferous tubules of the testes. The process can be subdivided into three phases; proliferation (clonal expansion), maturation (meiosis) and differentiation (spermiogenesis) (Fig. 6). Proliferation phase begins with mitotic divisions of the germline stem cells, spermatogonia. Spermatogonia are located next to the basal lamina of the seminiferous tubules, where they divide continuously by mitosis, giving rise to two types of daughter cells; type A and type B spermatogonia. Type A

spermatogonia are self-renewing cells that serve to replenish the stock of the stem cells, while type B spermatogonia divide and give rise to primary spermatocytes. Primary spermatocytes migrate towards the lumen of the seminiferous tubules and enter the first meiotic division to produce secondary spermatocytes. These undergo the second meiotic division and give rise to haploid round spermatids. Spermatids go through morphological differentiation into spermatozoa (spermiogenesis), which are then expelled to the lumen of seminiferous tubules (spermiation). Besides the germ cells, seminiferous epithelium consists of somatic cells called Sertoli cells. These cells have supportive and nourishing functions throughout the development, secret hormones and phagocytize cell fragments produced during spermatogenesis (Hess 1999). Spermatogenesis is a continuous process throughout the reproductive lifetime and it is highly regulated to assure the continuum of sperm production. In human, the time required to generate spermatozoa from spermatogonia is roughly 74 days (Amann 2008), while in mice the first wave of spermatogenesis is complete by day 35 after birth (Vergouwen et al. 1993).

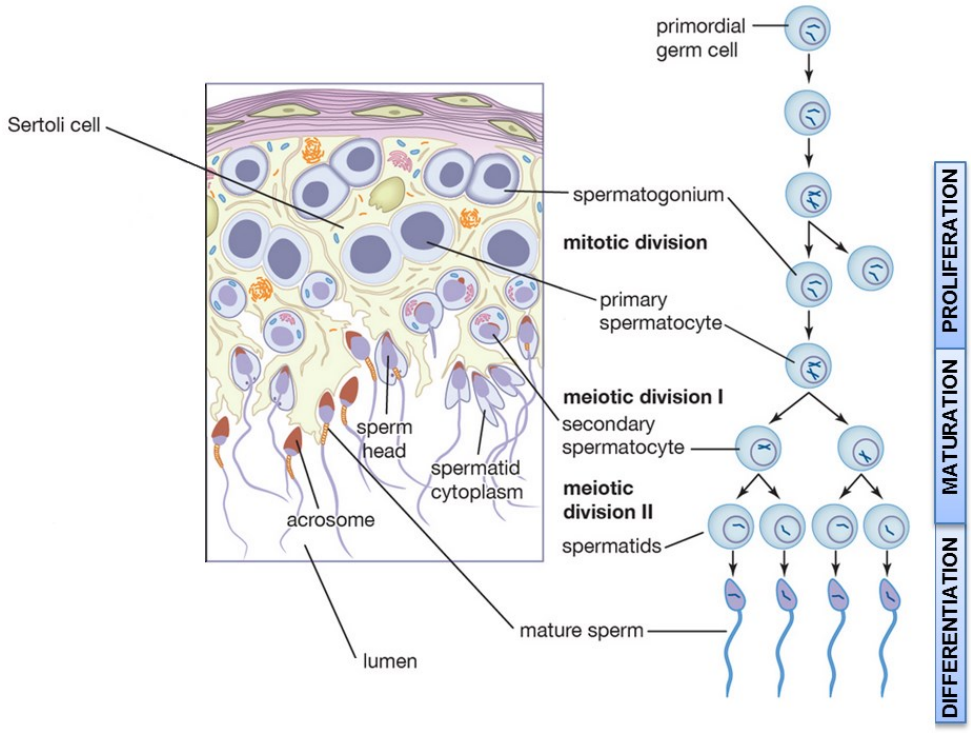

Figure 6. Schematic representation of mammalian spermatogenesis (modified from http://www.britannica.com/science/spermatogenesis).

1.4.1 Structure of human spermatozoa

Spermatozoa are composed of two morphologically and functionally distinct regions; a head and a flagellum, enclosed within the same plasma membrane (Fig. 7A). The sperm head contains a haploid nucleus with a densely packed DNA. The anterior part of the nucleus is surrounded by the acrosome, a specialized secretory vesicle that contains hydrolytic enzymes necessary for fertilization. The flagellum is essential for sperm motility. It is structurally divided into four parts: the connecting, the mid-, the principal, and the end piece. The internal cytoskeletal structure running throughout the flagellum is called axoneme. The axoneme is composed of a set of nine peripheral double microtubules and two single ones in the center (9+2 structure) (Fig. 7B). In addition, outer and inner arms of axonemal dyneins are bound to the outer double microtubules. Highly organized network of dyneins and associated proteins assures the sperm motility by enabling the sliding of the microtubules. In the midpiece and principal piece, the axoneme is surrounded by outer dense fibers (ODFs). ODFs are stiff and non-contractile fibers which play a role in the structural maintenance of flagellar elasticity, but are also important for regulation of the sperm motility (Inaba 2011).

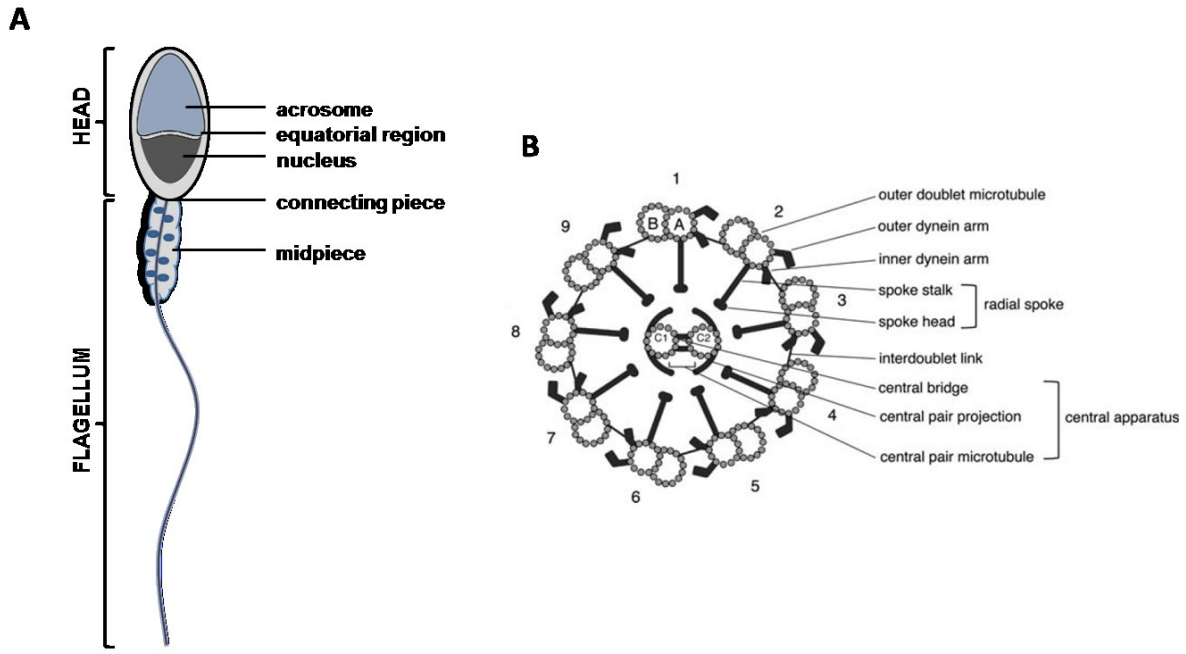

Figure 7. Human sperm structure. (A) Simplified scheme of human spermatozoon. (B) Structure of the flagellar axoneme (from (Inaba 2011)).

2 Aims of the study

SKAP is a multifunctional protein with proposed roles in mitosis, apoptosis and cell migration. It has recently drawn attention, not only because of the functions in vital biological processes, but also because of mutations associated with cancer suggesting it may act as an oncogene. Precise mechanisms behind SKAPs activities in these cellular processes are not completely understood. SKAP is putatively expressed in different isoforms, however, previous studies did not discriminate between them. As different molecular architectures of protein isoforms often determine their localization and functions, this study aimed to investigate the expression profile and possible functional differences between SKAP isoforms in human and mouse.

Some proteins assemble into homo-oligomeric complexes in order to perform their cellular functions. Sometimes transitions between different oligomeric states also regulate protein activities. Therefore, defining protein stoichiometry is crucial to understand its molecular function. In this respect, based on the primary structures of SKAP, another aim of this project was to address its ability to self-associate.

SKAP is a relatively newly identified protein and its functions are just beginning to be understood. As a crucial step to define and better understand functions of SKAP, this work also aimed to discover its unknown interaction partners and its potential oncogenic nature.

3 Materials and methods

3.1 Materials

3.1.1 Bacterial strains and media

Escherichia coli (*E. coli*) strains used in this work are listed and described in Tab. 1.

Table 1. *E. coli* strains used for plasmid DNA amplification and recombinant protein expression.

Strain	Genotype
XL1-Blue	*endA1 gyrA96 (nal^R) thi-1 recA1 relA1 lac glnV44 F'[::Tn10 proAB$^+$ lacI^{q}Δ (lacZ) M15] hsdR17(r_K-m_K+)*
DH5α	*deoR endA1 gyrA96 hsdR17 (r_K– m_K+) recA1 relA1 supE44 thi-1 D (lacZYA- argFV169) f80lacZDM15 F-*
BL21 (DE3)	*F– ompT gal dcm lon hsdSB(r_B- m_B-) λ (DE3 [lacI lacUV5-T7 gene 1 ind1 sam7 nin5])*
BL21 (RE4)	*F- ompT gal dcm lon hsdS(r_B-m_B-) gal;* transfected with pREP4

Media used for cultivation of bacteria:

LB medium
1% (w/v) Peptone-casein
0.5% (w/v) Yeast extract
85.6 mM NaCl

LB-agar plates
LB medium with 1.5% (w/v) agar

Selective media
LB medium or LB-agar plates with appropriate antibiotics (50 µg/ml ampicillin, 25 µg/ml kanamycin, 34 µg/ml chloramphenicol)

3.1.2 Eukaryotic cells and cell culture materials

Eukaryotic cells and cell lines used in this work are listed in Tab. 2.

Table 2. List of eukaryotic cells.

Cells	Description	
Human		
HEK-293	embryonic kidney cells	
HeLa	cervical carcinoma cells	
MCF-7	breast adenocarcinoma cells	
U-2 OS	osteosarcoma cells	
Cal 29	bladder cancer cells	
Daoy	medulloblastoma cells	
SH-SY5Y	neuroblastoma cells	
HCT 116	colorectal carcinoma cells	
Caco-2	colorectal adenocarcinoma cells	
HaCaT	keratinocytes	
A-431	epidermoid carcinoma	
H-157	lung epithelial cells	
HEp-2	HeLa contaminant cell line	
NHEK	adult normal epidermal keratinocytes	Cell pellets kindly provided by Dr. Cagatay Günes
NHEK-Neo	neonatal normal epidermal keratinocytes	
HMEC	mammary epithelial cells	
ImR-90	lung fibroblasts	
BJ	foreskin fibroblasts	
HFF	foreskin fibroblasts	
Murine		
Neuro-2a	neuroblastoma cells	
CMT-93	rectal polyploid carcinoma cells	
C57MG	mammary epithelial cells	
Hybridoma cells	monoclonal antibody-producing cells, generated as fusion of murine B-cells and myeloma cells	Produced in the group of Prof. Karlheinz Friedrich

Media used for eukaryotic cell culture:

Eukaryotic cell medium	*Dulbecco´s Modified Eagle´s Medium* (DMEM) 10% (v/v) fetal calf serum (FCS) 100 U/ml penicillin, 100 µg/ml streptomycin
IgG-depleted hybridoma cell medium	*Roswell Park Memorial Institute* (RPMI)-1640 10% (v/v) FCS without IgG 2% (v/v) HT supplement (hypoxanthine/thymidine) 20 ng/ml human interleukin 6 (IL-6)

Freezing medium	corresponding cell culture medium 20% (v/v) FCS 10% (v/v) dimethyl sulfoxide (DMSO)

3.1.3 Human and mouse material

Total RNA from human tissues was kindly provided by Dr. Cagatay Günes (Fritz Lipmann Institute on Aging, Jena). RNAs from normal human colon and colon cancer were kindly provided by Dr. Yuan Chen (Institute of Pathology, University Hospital Jena). Human semen samples were obtained from a healthy 30 year-old donor. Informed consent was obtained from the donor. Human testicular biopsies were kindly provided by Prof. Dr. Christiane Kirchhoff (University Hospital Hamburg-Eppendorf). These were obtained and characterized as described (Feig et al. 2007). To analyze SKAP isoforms in mouse, testes were collected from wild type C57BL/6 mice (provided by Dr. Cagatay Günes) at different time points after birth as described (Weise and Günes 2009).

3.1.4 cDNAs, plasmids and shRNA constructs

Human KNSTRN1 cDNA (GenBank ID: NM_033286.3) was obtained previous to this work. It was purchased as IMAGE clone (IMAGp998L111825Q3; RZPD Deutsches Ressourcenzentrum für Genomforschung GmbH) and cloned into various expression vectors. As part of this work, human KNSTRN16 cDNA (Ensembl ID: ENST00000608100) was amplified by PCR from KNSTRN1 cDNA with oligonucleotides ON1217 and ON224 (Tab. 5). Mouse Knstrn1 (GenBank ID: NM_026412.3) cDNA was amplified by RT-PCR from total RNA of adult mouse testis using oligonucleotides ON1315 and ON1317 (Tab. 5). All amplified cDNAs were cloned into pCS2+ vector, sequenced for verification and subsequently subcloned into other expression vectors (Tab. 3). Pontin and Reptin (Weiske and Huber 2005), β-catenin (Aberle et al. 1994) and Tip60 (Huber and Weiske 2008) expression constructs were described previously.

Table 3. List of plasmid vectors used in this work.

Vector	Description
Prokaryotic expression vectors	
pGEX-4T1	for expression of recombinant N-terminal Glutathione S-transferase (GST)-fusion proteins
pMAL-c2X	for expression of recombinant N-terminal Maltose-binding protein (MBP)-fusion proteins
Eukaryotic expression vectors	
pCS2+	CMV promotor
pCS2+myc$_6$	codes for C-terminal 6x myc-tag
pCS2+FLAG	codes for C-terminal FLAG-tag
p3xFLAG-CMV™-10	codes for N-terminal 3x FLAG-tag
p3xFLAG-CMV™-14	codes for C-terminal 3x FLAG-tag
pDONR221	Gateway® donor vector
pH-Ch-N*	Gateway® destination vector for expression of N-terminal mCherry-fusion proteins
pH-mRub-N*	Gateway® destination vector for expression of N-terminal mRuby2-fusion proteins
pH-mRub-C*	Gateway® destination vector for expression of C-terminal mRuby2-fusion proteins
pH-Clov-N*	Gateway® destination vector for expression of N-terminal Clover-fusion proteins
pH-Clov-C*	Gateway® destination vector for expression of C-terminal Clover-fusion proteins
pH-G-N*	Gateway® destination vector for expression of N-terminal EGFP-fusion proteins

*Gateway expression vectors were designed in the group of Prof. Dr. Stephan Diekmann (Fritz Lipmann Institute on Aging, Jena) and kindly provided by Dr. Christian Hoischen

To reduce protein levels of SKAP, a set of ready-cloned shRNA expression vectors was purchased from OriGene Technologies (TL306156), where every shRNA vector is cloned in pGFP-C-shLenti plasmid under U6 promoter for mammalian cell expression. Sequences of 29mer shRNAs and scrambled control are listed in Tab. 4.

Table 4. Anti-KNSTRN shRNA and scrambled control nucleotide sequences.

	Name	Sequence (5´→3´)
anti-KNSTRN	TL306156A	CACTTCTAAGAGTCTCTTACCTGTTAGGT
	TL306156B	TTCAGGAGGTCCAGAGAATGATGTTACAA
	TL306156C	CTGTTAGAAGCCGTCAACAAGCAGTTGCA
	TL306156D	ACTTAGCCGGTGGCACGACAGTTGCTGCA
scrambled control	TR30021	GCACTACCAGAGCTAACTCAGATAGTACT

3.1.5 Oligonucleotides

All oligonucleotide primers (except the ones used for Gateway® cloning (biomers.net, Ulm, Germany)) in this work were synthesized by Metabion (Steinkirchen, Germany) and are listed in Tab. 5. Tab. 6 summarizes oligonucleotide combinations used in PCR reactions for cloning of expression constructs of truncated SKAP proteins. Primers used for Gateway® cloning are listed in Tab. 7.

Table 5. List of oligonucleotide primers.

Name	Description	Sequence (5´→3´)
Human KNSTRN		
ON223	hKNSTRN1-F	gcgggatcc**gccacc**ATGGCGGCTCCCGAAGCCCCG
ON224	hKNSTRN1/16-R	gcgggatccTTACATTTCTAATAGCTGCTCCA
ON225	hKNSTRN1/16-R	gcgggatccCATTTCTAATAGCTGCTCCATT
ON1139	hKNSTRN1(aa166)-F	cgcggatcc**gccgcc**ATGAGTAAGCAAAAATCAGAGGAAG
ON1140	hKNSTRN1(aa168)-R	cgcggatccTTACTTACTCAGTGGTTTGTAGCC
ON1141	hKNSTRN1(aa216)-F	cgcggatcc**gccgcc**ATGTGTTTGGCAATTTTGGAGAGC
ON1142	hKNSTRN1(aa215)-R	gcgggatccTTAGTTGTCCCGAAACTTCTCC
ON1143	hKNSTRN1(aa246)-F	gcgggatcc**gccgcc**ATGGACTCTATGTTGCTGTTAG
ON1144	hKNSTRN1(aa248)-R	gcgggatccTTAAGAGTCCATGTGATCAGTAG
ON1217	hKNSTRN16-F	gcgggatcc**gccgcc**ATGACCAGTGTGGTTAAGACAG
ON1227	hKNSTRN2-R	gcgggatccCTACATTTGGTGCAATATCCCATG
ON1228	hKNSTRN3-R	gcgggatccTTAAAAGCTTCAGCTCCTCTTGC
ON1230	hKNSTRN1-F	gcgggatccATGGCGGCTCCCGAAGCC
ON1232	hKNSTRN1(aa78)-R	gcgggatccTTACGTAACGAGGCGGCACGG
ON1303	hKNSTRN qPCR-F	ATGGGCAAATGAAAGCTACTG
ON1304	hKNSTRN qPCR-R	TGCTTACTCAGTGGTTTGTAGCC
ON1470	hKNSTRN1(S24F)-F	TCTACAGAGTGCGATTTCCACCCACTTCCGCCTAGC
ON1471	hKNSTRN1(A40E)-F	CTATTTGAAACCCAGGAGGCCGACTTAGCCGGTGGC
Murine Knstrn		
ON1305	mKnstrn1-F	GAGACAGCCTTCCGTACAACA
ON1306	mKnstrn4-F	GTGCTAAGACGGTGTGCGAT
ON1307	mKnstrn1/4-R	TTCTAAGAGCTGCTCCATTTCCTC
ON1315	mKnstrn1-F	gcgggatcc**gccgcc**ATGGCGGCTCCCGAGGCC
ON1316	mKnstrn4-F	gcgggatcc**gccgcc**ATGGCCAGTGCTAAGACGG
ON1317	mKnstrn1/4-R	gcgggatccCTACATTTCTAAGAGCTGCTCC
Other		
ON140	hβ-actin-F	TCCTGGGCATGGAGTCCTGTG
ON141	hβ-actin-R	CGCCTAGAAGCATTTGCGGTG
ON182	hGAPDH-F	AGCAATGCCTCCTGCACCACCACC
ON183	hGAPDH-R	CCGGAGGGGCCATCCACAGTCT

Table 5. List of oligonucleotide primers (continued).

ON983	mGAPDH-F	CCACTCTTCCACCTTCGATG
ON984	mGAPDH-R	TCCACCACCCTGTTGCTGTA
ON1151	h/m 18S rRNA-F	GCA ATT ATT CCC CAT GAA CG
ON1152	h/m 18S rRNA-R	GGG ACT TAA TCA ACG CAA GC
ON1472	mutagenesis-R	GTCAGAAGTAAGTTGGCCGCAGTGTTATCACTCATG

F: forward; R: reverse; h: human; m: murine; aa: amino acid; BamHI restriction site is underlined; Kozak sequence is written in **bold** letters; nucleotides complementary to the original cDNA sequence are written in capitals; start and stop codons are marked in blue; in mutagenesis primers, nucleotides that differ from the original sequence are marked in red

Table 6. List of primer combinations used for cloning of SKAP deletion constructs.

SKAP1		SKAP16	
Deletion construct	**Primer pair**	**Deletion construct**	**Primer pair**
1-78	F: ON223 R: ON1232	**1-90**	F: ON1217 R:ON1140
79-316	F: ON1217 R: ON224	**89-238**	F: ON1139 R: ON224
1-168	F: ON223 R:ON1140	**1-138**	F: ON1217 R: ON1142
167-316	F: ON1139 R: ON224	**139-238**	F: ON1141 R: ON224
1-216	F: ON223 R: ON1142	**1-170**	F: ON1217 R: ON1144
217-316	F: ON1141 R: ON224	**169-238**	F: ON1143 R: ON224
1-248	F: ON223 R: ON1144	**89-138**	F: ON1139 R: ON1142
247-316	F: ON1143 R: ON224	**139-170**	F: ON1141 R: ON1144

F: forward; R: reverse

Table 7. List of primers used to generate Gateway® expression clones.

		Sequence (5´→3´)
SKAP1	attB1F	ggggacaagtttgtacaaaaaagcaggcttcgaaaacctgtattttcagggcgccacc ATGGCGGCTCCCGAAGCCC
	attB2R	ggggaccactttgtacaagaaagctgggtCATTTCTAATAGCTGCTCCATTTCCTTAAGG
SKAP16	attB1F	ggggacaagtttgtacaaaaaagcaggcttcgaaaacctgtattttcagggcgccacc ATGACCAGTGTGGTTAAGACAGTGTATAG
	attB2R	same as for SKAP1

F: forward; R: reverse; attB overhangs are underlined; nucleotides complementary to the original cDNA sequence are written in capitals; start and stop codons are marked in blue

3.1.6 Antibodies

Table 8. Primary antibodies used in this work.

Antibody	Manufacturer	Stock concentration	Used dilution
Anti-SKAP			
Rabbit polyclonal	Atlas Antibodies AB Sigma	0.5 µg/µl	WB:0.5 µg/ml IF: 1:1.000 or 1:200 IP: 1 µg
Mouse monoclonal (A12-11)	produced as part of this PhD project	0.4 µg/µl	WB: 1 µg/ml IF: 1:100 IP: 1 µg
Mouse monoclonal (C11-32)	produced as part of this PhD project	0.64 µg/µl	WB: 1 µg/ml IF: 1:200 IP: 1 µg
Mouse monoclonal (F5-13)	produced as part of this PhD project	0.55 µg/µl	WB: 1 µg/ml IF: 1:200 IP: 1 µg
Anti-Pontin			
Rabbit polyclonal (E12-TC)	described in (Bauer et al. 1998)	Unpurified rabbit serum	IF: 1:300
Mouse monoclonal (5G3-11)	described in (Weiske and Huber 2005, Cvackova et al. 2008)	0.5 µg/µl	WB: 1:500
Other			
Rabbit polyclonal anti-GST	described in (Weiske and Huber 2005)	-	WB: 1:10.000
Mouse monoclonal anti-MBP (D7-42)	produced as part of this PhD project	0.58 µg/µl	WB: 1 µg/ml
Mouse monoclonal anti-FLAG M2	Sigma	3.8 µg/µl	WB: 1:10.000 IP: 2 µg
Mouse monoclonal anti-myc (9E10)	Sigma	1.5 µg/µl	WB: 1:4.000 IP: 2 µg
Mouse monoclonal anti-GFP (JL-8)	Clontech	1 µg/µl	IP: 1 µg
Mouse monoclonal anti-GAPDH	Merck Millipore	1 µg/µl	WB: 1:1.000

WB: Western blot; IF: immunofluorescence; IP: immunoprecipitation

Table 9. Secondary antibodies used in this work.

Antibody	Manufacturer	Stock concentration	Used dilution
Antibodies for Western blot			
HRP-conjugated goat anti-mouse IgG	Dianova	0.5 µg/µl	1:10.000
HRP-conjugated goat anti-rabbit IgG	Dianova	0.5 µg/µl	1:10.000
HRP-conjugated goat anti-mouse IgG (light chain)	Dianova	0.5 µg/µl	1:5.000

Table 9. Secondary antibodies used in this work (continued).

Antibodies for immunofluorescence			
Goat anti-mouse Alexa Fluor™ 488-labeled	Molecular Probes (Invitrogen)	2 µg/µl	1:1.000
Goat anti-rabbit Alexa Fluor™ 594-labeled	Molecular Probes (Invitrogen)	2 µg/µl	1:1.000

HRP: horseradish peroxidase

3.1.7 Enzymes, reaction kits and molecular weight standards

Enzymes:

BP Clonase™ II enzyme mix	Invitrogen
LR Clonase™ II enzyme mix	Invitrogen
Phusion® High-Fidelity DNA-Polymerase	New England Biolabs
T4-Polynucleotide kinase (PNK)	New England Biolabs
Proteinase K	Invitrogen
Quick T4 DNA-ligase	New England Biolabs
RNAse A	Carl Roth
Shrimp alkaline phosphatase (SAP)	Fermentas
Taq DNA-Polymerase	New England Biolabs
Type II restriction endonucleases	Fast Digest by Fermentas, Roche

Commercial reaction kits:

CloneJET PCR Cloning Kit	Thermo Fisher Scientific
DNA Clean and Concentrator™-5	Zymo Research
Expand High Fidelity PCR System	Roche
GoTaq® qPCR Master Mix	Promega
High Capacity cDNA Reverse Transcription Kit	Applied Biosystems
NucleoBond® Xtra Midi	Macherey-Nagel
NucleoSpin® RNA II	Macherey-Nagel
Pwo Master	Roche
Quick Ligation™ Kit	New England Biolabs
SMART™ RACE cDNA Amplification Kit	Clontech
SuperScript™ First-Strand Synthesis System for PCR	Invitrogen
The Original TA Cloning® Kit	Invitrogen
Zymoclean™ Gel DNA Recovery Kit	Zymo Research
Zyppy™ Plasmid Miniprep Kit	Zymo Research

DNA and protein molecular weight standards:

GeneRuler™ 100 bp DNA Ladder (100-1.000 bp)	Thermo Fisher Scientific
GeneRuler™ 1 kb DNA Ladder (250-10.000 bp)	Thermo Fisher Scientific
PageRuler™ Prestained Protein Ladder (10-170 kDa)	Thermo Fisher Scientific
PageRuler™ Unstained Protein Ladder (10-200 kDa)	Thermo Fisher Scientific

3.1.8 Chemicals

1,4-Diazabicyclo-(2.2.2)-octane solution (DABCO)	Carl Roth
4',6-diamidino-2-phenylindole (DAPI)	Sigma
4-iodophenylboronic acid (IPBA)	Sigma
Acetic acid	Carl Roth
Agar	BD
Agarose	Invitrogen
Ammonium persulfate (APS)	Serva
Ampicillin	Ratiopharm
Amylose beads	New England Biolabs
Bromphenolblue	Merck
Chloramphenicol	Fluka
Complete™-EDTA	Roche
Coomassie Brilliant Blue R250	Merck
Deoxynucleotide triphosphates (dNTPs)	New England Biolabs
DMEM	Sigma
DMSO	Merck Millipore
Dynabeads® Protein A	Invitrogen
Ethanol	Echter Nordhäuser Spirituosen
Ethylene glycol-bis(2-aminoethylether)-N,N,N′,N′-tetraacetic acid (EGTA)	Serva
Ethylenediaminetetraacetic acid (EDTA)	Carl Roth
FCS	PAN Biotech
FuGENE® HD transfection reagent	Promega
Glucose-monohydrate	Carl Roth
Glutathione (GSH)-agarose beads	Sigma
Glycerol	Carl Roth
Glycine	Carl Roth
Goat serum	PAA
HCl	Carl Roth
HT supplement	Life Technologies
Imidazole	Carl Roth
Ingenio® electroporation solution	Mirus Bio LCC
Isopropanol	VWR
Isopropylβ-D-1-thiogalactopyranoside (IPTG)	AppliChem
Kanamycin	Merck
KCl	Carl Roth
Luminol	Carl Roth
Methanol	VWR
$MgCl_2$	Carl Roth
Na_2HPO_4 x H_20	Merck
Na_2MoO_4	Sigma
Na_3VO_4	Sigma
NaCl	Carl Roth
NaF	VEB Flourwerke Dohna
NaH_2PO_4 x H_20	Merck
Nonidet P-40	Roche
Paraformaldehyde	Carl Roth
PBS	Sigma

Penicillin/streptomycin	Sigma
Peptone-casein	Carl Roth
Polyethyleneimine (PEI)	Polysciences, Inc.
Polyethylene-glycol 8000 (PEG 8000)	Fluka
Poly-L-Lysine	Sigma
ProLong® Gold Antifade Mountant with DAPI	Life Technologies
Protein A sepharose™ CL-4B	GE Healthcare
Pyronine G	Sigma
RedSafe™ Nucleic Acid Staining Solution	iNtRON Biotechnology
Rotiphorese® (30% (w/v) Acrylamide, 0.8% (w/v) Bisarcylamide)	Carl Roth
RPMI-1640	Sigma
Sodium dodecyl sulfate (SDS)	Carl Roth
Sucrose	Carl Roth
Tetramethylethylenediamine (TEMED)	Carl Roth
Tris	Carl Roth
Triton X-100	Roche
Trypsin-EDTA	Sigma
TurboFect transfection reagent	Thermo Fisher Scientific
Tween 20	Carl Roth
Xylene cyanol	Carl Roth
Yeast extract	Carl Roth
β-mercaptoethanol	Carl Roth

3.1.9 Equipment and consumables

Laboratory equipment:

2720 Thermal cycler	Applied Biosystems
761 Calimatic pH-meter	Knick
ÄKTA purifier™ 10 FPLC device	GE Healthcare
AMAXA Nucleofector®II	Amaxa Biosystems
Benchtop centrifuges: Mikro 220R	Andreas Hettich
Rotina 380R	
Rotina 420R	
Bioview blue light transilluminator	Biostep
Casy® cell counter and analyzer model TT	Roche Innovatis
CO_2 incubator	BINDER
Comfort thermomixer	Eppendorf
CONSORT ev 261 electrophoresis power supply	CONSORT nv
FiberLite® rotor F14-6x250y	Piramoon Technologies
G:BOX gel documentation system	Syngene
Gel dryer model 583	Bio-Rad
HERAsafe® biological safety cabinet	Thermo Fisher Scientific
Incubator shaker Ecotron	Infors
INCU-Line incubator	VWR
MC1 Analytik AC120S precisions balance	Sartorius
Microscopes: AE21 Inverted microscope	Motic
Axio Observer.Z1 ApoTome	ZEISS
LSM 710 Confocor3 microscope	ZEISS
Mini centrifuge Sprout™	Biozym Scientific

Mini-PROTEAN® Tetra Cell Electrophoretic chamber	Bio-Rad
Mini-Trans-Blot® Electrophoretic transfer cell	Bio-Rad
MR3001 magnetic stirrer	Heidolph
MW81W microwave	Samsung
NanoDrop 2000 spectrophotometer	PEQLAB
NICOOL LM10 mini freezer	Air Liquide
QBD2 Block heater	Grant Instruments
Sorvall RC-5B Refridgerated Superspeed Centrifuge	Dupont Sorvall Instruments
Sorvall® SS-43 centrifuge rotor	Dupont Sorvall Instruments
Spectrophotometer	Eppendorf
Standard power pack P25 power supply	Biometra
StepOnePlus™ Real-Time PCR System	Applied Biosystems
TE412 scale	Sartorius
Trans-Blot® SD Semi-dry electrophoretic transfer cell	Bio-Rad
Ultra turrax tissue homogenizer	IKA-Werke
Ultrasonic processor UP100H	Hielscher Ultrasonics
Veriti® 96-Well Thermal Cycler	Applied Biosystems
Vortex	VWR

Laboratory consumables:

Cell culture plates (10 cm, 6-well, 12-well, 24-well)	Greiner Bio-One
CELLSTAR® Filter Cap Cell Culture Flasks (75 cm², 175 cm²)	Greiner Bio-One
Cellstar® tubes (15 ml and 50 ml)	Greiner Bio-One
Ingenio® Electroporation cuvettes	Mirus Bio LCC
Microscope slides and coverslips	Thermo Fisher Scientific
Nunc™ Cell scrapers	Thermo Fisher Scientific
PCR tubes (0.2 ml)	Biozym
Pipette tips (volume range: 10 µl, 200 µl and 1000 µl)	Greiner Bio-One
Plastic pipettes (2 ml, 5 ml and 10 ml)	Greiner Bio-One
Poly-Prep® chromatography columns	Bio-Rad
Polyvinylidene fluoride (PVDF) membrane Roti®	Carl Roth
Reaction tubes (0.5 ml, 1.5 ml and 2 ml)	Eppendorf, Sarstedt
Sterile filters Minisart® (poresize 0.2 µm)	Sartorius
Visking dialysis tubing (exclusion limit: 14 kDa)	Carl Roth
Whatman® chromatography paper (3mm)	Biometra

3.1.10 Software

Software	Made/Copyright by
Adobe® Illustrator® CS4	Adobe Systems Incorporated
ApE (A plasmid Editor)	M. Wayne Davis
AxioVision 4.8	ZEISS
BLAST	NCBI
EndNote x7	Thomson Reuters
FigureJ	Jerome Mutterer, Edda Zinck
FIJI/ImageJ	Wayne Rasband
SigmaPlot	SYSTAT Software
WormWeb (Exon-Intron Graphic Maker)	Nikhil Bhatla
ZEN	ZEISS

3.2 Methods

3.2.1 Molecular biological methods

3.2.1.1 Transformation of *Escherichia coli (E. coli)*

E.coli XL1-Blue and DH5α strains were used for plasmid amplification and BL21 (DE3) and BL21 (RE4) for protein expression. For transformation, frozen aliquots of competent cells were thawed on ice and 20 µl of bacterial suspension was mixed with about 100 ng of plasmid DNA. After 10 min incubation on ice, bacteria were heat-shocked for 1 min (XL1-Blue, DH5α, BL21 (DE3)) or 2 min (BL21 (RE4)) at 42°C. Subsequently, 500 µl of LB medium without antibiotics were added to the cells and further incubated for 30 min at 37°C to allow the bacteria to start the expression of antibiotic resistance genes. Afterwards, 30-50 µl of the suspension were plated on LB-agar plates with corresponding antibiotics. Bacteria were grown over night at 37°C.

3.2.1.2 Plasmid DNA purification

For purification of small amounts of plasmid DNA, single colonies of transformed bacteria were grown in 3 ml LB medium with antibiotics for 8-12 h at 37°C. Two ml of bacterial suspension were centrifuged twice at 6.000 g for 5 min at 4°C to pellet the cells and remove the LB medium. Bacterial pellet was resuspended in 150 µl buffer P1 and lysed with 150 µl buffer P2 by inverting the tubes. The solution was neutralized with the addition of 150 µl buffer P3. Bacterial cell debris, proteins and genomic DNA were pelleted by centrifugation at 20.800 g for 10 min at 4°C. Supernatant was transferred to a new tube and plasmid DNA was precipitated with 900 µl cold absolute ethanol by centrifugation (20.800 g, 10 min, 4°C). After washing with 200 µl of 70% (v/v) ethanol, the pellet was dried at 42 °C and afterwards dissolved in 20-30 µl ddH_2O.

Buffer P1 (resuspension)	50 mM Tris/HCl, pH 8.0 100 µg/ml RNaseA 10 mM EDTA
Buffer P2 (lysis)	200 mM NaOH 1% (w/v) SDS
Buffer P3 (neutralization)	3 M potassium acetate, pH 5.5

Alternatively, DNA was isolated and purified using the NucleoSpin® Plasmid QuickPure kit following the manufacturer´s instructions.

For purification of bigger amounts of plasmid DNA, single colonies of transformed bacteria were picked using a sterile pipette tip and grown in 100 ml LB medium containing antibiotics for 12-16 h at 37°C under constant agitation. Plasmid DNA was purified using the NucleoBond® Xtra DNA plasmid purification kit according to the manufacturer´s instructions. Purified DNA was dissolved in 0.1x TE buffer and stored at -20°C.

0.1x TE buffer 10 mM Tris/HCl, pH 8
0.1 mM EDTA

3.2.1.3 DNA concentration measurements

Concentration and purity of DNA were determined on the NanoDrop 2000 spectrophotometer. Measurements of absorbance at 260 nm (DNA/RNA absorption maximum) were done in 1-2 µl of DNA solution. Before the measurements, NanoDrop was calibrated with the corresponding solvent.

3.2.1.4 DNA restriction digest

For restriction digest, approximately 1 µg of DNA was mixed with the appropriate restriction enzyme in a reaction mix and incubated as suggested by the manufacturer. After the digest, DNA was separated by agarose gel electrophoresis and purified from the gel.

Example of a restriction digest reaction using Roche BamHI restriction enzyme:

1 µg DNA
2 µl SuRE/Cut A reaction buffer (10x)
0,5 µl BamHI (10 U/µl)
nuclease-free H_2O up to 20 µl
→1h, 37°C

3.2.1.5 Dephosphorylation of DNA

After the restriction digest, 5´-ends of the vectors were dephosphorylated using shrimp alkaline phosphatase (SAP) to prevent the self-ligation of linearized vectors. Dephosphorylation was done after the inactivation of the restriction enzyme (20 min at 65°C) by adding the 10x SAP buffer and 1 µl SAP (1 U/µl) directly to the restriction reaction. The reaction was incubated for 60 min at 37°C, followed by inactivation of

SAP for 15 min at 65°C. The reaction mix was then separated by agarose gel electrophoresis and the linearized, dephosphorylated vector DNA was extracted from the agarose gel.

3.2.1.6 Agarose gel electrophoresis

Agarose gel electrophoresis was performed for analyses and purification of PCR products and DNA fragments after restriction digest. To prepare the agarose gels, depending on the size of the DNA fragment, appropriate amount of agarose (0.8-2% (w/v)) was dissolved in 1x TAE buffer by heating in the microwave. After cooling down to 60-70°C, 2 µl of RedSafe™ nucleic acid staining solution were added per 50 ml agarose solution, the solution was poured into the gel chamber and left to polymerize. DNA samples were mixed with the 6x DNA loading buffer and loaded into the gel slots. Electrophoresis was run in 1x TAE buffer at 80-100 V. After electrophoresis, DNA in the gel was visualized using Bioview blue light transilluminator or under UV light in a G:BOX gel documentation system. GeneRuler 1 kb or GeneRuler 100 bp were used as reference size markers.

1x TAE buffer
40 mM Tris/HCl, pH 8.5
50 mM acetic acid
1 mM EDTA

6x DNA loading buffer
0.25% (w/v) Xylenecyanol
0.25% (w/v) Bromphenolblue
30% (v/v) glycerol
1 mM EDTA

3.2.1.7 Extraction of DNA from agarose gels

After electrophoretic separation of DNA, desired bands were visualized under blue light transilluminator and cut out from the agarose gels with a scalpel. DNA was extracted from the gel using the Zymoclean™ Gel DNA Recovery kit according to manufacturer´s instructions.

3.2.1.8 Ligation

For the ligation of DNA fragments and linearized vectors, Quick Ligation™ kit was used.

Ligation reaction:

About 3:1 ratio of DNA fragment and linearized dephosphorylated vector
5 µl Quick ligase buffer (2x)
1 µl Quick T4 DNA-ligase
nuclease-free H_2O up to 10 µl

The ligation reaction was performed for 5 min at 25°C and subsequently transformed into *E.coli* XL1-Blue. For transformation, 10 µl of the ligation reaction was mixed with 150 µl of competent *E.coli* XL1-Blue cells and transformation was performed as described. Hundred µl of transformed bacterial suspension was plated on LB-agar plates with antibiotics and incubated over night at 37°C. Single colonies were picked and grown in LB medium with selection antibiotics over night. DNA was isolated and correct clones were identified by restriction digest or by PCR.

3.2.1.9 RNA isolation

Total RNA from eukaryotic cells and tissues was isolated using NucleoSpin® RNA II isolation kit (Macherey-Nagel) following the manufacturer´s recommendations. RNA was eluted with nuclease-free H_2O and quantification and purity determination were done spectrophotometrically on the NanoDrop. RNA was stored for short time periods at -20°C and for long-term at -80°C.

3.2.1.10 cDNA synthesis

RNA was reverse-transcribed using random hexamers and oligo-$(dT)_{18}$ using the High-Capacity cDNA reverse transcription kit.
Typical reverse transcription reaction:

2 µg RNA
4 µl RT buffer (10x)
4 µl RT Random Primers (10x)
2 µl oligo-$(dT)_{18}$ (0.5 µg/µl)
1.6 µl dNTPs (25x)
1 µl MultiScribe™ Reverse Transcriptase (50 U/µL)
nuclease-free H_2O up to 40 µl

Program:

Temperature	Time
25°C	10 min
37°C	2 h
85°C	5 min
4°C	∞

3.2.1.11 Polymerase chain reaction (PCR)

PCR with *Taq* DNA-Polymerase

Standard PCR reactions using *Taq* DNA-polymerase were performed to amplify cDNAs from different cells and tissues, as well as for the analyses of clones generated after ligation.

Typical PCR reaction:

20-500 ng DNA
1 µl forward primer (10 µM)
1 µl reverse primer (10 µM)
0.4 µl dNTP mix (10 mM)
2 µl ThermoPol® Reaction Buffer (10x)
0.2 µl *Taq* DNA-Polymerase (5 U/µl)
nuclease-free H_2O up to 20 µl

PCR program used for amplification of KNSTRN cDNA in human cells and tissues:

Step	Temperature	Time	Cycles
Initial denaturation	95°C	30 sec	1 x
Denaturation	95°C	30 sec	40 x
Primer annealing	55°C	30 sec	
Elongation	68°C	1 min	
Final elongation	68°C	5 min	1 x
Cooling	4°C	∞	

PCR with proofreading DNA-polymerases

For high-fidelity amplification of DNA prior to cloning or sequencing, Pwo Master or Phusion® High-Fidelity DNA-Polymerase were used following the manufacturer´s instructions.

3.2.1.12 Quantitative real-time PCR (qPCR)

Relative differences in the SKAP mRNA expression between normal colon and colon cancer were determined by qPCR using GoTaq® qPCR Master Mix according to manufacturer´s instructions. Reactions were performed on approximately 100 ng cDNA in triplicates, using the ON1303 and ON1304 oligonucleotides (Tab. 5). For normalization, 18S rRNA amplification was performed.

3.2.1.13 Rapid amplification of cDNA ends (5´-RACE)

To identify 5´-ends of human KNSTRN cDNA in HEK-293 cells, 5´-RACE reactions were performed (Fig. 8). In this work, 5´-RACE reactions were done using the SMART™ RACE cDNA Amplification Kit.

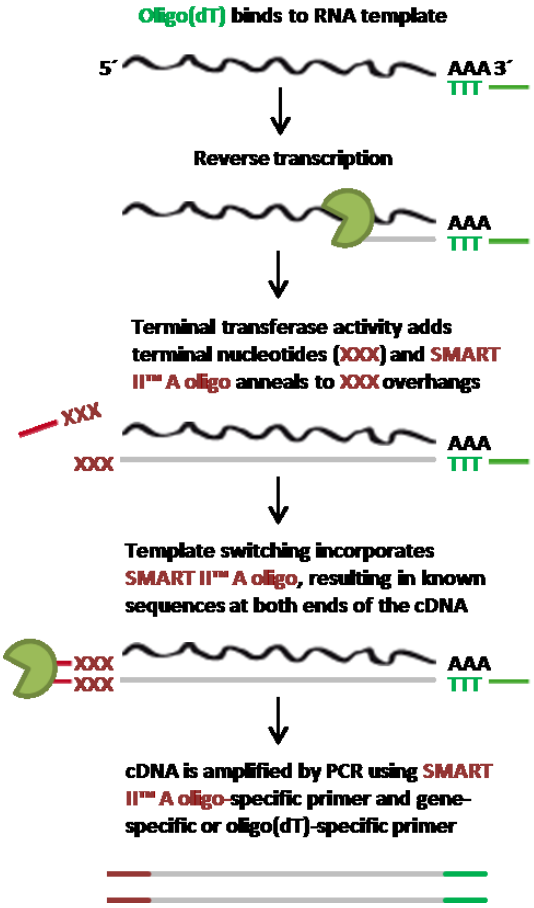

Figure 8. Schematic representation of a SMART™ 5´-RACE-PCR reaction.

cDNA was synthesized from HEK-293 RNA using the KNSTRN-specific anti-sense oligonucleotide (ON1142; Tab. 5) in the presence of an adapter SMART II™ A oligonucleotide.

5´-RACE-ready cDNA synthesis reaction:

1 µg HEK-293 RNA
1 µl ON1142 (10 µM)
1 µl SMART II™ A oligonucleotide
nuclease free H_2O up to 5 µl
→2 min, 70°C
→2 min, 4°C

Added: 2 µl First-strand buffer (5x)
1 µl DTT (20 mM)
1 µl dNTP Mix (10 mM)
1 µl SuperScript™ II RT (50 U/µl)
→90 min, 42°C
→added 100 µl Tricine-EDTA buffer
→7 min, 72°C

SMART II™ A-tailed cDNA (2.5 µl) was amplified with Taq DNA-polymerase by either touch-down or classical PCR program using an adapter-specific forward primer (Universal Primer Mix; UPM) in combination with a reverse gene-specific oligonucleotide (ON1142).

Touchdown PCR program:

	Temperature	Time	Cycles
Phase 1			
Step			
Denaturation	94°C	30 sec	5 x
Annealing/elongation	72°C	3 min	
Phase 2			
Step			
Denaturation	94°C	30 sec	5 x
Annealing	70°C	30 sec	
Elongation	72°C	3 min	
Phase 3			
Step			
Denaturation	94°C	30 sec	25 x
Annealing	68C	30 sec	
Elongation	72°C	3 min	
Cooling	4°C	∞	

Classical PCR program:

Step	Temperature	Time	Cycles
Initial denaturation	95°C	30 sec	1 x
Denaturation	95°C	15 sec	30 x
Primer annealing	50°C	15 sec	
Elongation	68°C	40 sec	
Final elongation	68°C	2 min	1 x
Cooling	4°C	∞	

The PCR products were used in a nested PCR reaction using the adapter-specific forward (Nested Universal Primer; NUP) and reverse oligonucleotide that anneals 3´ to ON1142 (ON1140; Tab. 5). PCR reaction was performed with classical PCR program.

3.2.1.14 Purification of PCR products

Before using the PCR products as a template in a nested PCR reaction, they were purified using DNA Clean and Concentrator™-5 kit, following the manufacturer´s instructions.

3.2.1.15 Cloning of PCR products into pCR™2.1 and pJET1.2/blunt vectors

Prior to sequencing, some PCR products were cloned into plasmid vectors and amplified in *E. coli*. PCR products amplified by *Taq* DNA-polymerase were cloned into pCR™2.1 vector using The Original TA Cloning® Kit. PCR products generated by a proofreading Phusion® High-Fidelity DNA-Polymerase, were cloned into pJET1.2/blunt using the CloneJET PCR Cloning Kit. For the ligation, 2 µl of pCR™2.1 (25 ng/µl) and 0.5 µl of pJET1.2/blunt (50 ng/µl) were used in combination with 3 µl of PCR product. Ligation was performed with Quick T4 DNA-Ligase.

3.2.1.16 Gateway® cloning

Gateway® cloning technology is based on the bacteriophage λ site-specific recombination system (Hartley et al. 2000). It allows rapid transfer of the desired DNA fragment between different cloning vectors while maintaining orientation and reading frame. In this work, Gateway® cloning was used to prepare expression clones used for FRET and FCCS experiments. The cloning procedure consists of several steps depicted in the Fig. 9.

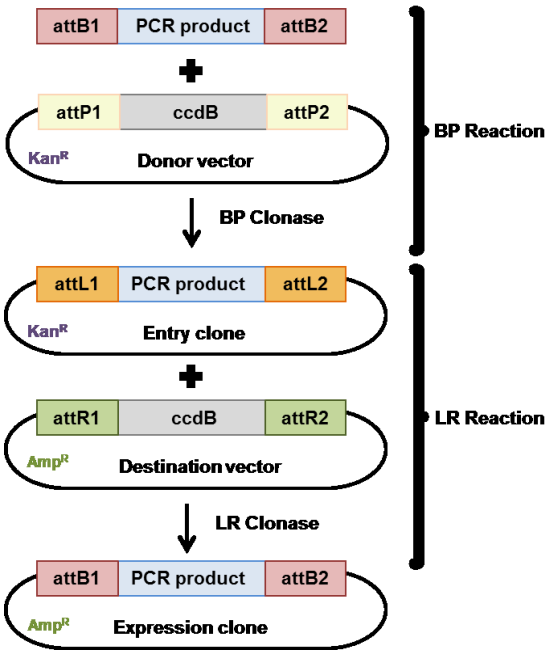

Figure 9. Gateway® cloning scheme. DNA sequence of interest is PCR amplified using a proofreading DNA-polymerase and primers with attB overhangs. PCR product is mixed with the donor vector in the presence of BP clonase mix which catalyzes the recombination reaction between target attB and vector attP sequences. Recombination generates the entry clone with attL sites flanking the cloning site. In a subsequent reaction, the entry clone is mixed with the destination vector in the presence of the LR clonase enzyme mix. LR clonase mix contains enzymes needed for recombination between attL and attR sites and allows recombination of the target sequence into a desired vector of choice, thereby generating an expression clone. ccdB gene located between the attP/R sites of the donor and destination vectors is lethal to most strains of *E. coli* and it helps the selection of the bacteria transformed with successfully recombined plasmids.

PCR

SKAP1 and SKAP16 cDNAs were PCR-amplified using primers with attB overhangs (Tab. 7) in a reaction using the Expand High Fidelity PCR System following the manufacturer´s recommendations.

Mix 1
110 ng pCS2+KNSTRN1
0.5 µl forward primer (100 µM)
0.5 µl reverse primer (100 µM)
nuclease-free H_2O up to 25 µl

Mix 2
10 µl buffer with $MgCl_2$ (5x)
1 µl dNTPs (10 mM)
0.3 µl $MgCl_2$ (25 mM)
1 µl Enzyme mix (5 U/µl)
nuclease-free H_2O up to 25 µl

Mix 1 and mix 2 were combined and the PCR reaction was performed using the program:

Step	Temperature	Time	Cycles
Initial denaturation	94,2°C	1 min 30 sec	1 x
Denaturation	94,2°C	25 sec	8 x
Primer annealing	62.5°C	30 sec	
Elongation	72°C	1 min 20 sec	
Denaturation	94.2°C	25 sec	23 x
Primer annealing	71°C	30 sec	
Elongation	72°C	1 min 30 sec	
Final elongation	72°C	10 min	1 x
Storage	4°C	∞	

BP reaction

PCR products were separated in agarose gel electrophoresis, purified from the gel and cloned into donor vector pDONR221 in a reaction mix:

100 ng PCR product
100 ng pDONR221
1 µl BP Clonase™ II enzyme mix
0.1x TE buffer up to 6 µl

After over night incubation at 25°C, 1 µl Proteinase K was added to the mix and the reaction was further incubated 30 min at 37°C. Subsequently, the reaction was transformed into DH5α competent *E.coli* cells. DNA was isolated from 8 clones and analyzed by restriction digest using BsrGI restriction enzyme. Appropriate entry clones were then analyzed by sequencing and used for the LR reactions.

LR reaction

To subclone SKAP1 and SKAP16 cDNAs from the entry clones into the destination vectors, corresponding entry clones were mixed with the appropriate destination vectors in a reaction:

150 ng entry clone
150 ng destination vector
1 µl LR Clonase™ II enzyme mix
0.1x TE buffer up to 6 µl

Reaction was incubated over night at 25°C. Next day, 1 µl Proteinase K was added to the mix and the reaction was further incubated 30 min at 37°C. Subsequently, the reaction was transformed into DH5α competent *E.coli,* DNA was isolated from 8 clones and analyzed by restriction digest using BsrGI. Generated expression clones were used in FRET and FCCS experiments.

3.2.1.17 Site-directed mutagenesis

Site-directed mutagenesis PCR was performed to generate SKAP1 mutants. Prior to PCR, mutation-carrying primers were phosphorylated in the following reaction:

1 µl mutagenesis primer (100 µM)
2 µl ATP (10 mM)
0.4 µl Mg_2SO_4 (25 mM)
1 µl PNK buffer (10 x)
0.25 µl PNK (1U/µl)
nuclease-free H_2O up to 10 µl
→ 30 min 37°C
→ 15 min 60°C

Phosphorylated primers were used together with pCS2+KNSTRN1-myc_6 (template) in PCR reactions using Pwo Master mix. Oligonucleotides used for amplification of KNSTRN1-S24F were ON1470 and ON1472, and for KNSTRN1-A40E, ON1471 and ON1472 (Tab. 5). Generated pCS2+KNSTRN1-S24F-myc_6 and pCS2+KNSTRN1-A40E-myc_6 were sequenced for verification.

Mutagenesis PCR reaction setup:

10 ng template
1 µl forward primer (10 µM)
1 µl reverse primer (10 µM)
10 µl Pwo Master
nuclease-free H_2O up to 20 µl

Mutagenesis PCR program:

Step	Temperature	Time	Cycles
Initial denaturation	95°C	2 min	1 x
Denaturation	95°C	30 sec	30 x
Primer annealing	60°C	30 sec	
Elongation	68°C	15 min	
Final elongation	68°C	15 min	1 x
Cooling	4°C	∞	

3.2.1.18 DNA sequencing

To control the nucleotide sequence of DNA, all cloned expression constructs and some PCR products in this work were sequenced by companies GATC Biotech (Konstanz, Germany), Macrogen (Amsterdam, Netherlands) or Eurofins Genomics (Ebersberg, Germany). Analyses of the DNA nucleotide sequences were performed with the ApE software.

3.2.2 Cell biological methods

3.2.2.1 Eukaryotic cell culture

All used cell lines were cultured in a 5% CO_2 incubator at 37°C under sterile conditions.

Adherent human and murine cell lines were cultured in eukaryotic cells culture medium in 10 cm culture dishes. Depending on the cell type and density, cells were passaged every 3-4 days. First, the medium was aspirated, cells were washed with 10 ml PBS and detached from the dish bottom with 2 ml Trypsin-EDTA at 37°C for 3-10 min, depending on the cell type. Trypsin reaction was stopped by addition of fresh medium and the detached cells were pelleted by centrifugation at 200 g for 5 min. After centrifugation, cells were resuspended in fresh medium and seeded out in a new culture dish, in a ratio 1:5 to 1:15.

Hybridoma cells were grown as suspension culture in IgG-depleted medium in 75 cm² and 175 cm² cell culture flasks. They were passaged every 4-5 days by diluting a part of cell suspension with fresh medium. Supernatants for purification of antibodies were collected from hybridoma cells that were grown until they died off.

For cryopreservation of cells, trypsinized cells or suspension cells were centrifuged for 5 min at 200 g, medium was removed and cells were resuspended in corresponding freezing medium. Cell suspension was transferred into cryopreservation tubes in 1 ml fractions and left in the NICOOL mini freezer for gradual freezing. After 30 min, tubes were moved to -196°C for long term storage. To take the cryopreserved cells back in culture, cells were thawed at 37°C, immediately resuspended in 20 ml of corresponding medium and centrifuged for 5 min at 200 g. After centrifugation, cells were resuspended in fresh medium and seeded into culture plates or flasks.

Before seeding out for experiments, cells were counted using Casy® cell counter following the manufacturer´s instructions.

3.2.2.2 Transient transfection of eukaryotic cells

Chemical-based transfection (PEI, TurboFect, FuGENE® HD)

Transfection of the cells was performed 24 h after seeding using PEI (1 mg/ml), TurboFect or FuGENE® HD transfection reagents. Transfection reagent was added to serum-free DMEM pre-mixed with the appropriate amount of DNA and the mixture was incubated at room temperature. Amounts of components and incubation times used for transfection with different transfection reagents are shown in the Tab. 10. After incubation, the transfection mix was added dropwise to the cells and cells were further grown for 48 h before analyses.

Table 10. Components and incubation times used for transfection with different transfection reagents. Amounts of DMEM, DNA and transfection reagent are given for a typical transfection of cells in 1 well of a 6-well culture plate.

	DMEM (µl)	DNA (µg)	Transfection reagent (µl)	Incubation time (min)
PEI	200	2	8	30
TurboFect	200	2	4	15
FuGENE®HD	100	2	4.5	20

Electroporation

Prior to FCCS experiments, HEp-2 cells were transfected using Amaxa Nucleofector®II electroporation system. Confluent cells were washed twice with PBS and trypsinized. Approximately 1/12 of the cells was resuspended in 100 µl Ingenio® electroporation solution (pre-mixed with 2 µg DNA) and transferred to the electroporation cuvettes. The cuvettes were transferred to the Amaxa apparatus and cells were transfected using program 0-017. Transfected cells were resuspended in fresh medium, placed into wells of a 6-well plate and grown for 48 h before analyses.

3.2.2.3 RNA interference

To reduce SKAP protein levels, HEK-293 cells were seeded in 6-well plates in a density of $5x10^5$ cells per well. Twenty-four hours after seeding, cells were transiently transfected either with KNSTRN-specific shRNA constructs alone (Tab. 4) or in combination with pCS2+KNSTRN1 using TurboFect. A scrambled shRNA cassette served as a negative control. SKAP protein levels were analyzed by SDS-PAGE and Western blot 5 days after transfection.

3.2.2.4 Preparation of cell lysates

Total cell lysates for SDS-PAGE and Western blot were prepared by incubating the cells in RIPA buffer supplemented with Complete™ protease inhibitor mix for 10 min on ice. After sonication and centrifugation (20.800 g for 10 min at 4°C), supernatants were diluted 1:2 with 2x SDS-loading buffer. Proteins were separated by SDS-PAGE and Western blotting was performed.

RIPA buffer 150 mM NaCl
2 mM EDTA
10% (v/v) glycerol
1% (v/v) Triton-X-100
0.5% (w/v) Na-deoxycholate
0.2% (v/v) SDS

3.2.3 Biochemical methods

3.2.3.1 SDS-polyacrylamide gel electrophoresis (SDS-PAGE)

Proteins were separated in a reducing SDS-PAGE using the Mini-PROTEAN® vertical electrophoresis system. Depending on the expected molecular weight of the proteins, separating gels were prepared with different concentrations of acrylamide. Composition of a 10% polyacrylamide gel is shown in Tab. 11.

Table 11. Composition of polyacrylamide gels.

Component	Separating gel (10%)	Stacking gel (5%)
30% (w/v) acrylamide/0,8% (w/v) bisacrylamide	1.67 ml	0.26 ml
1.5 M Tris/HCl, pH 8.8	1.25 ml	-
0.5 M Tris/HCl, pH 6.8	-	0.41 ml
10% (v/v) SDS	50 µl	16.65 µl
ddH_2O	1.98 ml	0.78 ml
10% (w/v) APS	50 µl	16.65 µl
TEMED	6.7 µl	3.35 µl
Total volume:	5 ml	1.5 ml

For SDS-PAGE, samples were diluted in a 1:1 ratio with 2x SDS-sample buffer, boiled for 5 min at 95°C and loaded into the gel slots. Electrophoresis was performed with 80 V until the proteins concentrated in the separating gel and afterwards at 120-150 V. PageRuler™ prestained or unstained protein ladders were used as reference molecular-weight markers. After electrophoresis, the gels were used for Western blot or for direct staining of the proteins in the gels.

2x SDS-sample buffer
65 mM Tris/HCl, pH 6.8
3% (w/v) SDS
30% (v/v) glycerol
716 mM β-mercaptoethanol
0.01% (w/v) Bromphenolblue
0.01% (w/v) Pyronine G

SDS-PAGE running buffer
25 mM Tris
192 mM glycine
0.1% (w/v) SDS

3.2.3.2 Western blot and immunodetection

Semi-dry or tank-blot were performed to transfer the proteins to PVDF-membranes after SDS-PAGE. PVDF-membranes were shortly activated in methanol and equilibrated in the transfer buffer. Semi-dry transfer was performed in a Trans-Blot® SD Semi-dry electrophoretic transfer cell at 20 V for 30 min to 1 h, depending on the molecular weight of the proteins. Tank-blot transfer was done using Mini-PROTEAN® electrophoretic chamber at 100 V for 1 h.

Semy-dry blotting buffer
25 mM Tris
192 mM Glycine
20% (v/v) Ethanol

Tank-blot buffer
25 mM Tris
192 mM Glycine
10% (v/v) Ethanol

For immunodetection of the proteins after Western blotting, PVDF-membranes were first incubated in TBS-T buffer for 1 h at room temperature to prevent unspecific binding of the antibodies. Subsequently, membranes were left over night at 4°C with the primary antibodies diluted in TBS-T. After three washes with TBS-T buffer, 5 min each, membranes were incubated for 1 h with peroxidase-conjugated secondary antibodies diluted in TBS-T. After three washing steps with TBS-T buffer, chemiluminescence detection was performed using self-made ECL-solution on a G:BOX gel documentation system.

TBS-T
10 mM Tris/HCl, pH 7.5
150 mM NaCl
0.1% (v/v) Tween 20

ECL-solution
0.022% (w/v) luminol
100 mM Tris/HCl, pH 8.8
0.04 mM IPBA

3.2.3.3 Coomassie Blue staining of proteins in SDS-polyacrylamide gels

Coomassie Brilliant Blue R-250, a dye that unspecifically binds to proteins, was used for visualization of the proteins in the polyacrylamide gels after SDS-PAGE. After electrophoresis, gels were incubated in the Coomassie solution for approximately 30 min and then destained by changing the destaining solution until only proteins were visible and there was no background staining of the gel matrix. Afterwards the gels were washed in dH_2O and dried for storage.

Coomassie solution 0.1% (w/v) Coomassie Brilliant Blue R-250
30% (v/v) methanol
10% (v/v) ethanol

Destaining solution 10% (v/v) acetic acid
40% (v/v) ethanol

3.2.3.4 Expression and purification of recombinant proteins

For the expression of GST- and MBP-tagged proteins, 100 ml bacterial pre-culture (LB-ampicillin medium) was inoculated from a single colony and grown over night at 37°C in a shaking incubator. Thirty ml of the pre-culture were added to 400 ml LB-ampicillin medium with 1% (w/v) glucose and grown at 30°C in a shaking incubator. At the OD_{578} 0.5-0.6, protein synthesis was induced with 1 mM IPTG and the bacteria were incubated at 30°C for 1 h. Bacterial cells were then harvested by centrifugation 6.000 g, 4°C for 15 min. Pelleted cells were washed with 20 ml corresponding lysis buffer and centrifuged again at 6.000 g, 4°C for 15 min. Subsequently, bacteria were resuspended in 5 ml lysis buffer supplemented with Complete™ protease inhibitor mix and sonicated four times with 30 pulses (intensity 80%, cycle 0.5). Bacterial cell debris was removed by centrifugation at 20.800 g for 45 min at 4°C. Cleared lysates were subjected to affinity chromatography. GST-tagged proteins were purified on GSH-agarose beads and MBP-fusion proteins were purified using amylose beads. Columns for purification were prepared using Poly-Prep® chromatography columns with 1 ml of corresponding beads. Bacterial lysates were added to the beads equilibrated in lysis buffer. After loading of the lysates, columns were washed twice with 10 ml of washing buffer and the fusion proteins were eluted in 0.5 ml fractions using the corresponding elution buffers. To control the protein expression, eluted proteins were separated by SDS-PAGE and stained using Coomassie Blue.

	GST-fusion proteins	MBP-fusion proteins
Lysis/washing buffer	PBS	100 mM NaCl 40 mM Tris/HCl pH 8.0
Elution buffer	100 mM NaCl 40 mM Tris/HCl, pH 8.0 20 mM Glutathione	100 mM NaCl 40 mM Tris/HCl, pH 8.0 20 mM Maltose

3.2.3.5 Dialysis of GST-fusion proteins

After affinity purification, eluted protein-containing fractions were dialysed using dialysis tubing with 14 kDa exclusion limit. Dialysis was performed over night in 2 l of the dialysis buffer at 4°C.

Dialysis buffer 20 mM Tris/HCl, pH 8.0
50 mM NaCl

3.2.3.6 Pull-down

For *in vitro* protein interaction assays, GST or GST-fusion proteins were incubated with MBP-fusion proteins in pull-down buffer for 1 h at 4°C. After incubation, samples were centrifuged (10 min, 20.800 g at 4°C), 30 µl of GSH-beads were added to the supernatants and incubated for 30 min at 4°C under agitation. GSH-beads were pelleted (2 min, 2.700 g at 4°C) and washed three times with 350 µl pull-down buffer. After the last washing step, the beads were resuspended in 30 µl 2xSDS-sample buffer and protein complexes were analyzed by SDS-PAGE and Western blotting.

Pull-down buffer 50 mM Tris/HCl, pH 8.0
150 mM NaCl
2 mM $MgCl_2$
0.1% (v/v) Triton X-100

3.2.3.7 Immunoprecipitation

For immunoprecipitation of endogenous or overexpressed SKAP proteins, HEK-293 cells were seeded in a density of $4x10^6$ cells per 10 cm culture dish. After 24 h, cells were either non-transfected or transiently transfected with pCS2+KNSTRN1. Forty-eight hours after transfection, cells were lysed in lysis buffer A supplemented with Complete™ protease inhibitor mix for 10 min on ice. After lysis, cells were scraped off the plates and centrifuged 20.800 g for 10 min at 4°C. Protein complexes were isolated from 100 µl of each supernatant with 1 µg of the corresponding anti-SKAP

antibody (or anti-GFP antibody as a control) pre-bound to Dynabeads® Protein A under agitation for 1 h at 4°C. After three washing steps with lysis buffer A, precipitated proteins were resuspended in 2x SDS-loading buffer and analyzed by Western blotting with polyclonal anti-SKAP antibody.

For co-immunoprecipitation analyses, HEK-293 cells were seeded in a density of $8x10^5$ cells/well of a 6-well plate and transfected with appropriate plasmid constructs 24 h after seeding. The cells were lysed 48 h after transfection with 400 µl lysis buffer A/well and immunoprecipitation was done with 2 µg respective antibody using Protein A Sepharose™ CL-4B and following the same procedure as described for immunoprecipitation of endogenous proteins.

Lysis buffer A
10 mM imidazole, pH 6.8
100 mM KCl
2 mM $MgCl_2$
300 mM sucrose
10 mM EGTA
0.2% (v/v) Triton-X-100
1 mM NaF
1 mM Na_2MoO_4
1 mM Na_3VO_4,
0.3% (v/v) H_2O_2

3.2.3.8 Immunofluorescence staining and microscopy

To study SKAP localization using immunofluorescence microscopy, HEK-293 cells were seeded on coverslips in a density of $6x10^5$ cells per well in a 6-well plate. Twenty-four hours after seeding, cells were either non-transfected or transiently transfected with pCS2+KNSTRN1 or pCS2+KNSTRN16. After 48 h, cells were washed with PBS and fixed for 15 min in cold 3% (w/v) paraformaldehyde. Next, cells were washed in PBS, incubated for 15 min in 125 mM glycine in PBS and permeabilized in 0.5% (v/v) Triton-X-100 for 8 min. After 30 min blocking with 1% (v/v) goat serum in PBS, cells were incubated with anti-SKAP antibodies for 1 h at room temperature. After three washing steps, incubation with secondary antibodies and DAPI was done for 30 min at room temperature. After incubation, coverslips were washed and mounted with Mowiol supplemented with DABCO. Negative controls were incubated without the primary antibodies.

For immunofluorescence staining of human sperm cells, the cells were washed with PBS three times by centrifugation 5 min at 300 g, resuspended in PBS and attached

to poly-L-lysine coated coverslips. On the coverslips, cells were fixed for 10 min with either 3% (w/v) paraformaldehyde or cold methanol. After three washing steps with 0.2% (v/v) Triton-X-100 in PBS, cells were blocked with 5% (v/v) goat serum for 1 h at room temperature. After incubation with primary antibodies over night at 4°C, the cells were washed and incubated with secondary antibodies and DAPI for 1 h at room temperature. Negative controls were incubated without the primary antibodies. Images were taken on an inverse fluorescence microscope Axio Observer.Z1 ApoTome using 1.3 NA oil-immersion objective with 100x magnification. Figures were prepared using FigureJ.

3.2.3.9 Acceptor-bleaching FRET (Förster resonance energy transfer)

FRET experiments were performed in collaboration with Dr. Christian Hoischen (Fritz Lipmann Institute on Aging, Jena) mainly as described previously (Orthaus et al. 2008, Orthaus et al. 2009, Hellwig et al. 2011, Dornblut et al. 2014, Diekmann and Hoischen 2014). HeLa cells were double transfected with vectors for the simultaneous expression of Clover- and mRuby2-fusion proteins and analyzed in interphase and mitosis. Forty-eight hours after transfection, the cells were washed three times with PBS, fixed with 4% paraformaldehyde for 10 min and embedded using ProLong® Gold Antifade Mountant with DAPI. FRET measurements were performed on an LSM 710 Confocor3 microscope using 1.4 NA 63x oil immersion objective. FRET was measured using the acceptor photobleaching method (Bastiaens et al. 1996) (Fig. 10).

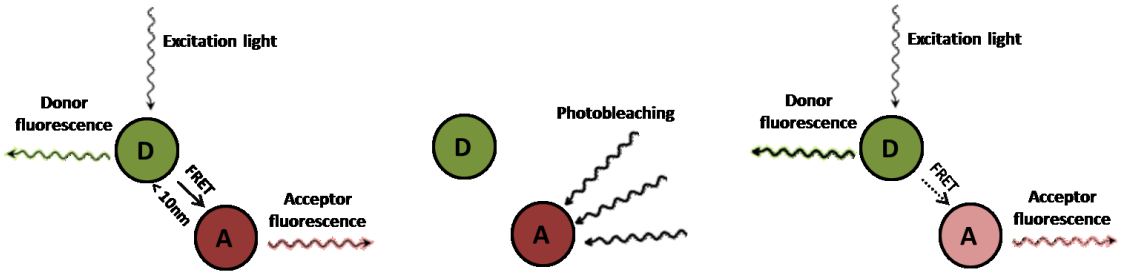

Figure 10. Acceptor photobleaching FRET scheme (modified from (Grzanka et al. 2014)). When two fluorophores are brought into close proximity to each other, the fluorescence of the donor (D) is quenched by the presence of the acceptor (A); the energy that would be released as a photon after donor excitation is passed to the acceptor molecule in a non-radiative transfer. In the acceptor photobleaching technique, the acceptor fluorophore is bleached, thereby reducing its ability to receive energy from the donor, which leads to an increase in fluorescence of the donor molecule. The pre- and post-bleach difference in donor fluorescence is used to estimate the level of FRET.

According to this procedure, if FRET is occurring, the donor fluorescence will be quenched. Consistently, photobleaching of the acceptor (mRuby2) should result in an increase in fluorescence of the donor (Clover). In our experiments, after 4 scans in the red and the green channel (pixel dwell 1.58 µsec), cells were bleached by scanning in a 2-5 µm region of interest (ROI) using the DPSS 561-10-laser line at 100% intensity with 25 iterations. After the bleach, 3 further images were collected to assess changes in donor fluorescence. Images were collected using the 488 nm laser line of a 25 mW Argon/2-laser at 0.5% of the laser intensity.

To calculate the FRET efficiency (E_{FRET}) as a percentage, following formula was used:

$$FRET\ efficiency\ (EFRET) = \frac{(Dpost - Dpre) \times 100}{Dpost}$$

where *Dpre* and *Dpost* are the donor fluorescence intensities analyzed using ZEN software before and after photobleaching the acceptor, respectively. Additionally, Clover fluorescence in an unbleached area of the same size as the bleached area was analyzed resulting in control FRET efficiency (E_{VAR}). The determined E_{FRET} and E_{VAR} values were classified into 4% deviating categories and the number of counts for each category is shown in a bar diagram. Both input groups (E_{FRET} and E_{VAR} values) were statistically evaluated using paired t-test in SigmaPlot software.

3.2.4 Fluorescence cross-correlation spectroscopy (FCCS)

FCCS is a variation of FCS (fluorescence correlation spectroscopy). It is a method which allows monitoring molecular interactions, enzymatic reactions, as well as dynamic co-localization in living cells (Bacia et al. 2006, Bacia and Schwille 2007) (Fig. 11).

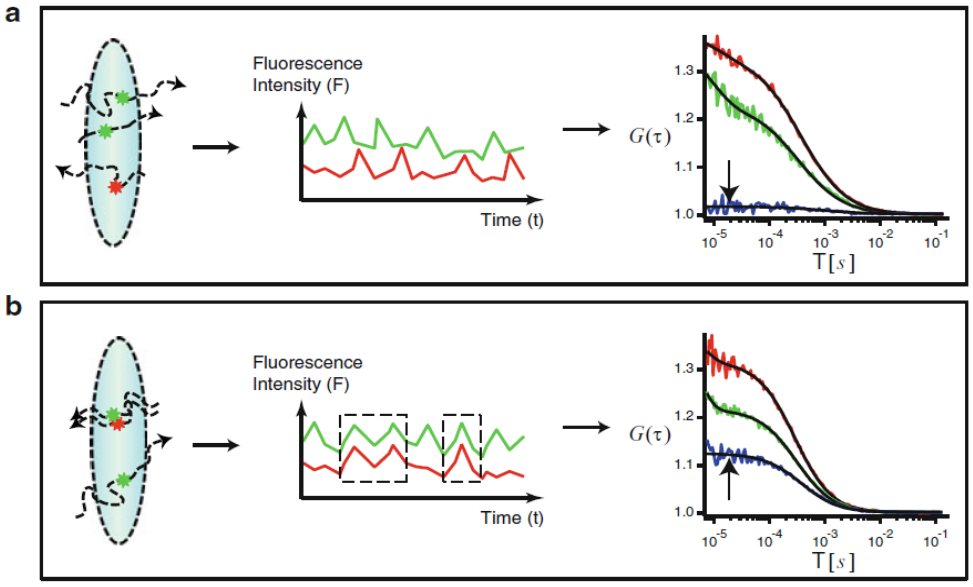

Figure 11. Principle of dual-color FCCS: (a) Differently tagged particles move independently through the observation volume. Therefore, the signals are not correlated and their CCF (cross correlation function) is flat (blue curve). (b) If particles form complexes and move together through the observation volume, the signals of the differently tagged particles will correlate resulting in an elevated CCF with respect to the green and red ACF (auto correlation function) (from (Foo 2011).

In this work, dual-color FCCS analyses were performed in collaboration with Dr. Christian Hoischen. Experiments were done at 37°C on an LSM 710 Confocor3 microscope using a C-Apochromat infinity-corrected 1.2 NA 40x water objective. HEp-2 cells were double-transfected with vectors for the simultaneous expression of EGFP- and mCherry-fusion proteins and analyzed in mitosis. On cells expressing both fusion proteins at relatively low and comparable levels, spots were selected for the FCCS measurements in areas of the nucleoplasm which were free of kinetochores. For illumination of the EGFP-fusion proteins, the 488 nm laser line of a 25 mW Argon/2-laser (ZEISS) was used. For simultaneous illumination of the mCherry-fusion proteins a DPSS 561-10-laser (ZEISS) was used. Both lasers were used at moderate intensities between 0.2 and 0.5%. The detection pinhole was set to a relatively small diameter of 40 µm. After passing a dichroic beam splitter for APDs (avalanche photodiode detector; NTF 565), the emission of mCherry was recorded in channel 1 through a BP-IR 615-680 nm bandpath filter by an APD (ZEISS), whereas the emission of EGFP was simultaneously recorded in channel 2 through a BP-IR 505-540 nm bandpath filter by a second APD. Before each measurement, possible crosstalk between the channels was analyzed and only cells without or with very little crosstalk were used. For the measurements, 10 x 10 time series of 10 sec each were

simultaneously recorded for mCherry and for EGFP. After averaging, the data were superimposed for fitting with the Fit-3Dfree-1C-1Tnw model of the ZEN-software, a diffusion model in three dimensions with triplet function. Applying this procedure, auto-correlations of channels 1 and 2 as well as the cross-correlation of channels 1 versus channel 2 were obtained. Before starting a set of experiments, the pinhole was adjusted.

3.2.5 Production and purification of monoclonal antibodies

Monoclonal anti-SKAP antibodies were generated in collaboration with the group of Prof. Dr. Karlheinz Friedrich (Institute of Biochemistry II, University Hospital Jena) by protein-based immunization of C57BL/6 mice. The mice were injected with 50 µg recombinant MBP-SKAP1 fusion protein four times in 12 weeks with a final boost three days before the spleenectomy. Spleen cells were fused with X63AG8.653 myeloma cells using ClonaCell™-HY PEG (STEMCELL™ Technologies). After fusion, hybridoma cells were selected in HAT (hypoxanthine–aminopterin–thymidine) medium for 1 week. Afterwards, hybridomas were subcloned three times to generate monoclonal clones. Supernatants of individual clones were screened for antibodies recognizing exclusively recombinant SKAP1 using ELISA (performed in the group of Prof. Friedrich) and Western blot. MBP controls were performed to distinguish SKAP-specific antibodies from anti-MBP-antibodies. For purification of monoclonal antibodies, hybridomas were cultivated in IgG-depleted medium and antibodies were purified from the supernatants by affinity chromatography using 1 ml HiTrap Protein G matrix on ÄKTA purifier™ FPLC system. Hybridoma supernatants were dialysed in dialysis buffer over night at 4°C and subsequently loaded on the Protein G matrix equilibrated in binding buffer. Column was washed with binding buffer and antibodies were eluted with elution buffer and immediately neutralized with neutralization buffer. Afterwards, purified antibodies were dialyzed against PBS, stabilized and preserved with 3% (v/v) sucrose/PEG 8000 and 0.01% (v/v) sodium azide. Antibodies were tested again for binding to SKAP on Western blot. The purity of antibodies was determined by SDS-PAGE and silver staining.

Dialysis/binding buffer	20 mM sodium phosphate, pH 7.0
Elution buffer	0.1 M glycine, pH 2.7
Neutralization buffer	1 M Tris/HCl, pH 9.0

4 Results

4.1 Generation of monoclonal anti-SKAP antibodies

In order to study the expression of the different SKAP isoforms, new antibodies against SKAP had to be produced. Therefore, monoclonal anti-SKAP antibodies were generated (in collaboration with the group of Prof. Dr. Karlheinz Friedrich) by protein-based immunization of C57BL/6 mice. The mice were injected with recombinant MBP-SKAP1 fusion protein and monoclonal antibodies were generated according to standard procedures. Using ELISA and Western blot, supernatants of individual clones were screened for antibodies exclusively recognizing recombinant SKAP1.

To define the epitopes recognized by the different SKAP-specific clones, full-length SKAP1 and its truncated constructs were expressed in bacteria as MBP- or GST-fusion proteins, purified and used in Western blotting for epitope mapping (Fig.12). Mapping experiments showed that the identified hybridoma produced antibodies that interact with different epitopes in SKAP. Anti-SKAP (A12-11) antibody binds to an epitope within the N-terminal region of SKAP1 (amino acids 1-78). Therefore, anti-SKAP (A12-11) antibody is able to distinguish between isoforms that contain the 78 N-terminal amino acids (SKAP1, SKAP5 and SKAP3) and SKAP16, which lacks amino acids 1-78. Comparable to a commercially available polyclonal anti-SKAP antibody, anti-SKAP (C11-32) antibody recognizes an epitope in the middle part of the protein present in all SKAP isoforms. Anti-SKAP (F5-13) antibody binds to the amino acids within the second coiled-coil domain, meaning it does not recognize the SKAP3 isoform. Because of their ability to specifically recognize certain SKAP isoforms, these antibodies represent a valuable tool to analyze the SKAP expression pattern.

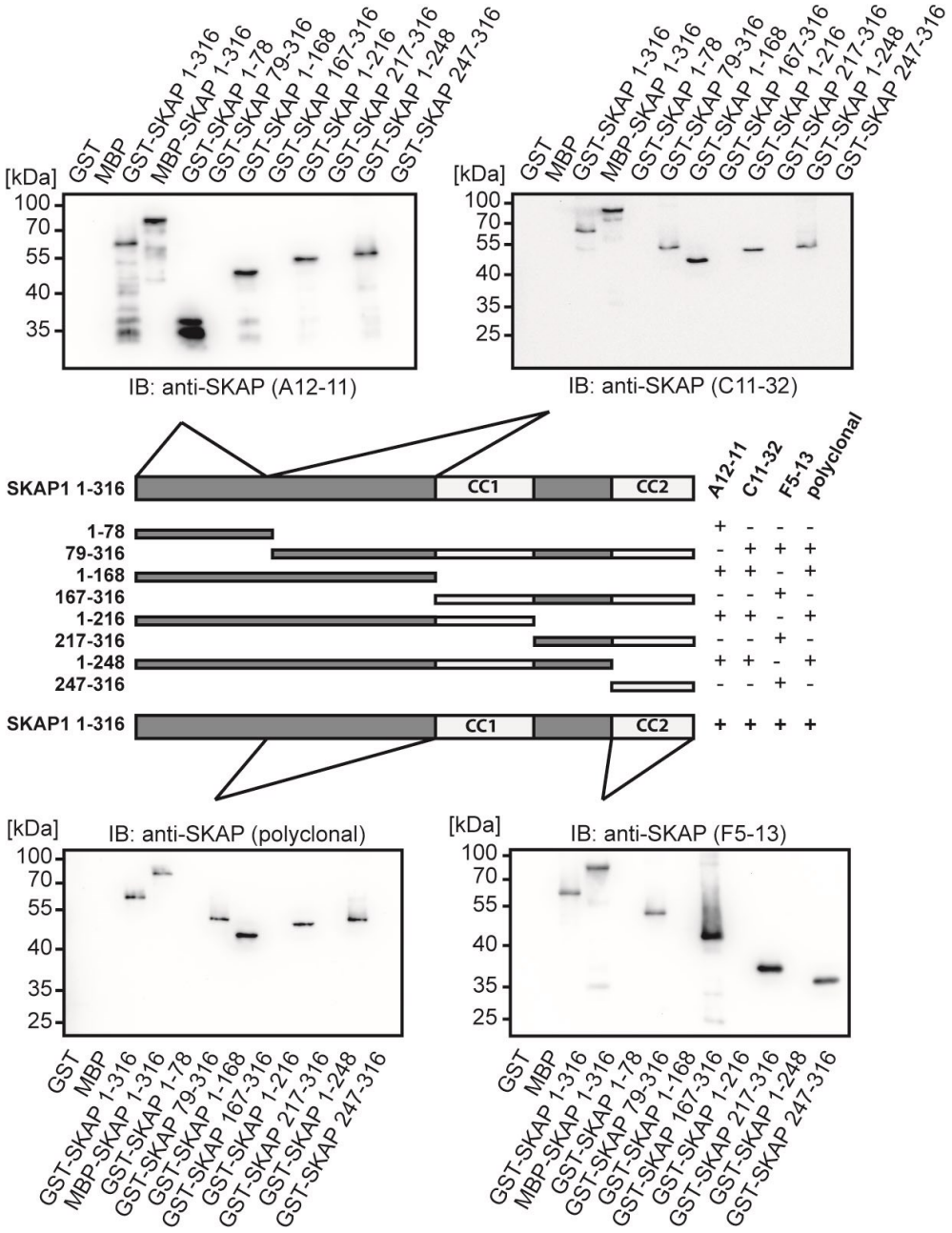

Figure 12. Mapping of epitopes recognized by anti-SKAP monoclonal antibodies. Recombinant full-length SKAP1 fusion proteins and its deletion constructs were analyzed by Western blotting. CC1 and CC2 represent two predicted coiled-coil domains. Representative blots of at least three independent experiments are shown (from (Cindric Vranesic et al. 2016)).

4.2 Expression profile of SKAP isoforms in human

4.2.1 SKAP 16 is the major SKAP isoform expressed in human cells

The potential differential expression pattern of the predicted protein-coding KNSTRN transcript variants was first investigated by RT-PCR using primer pairs designed to detect variants 1 and 16 (Fig. 13A). In human cell lines and primary cells of different origin KNSTRN16 was ubiquitously expressed. On the other hand, the KNSTRN1 transcript was not detectable in any of the cells analyzed. 5´-RACE-RT-PCR analyses of the HEK-293 RNA confirmed the presence of only one transcript whose sequence corresponded to KNSTRN16 (Fig. 13B).

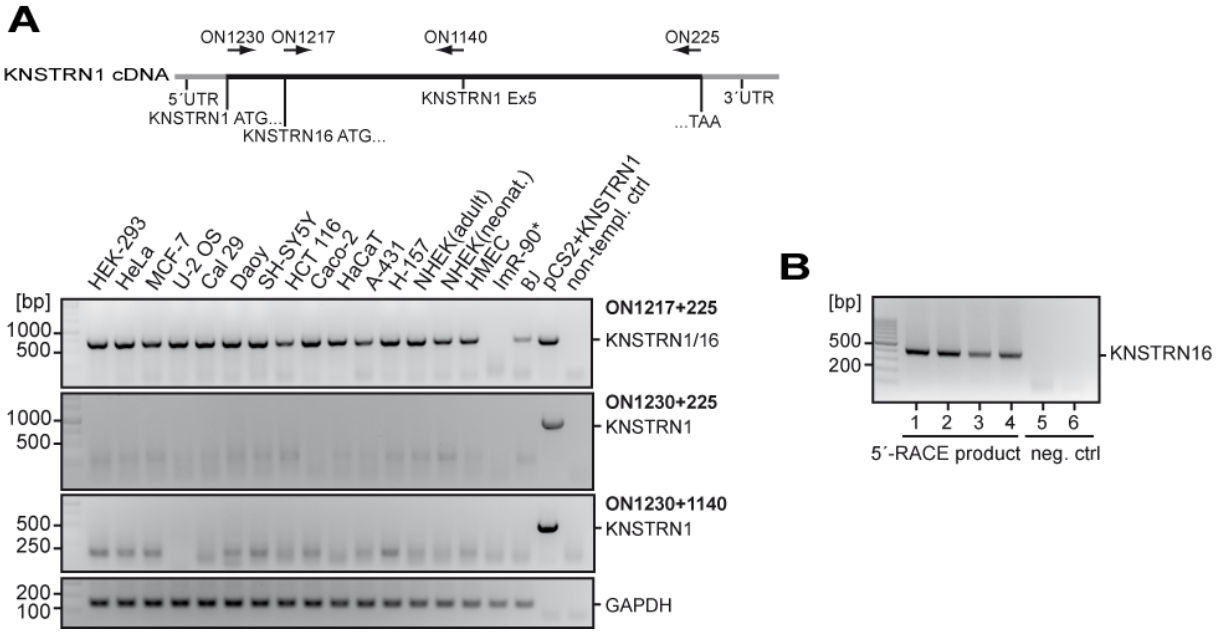

Figure 13. KNSTRN16 is the major KNSTRN transcript variant in human cells. (A) RT-PCR analysis of KNSTRN gene expression in human cells of different origin. The annealing sites of the used oligonucleotides are depicted in the upper part. pCS2+KNSTRN1 plasmid contains a full-length human KNSTRN1 cDNA and was used as a positive control. GAPDH was used as template control. *After higher number of PCR-cycles, low-abundant SKAP16 transcript is detectable also in ImR-90 cells. (B) 5´-RACE reactions with RNA isolated from HEK-293 cells showed the presence of only KNSTRN16 transcript as confirmed by sequencing. Lanes 1 to 4 represent products of nested PCR reactions using a touchdown PCR program (1 and 3) or classic PCR program (2 and 4) on unpurified (1 and 2) and purified (3 and 4) first PCR products; lanes 5 and 6 represent non-template controls for touch-down and classic PCR programs, respectively. Representatives of at least three experiments are shown (from (Cindric Vranesic et al. 2016)).

Next, the presence of SKAP isoforms was analyzed in cell lysates by Western blotting using different anti-SKAP antibodies (Fig. 14A). The SKAP1-specific (A12-11) antibody detected the overexpressed SKAP1 protein but it did not recognize any endogenous protein, proving the lack of SKAP1 expression. The rest of the anti-

SKAP antibodies detected one major band of molecular weight of around 32 kDa, which corresponds to SKAP16. Lysates of cells in which SKAP had been knocked down by shRNA were used to verify the specificity of anti-SKAP antibodies (Fig. 14B). Immunoprecipitation of endogenous SKAP protein from HEK-293 cells with different anti-SKAP antibodies confirmed that only the SKAP16 isoform is present in the cells (Fig. 14C).

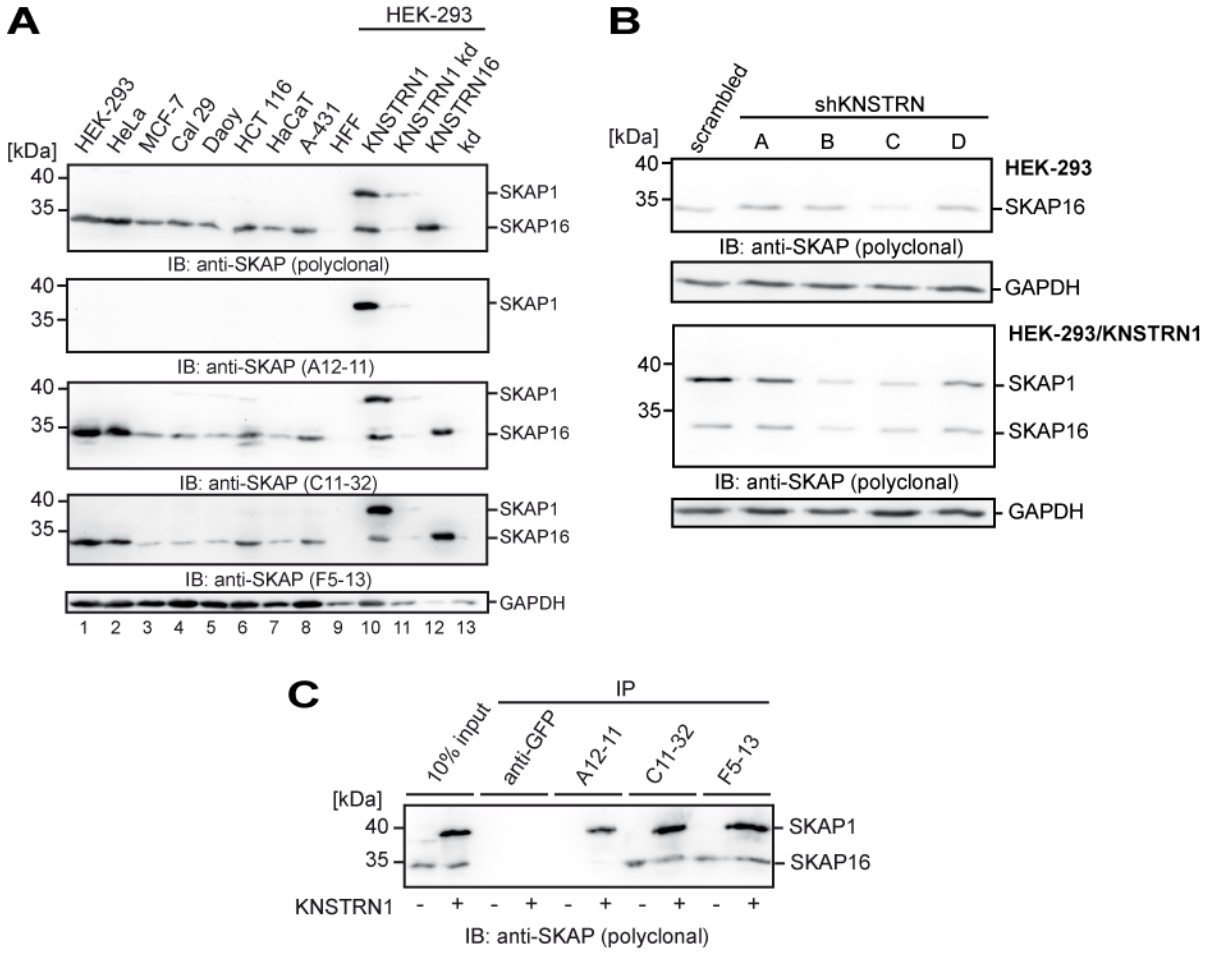

Figure 14. SKAP16 is the major SKAP isoform present in human cells. (A) Western blot analyses of total lysates of different cells using different anti-SKAP antibodies. Lysates of HEK-293 cells overexpressing SKAP1 and 16 (lanes 10 and 12) and extracts from HEK-293 cells treated with anti-SKAP shRNA (lanes 11 and 13) were used as controls to confirm the specificity of anti-SKAP antibodies. Anti-GAPDH antibody was used as a loading control. (B) SKAP knock-down in HEK-293 cells. HEK-293 cells were transfected with different shRNA constructs alone or in combination with pCS2+KNSTRN1. Five days after transfection, lysates of the cells were analyzed by Western blotting. shKNSTRN construct C resulted in the highest reduction in protein levels of both endogenous and SKAP1 protein and was used in further experiments as a control for anti-SKAP antibodies. (C) Immunoprecipitation of endogenous SKAP and overexpressed SKAP1 from extracts of HEK-293 cells using the different anti-SKAP antibodies. Precipitation with anti-GFP antibody was performed as a negative control. Representatives of at least three independent experiments are shown (from (Cindric Vranesic et al. 2016)).

In immunofluorescence stainings of endogenous SKAP protein in interphase HEK-293 cells, all anti-SKAP antibodies, except for anti-SKAP (A12-11), showed a mainly cytoplasmic staining and minor nuclear signals (Fig. 15A and 15C). In mitotic cells, spindle and kinetochore localized SKAP staining was observed (Fig. 15B), as reported previously (Fang et al. 2009, Dunsch et al. 2011, Schmidt et al. 2010, Wang et al. 2012). Anti-SKAP (A12-11) antibody readily detected overexpressed SKAP1, but no staining was observed in non-transfected cells or cells overexpressing SKAP16 (Fig. 15A). All the analyses of human cells lead to a conclusion that SKAP is expressed in human cells as the one major isoform, SKAP16, while the presence of endogenous SKAP1 or other isoforms predicted to include the N-terminal 78 amino acids could not be detected in any of the cells analyzed.

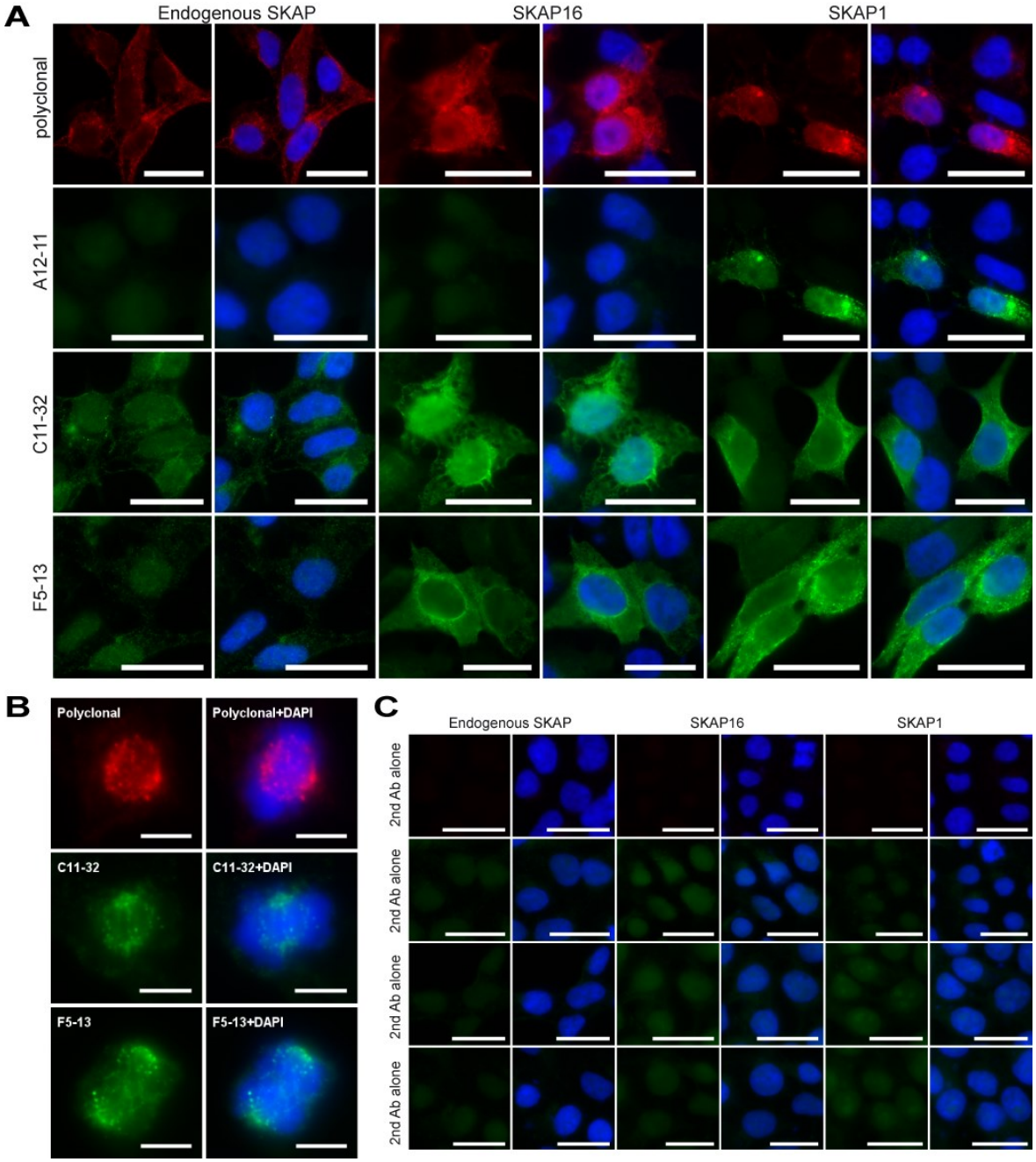

Figure 15. SKAP16 is the only SKAP isoform detectable in HEK-293 cells and it localizes to mitotic spindle and kinetochores in mitosis. (A) Immunofluorescence staining of HEK-293 cells with different anti-SKAP antibodies. Scale bars 20 µm. (B) SKAP localizes to mitotic spindle and kinetochores in mitotic HEK-293 cells, as shown by immunofluorescence staining using different anti-SKAP antibodies. Scale bars 5 µm. (C) Incubation with the Alexa Fluor™-conjugated antibodies alone was done as a control for immunofluorescence stainings. Scale bars 20 µm. Representatives of at least three experiments are shown (from (Cindric Vranesic et al. 2016)).

4.2.2 SKAP1 expression is testis/sperm-restricted

For further analyses of KNSTRN expression in human, twenty different human tissues were studied by RT-PCR (Fig. 16), using the same oligonucleotide combinations as for the cell lines. The KNSTRN16 transcript was detectable in all tissues analyzed, while KNSTRN1 expression showed to be testis-specific.

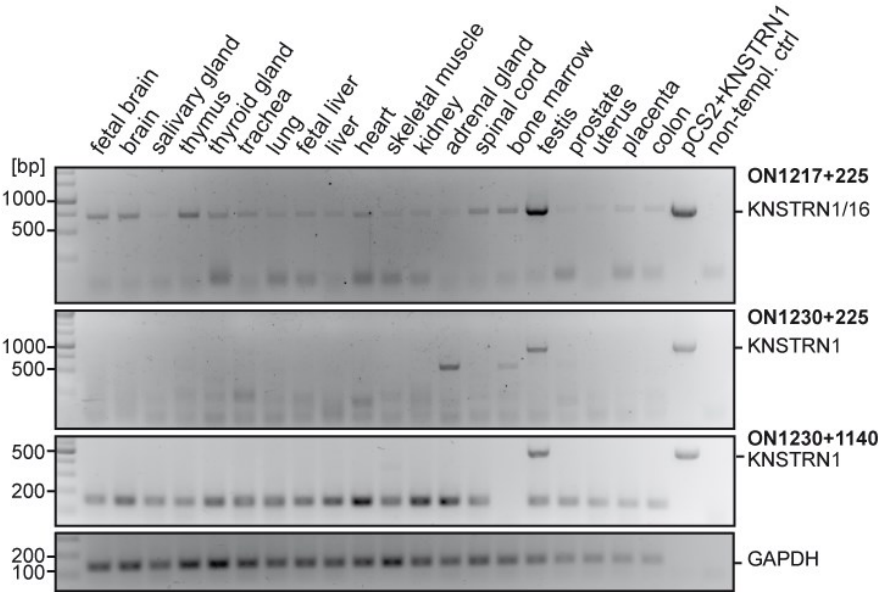

Figure 16. Human KNSTRN1 transcript is detectable only in testis. RT-PCR analysis of the expression of the KNSTRN gene in different human tissues (with primers depicted in Fig. 13A). KNSTRN16 transcript is present in all tissues, while KNSTRN1 is detected exclusively in testis. PCR products with primer combination ON1230+225 from heart (200 bp), adrenal gland (500 bp) and testis (950 bp), as well as ON1230+1140 from heart (150 bp) and skeletal muscle (350 bp) were cloned and sequenced, showing that only the PCR product from testis corresponds to KNSTRN. pCS2+KNSTRN1 and GAPDH were used as controls. Representatives of at least three experiments are shown (from (Cindric Vranesic et al. 2016)).

KNSTRN expression in testis was further closely investigated by RT-PCR on RNA obtained from men with normal spermatogenesis, patients with meiotic arrest or with Sertoli-cell-only syndrome (SCOS) (Feig et al. 2007) (Fig. 17). Because the hTERT (catalytic subunit of telomerase) in testis is expressed exclusively in spermatogonial stem cells, detection of the hTERT transcript was used to control the presence or absence of spermatogonia in the analyzed specimen (Weise and Günes 2009). KNSTRN16 was present in all samples analyzed, but KNSTRN1 transcript was detected only in samples acquired from men with normal spermatogenesis. These data implied that KNSTRN1 is expressed exclusively in spermatids and testicular sperm.

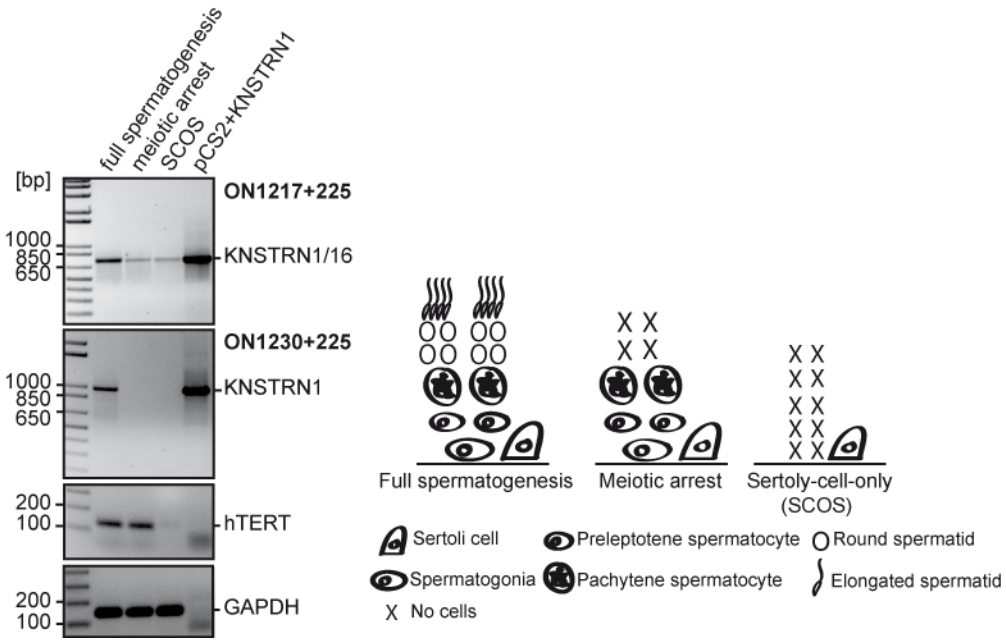

Figure 17. A KNSTRN1 transcript is present only in men with normal spermatogenesis. RT-PCR analysis of the KNSTRN expression in samples from men with full spermatogenesis, meiotic arrest and Sertoli-cell-only syndrome (SCOS). pCS2+KNSTRN1, hTERT and GAPDH were used as controls. The scheme represents different cell populations in the analyzed samples (adapted from (Feig et al. 2007)). Experiment was performed in the group of Dr. Cagatay Günes (from (Cindric Vranesic et al. 2016)).

To check whether SKAP1 is expressed in sperm, RT-PCR was performed on RNA isolated from ejaculated human sperm. RT-PCR reactions and subsequent sequencing confirmed the presence of KNSTRN1 transcript in spermatozoa (Fig. 18A). Additional analyses of human spermatozoa by Western blotting using the anti-SKAP antibodies characterized in Fig. 12 proved that SKAP1 is the only detectable SKAP isoform in these cells (Fig. 18B). The localization of SKAP1 in spermatozoa was defined by immunofluorescence microscopy. With the polyclonal anti-SKAP antibody, staining was detectable predominantly in the midpiece of the sperm flagellum (Fig. 18C). The anti-SKAP (C11-32) antibody additionally stained the equatorial region. Also on Western blots this antibody detected a hitherto unidentified additional band of a molecular weight lower than that of SKAP16 (Fig. 18B), therefore it cannot be excluded that the observed signal in the equatorial region might be a result of an unspecific antibody binding.

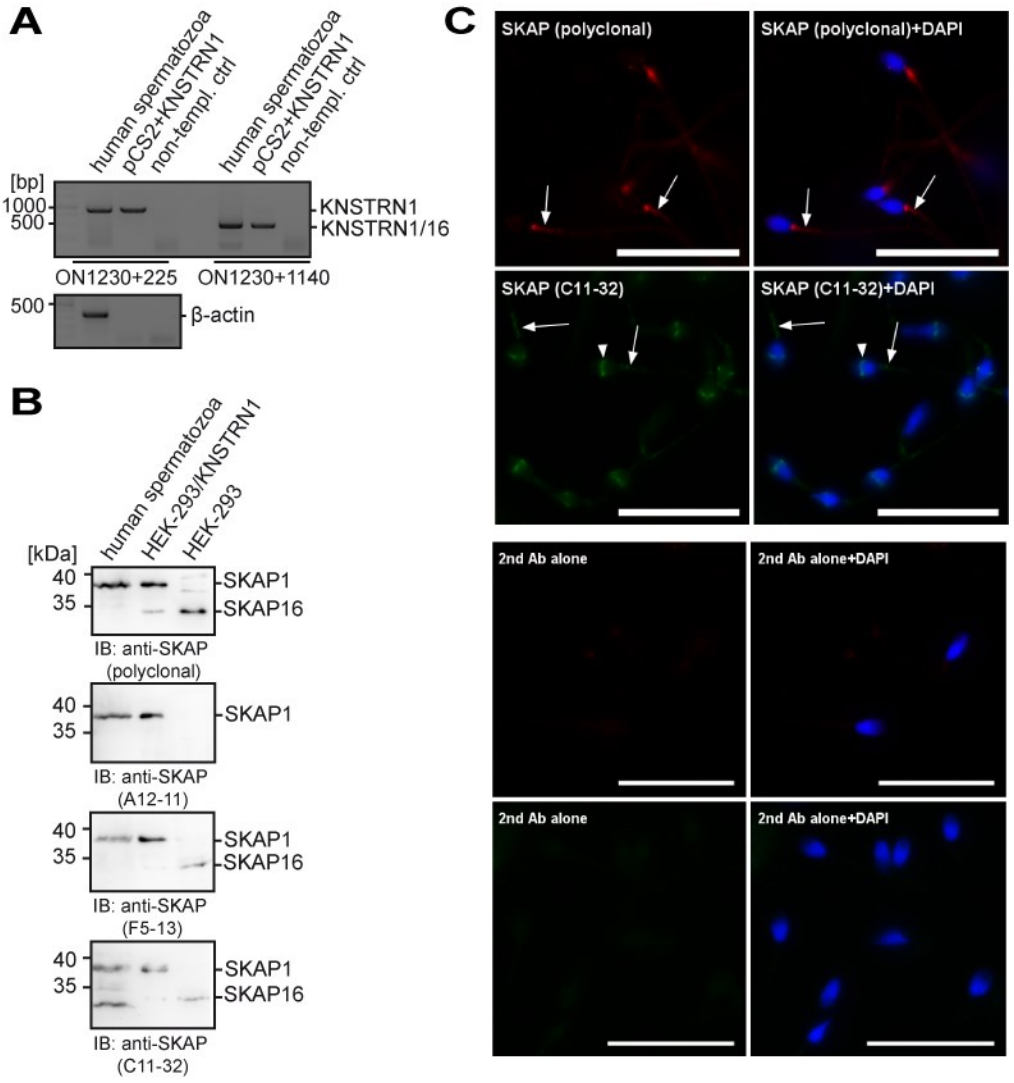

Figure 18. SKAP1 is expressed in the flagellum of human spermatozoa. (A) KNSTRN expression in human sperm was analyzed by RT-PCR. pCS2+KNSTRN1 and non-template control were used as positive and negative controls, respectively. β-Actin was used as a loading control. (B) SKAP expression in human sperm was analyzed by Western blotting with different anti-SKAP antibodies. (C) Immunofluorescence staining of human spermatozoa. SKAP1 localizes predominantly to the midpiece region (arrows). Anti-SKAP (C11-32) antibody in addition stains the equatorial region (arrowhead). As controls for SKAP stainings, fixed and blocked human spermatozoa were incubated with Alexa Fluor™-conjugated antibodies alone. Scale bars 20 µm. Representatives of at least three experiments are shown (from (Cindric Vranesic et al. 2016)).

Taken together, all the analyses of SKAP expression in human cells and tissues revealed the ubiquitous SKAP16 expression and testis/sperm-restricted expression pattern of SKAP1. Furthermore, protein products corresponding to the predicted SKAP3 and SKAP5 isoforms could not be detected in any of the analyzed cells and tissues.

4.3 Expression profile of SKAP isoforms in mouse

SKAP isoforms in mouse were studied with the aim to support the notion of testis/sperm-specific expression of human SKAP1. RT-PCR analysis of Knstrn transcripts (Knstrn1 and Knstrn4) in mouse cell lines showed the ubiquitous presence of Knstrn4, but no Knstrn1 was detectable (Fig. 19A and 19B). Analyses of Knstrn transcripts in various tissues revealed that both Knstrn1 and Knstrn4 are highly expressed in testis (Fig. 19C). While Knstrn1 expression was limited to testis, low-abundance Knstrn4 transcript could be detected in ovary (Fig. 19D), in addition to testis. Further investigation of mouse Knstrn1 expression in testis by RT-PCR was performed on RNA isolated from mouse testes at different time points after birth (Fig. 19E). The Knstrn4 transcript was present from earliest time point analyzed onwards, whereas Knstrn1 expression appears to start at around 4 weeks after birth. This time corresponds to the age in which spermatogenesis in mice is complete and the elongated spermatids are present in the testes (Vergouwen et al. 1993). This finding agrees with the data obtained by Grey et al., who reported that SKAP1 is present specifically in mouse spermatids (Grey et al. 2016). These data also support the discovery of testis/sperm-specific SKAP1 expression in human.

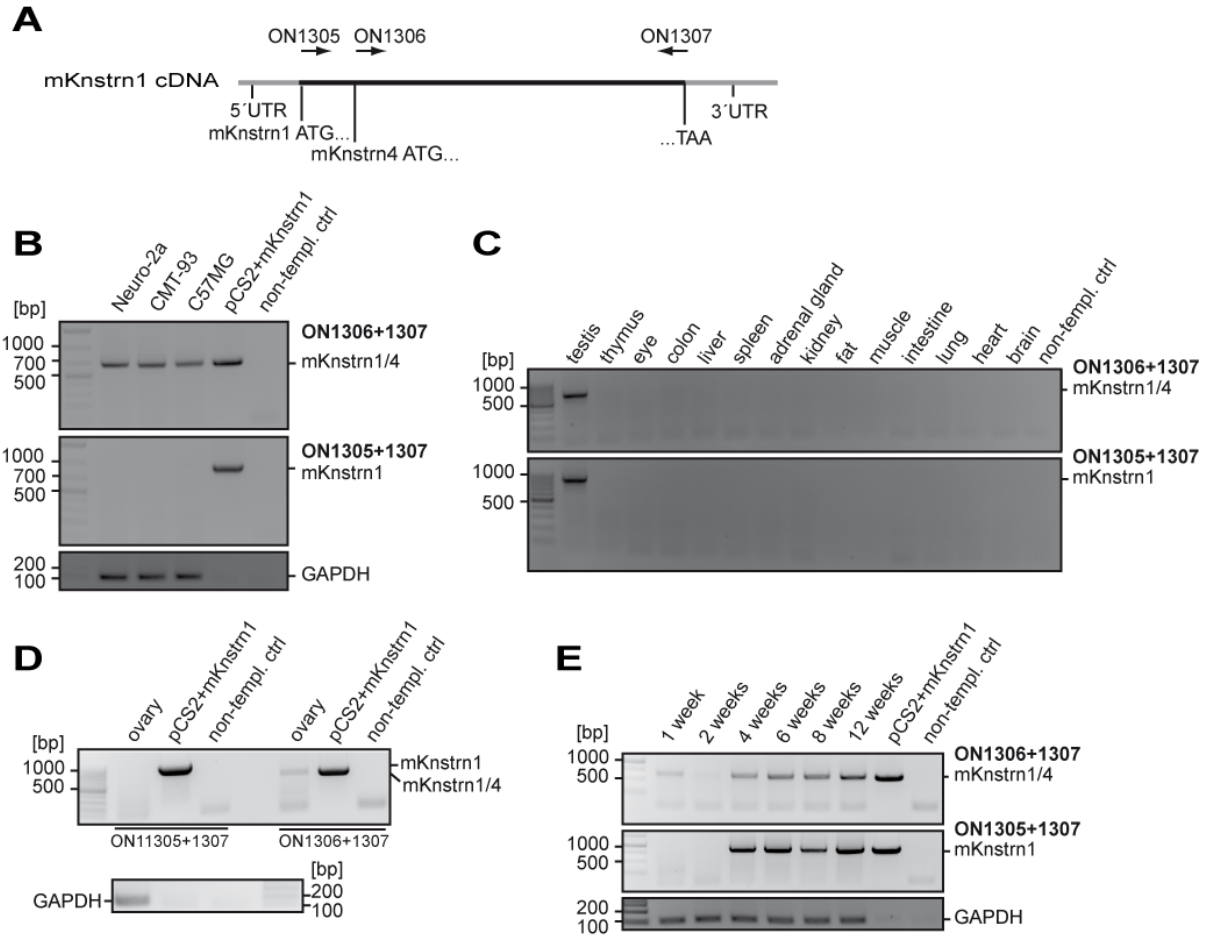

Figure 19. Knstrn expression in mice. (A) The annealing sites of oligonucleotides used for PCR reactions. (B) Analysis of mouse Knstrn transcripts in mouse cell lines using RT-PCR. (C) Analysis of the expression of the mouse Knstrn gene in different tissues by RT-PCR. (D) RT-PCR analysis of mouse Knstrn transcripts in mouse ovary. (E) RNA isolated from testes of mice of different age after birth was analyzed RT-PCR. pCS2+mKnstrn1 plasmid encoding mouse Knstrn1 cDNA and GAPDH were used as controls. Representatives of at least two experiments are shown (parts of the figure from (Cindric Vranesic et al. 2016)).

4.4 Human SKAP1 and SKAP16 stoichiometry

Defining a protein´s stoichiometry is an important step in trying to understand its molecular function. In this respect, with the aim to further contribute to better understanding of the function of SKAP, the ability of SKAP1 and SKAP16 to self-associate was investigated.

4.4.1 SKAP1 forms homomeric complexes

To test whether SKAP1 molecules directly interact with each other, pull-down assays were performed using the recombinant SKAP1 proteins. As shown in Fig. 20A, full-length GST-SKAP1 and MBP-SKAP1 do indeed directly bind to each other. A pull-down assay with full-length SKAP1 and its truncations indicated that this interaction might be mediated by the N-terminal domains (data not shown). SKAP1-SKAP1

interaction could also be shown using co-immunoprecipitation assays, where the overexpressed SKAP1 co-precipitated with SKAP1-myc$_6$ (Fig. 20B).

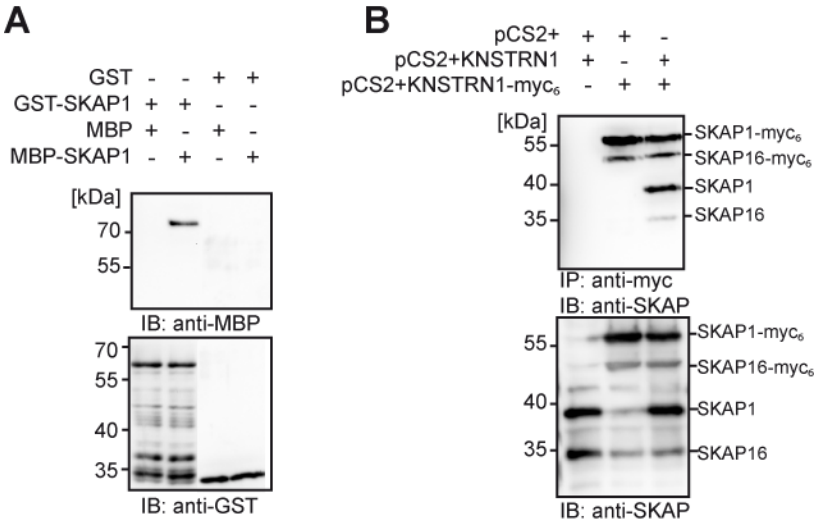

Figure 20. SKAP1 forms homomeric complexes. (A) GST-pull-down assay was performed with purified recombinant MBP-SKAP1 and GST- SKAP1. (B) HEK-293 cells were transiently transfected with pCS2+KNSTRN1 and pCS2+KNSTRN1-myc$_6$ as indicated. Protein complexes were immnunoprecipitated from the cell lysates with anti-myc (9E10) antibody and Western blotting was performed with polyclonal anti-SKAP and anti-myc (9E10) antibodies. Lower panel represents lysate controls. In the case of SKAP1-myc$_6$ overexpression, there is always a minor fraction of SKAP16-myc$_6$ co-expressed from the downstream in-frame SKAP16 start codon. Representatives of at least three experiments are shown.

Further analysis of SKAP1 self-association in the cells was performed with FRET (Fig. 21). For these experiments, HeLa cells were double-transfected with Clover-SKAP1 and mRuby2-SKAP1. For analyzing the FRET efficiency, the FRET donor fluorescence intensity of Clover-SKAP1 with or without photo-inactivation of the acceptor mRuby2-SKAP1 (acceptor-bleaching FRET, AB-FRET) was measured. In AB-FRET, the acceptor chromophore is destroyed by photo-bleaching, thereby preventing FRET from the donor to the acceptor. If the donor and acceptor were in a proximity sufficient for energy transfer, photo-bleaching the acceptor results in an observable increase in donor fluorescence. This method can only generate a positive result when the distance between donor and acceptor is less than ~10 nm. In FRET experiments in this study defined distance values from the measured FRET efficiencies were not deduced. Rather, the appearance of FRET was interpreted as an indication that donor and acceptor chromophores are close to one another within 10 nm. A mean E_{FRET} of 3.3% and a mean E_{VAR} (negative control) of -1.3% were

obtained in interphase cells (30 analyzed ROIs), resulting in a statistically significant difference between the two distributions ($p < 0.001$).

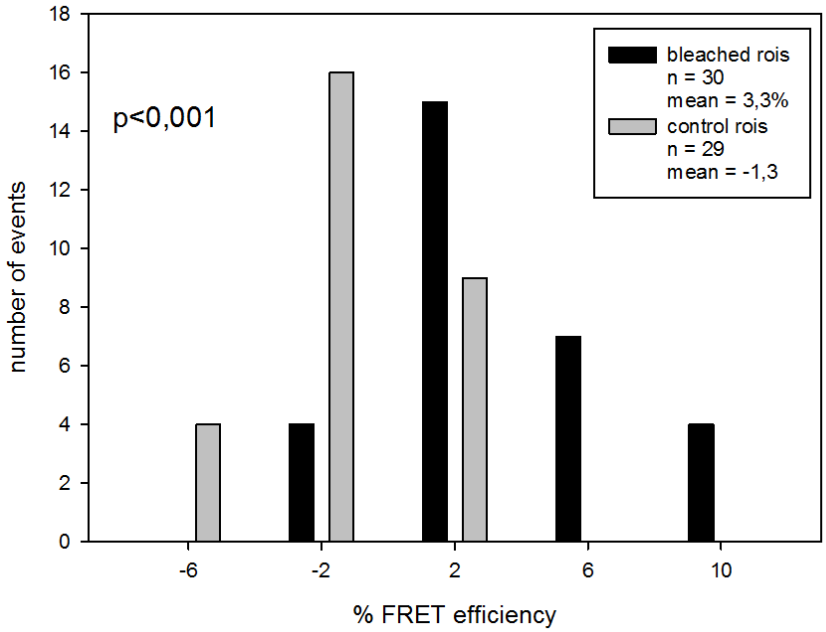

Figure 21. Acceptor-bleaching FRET between Clover-SKAP1 and mRuby2-SKAP1.The low *p*-value ($p<0.001$) indicates a strong FRET signal.

Finally, by FCCS it was determined whether SKAP1 forms complexes with itself in the cytoplasm of the living cells. In double-transfected HEp-2 cells, the protein pair EGFP-SKAP1/mCherry-SKAP1 was analyzed. For these proteins unequivocal cross-correlation was observed (Fig. 22A). From 27 FCCS experiments performed in 12 cells, all 27 showed clear cross-correlation indicating that at least two SKAP1 molecules move together, i.e. SKAP1 forms complexes with itself (there are at least two SKAP1 molecules within one and the same complex) in the cytoplasm of mitotic cells. Count rates were recorded simultaneously for both fluorophores. The count rate in a 1 sec resolution time scale is shown (insert b of Fig. 22A). The autocorrelations yielded 1.053 and 1.092 for EGFP-SKAP1 and mCherry-SKAP1, respectively. The amplitude of the cross-correlation curve A(CC), relative to the diffusion-related amplitude of one of the autocorrelation curves A(AC) of EGFP or mCherry, is a measure of binding or dynamic co-localization (Bacia and Schwille 2007). The cross-correlation analyses (with a magnified scale of G(Ƭ); insert a of Fig. 22A) resulted in a correlation of 1.015 indicating that 28% of the molecules are co-migrating in the cytoplasm of mitotic cells. The percentage of co-migrating SKAP1 molecules varied from 10% to 30%.

As a positive control, HEp-2 cells were transfected with pH-mR-G-C expressing a mRFP-EGFP fusion protein with comparable fluorescence intensities as in the FCCS analysis with EGFP-SKAP1 and mCherry-SKAP1. In Fig. 22B it is shown that the autocorrelations of EGFP (1.064) and mRFP (1.142) were comparable to the values obtained for EGFP-SKAP1 and mCherry-SKAP1 (Fig. 22A). The count rate is also shown in Fig. 22B (insert b). Cross-correlating the two channels against each other, a value of 1.029 was obtained indicating that about 45% of the molecules form a complex (Fig. 22B, with a magnified scale of G(τ) in insert a). The cross-correlation values obtained for the fusion EGFP-mCherry were in agreement with results of Kohl et al. (Kohl et al. 2005). For such fusion proteins, 100% cross-correlation should be observed. The lower value of about 50% could be explained by a much slower maturation and lower stability of mRFP compared to EGFP: EGFP molecules bound to an immature mRFP are interpreted by FCCS as free molecules. Thus, cross-correlation values seem to underestimate the percentage of co-migrating molecules. Consequently, oligomerization of EGFP-SKAP1 and mCherry-SKAP1 probably is higher than the calculated 10–30%, likely 20–60%.

As negative control, HEp-2 cells were transfected with vector pIRES2, separately expressing EGFP and mRFP as single molecules with comparable fluorescence intensities as in the FCCS analysis with EGFP-SKAP1 and mCherry-SKAP1 (Fig. 22C). The count rate is shown in insert b. The autocorrelations yielded 1.087 and 1.098 for EGFP and mRFP, repectively. The cross-correlation curve (with a magnified scale of G(τ) (insert a), resulted in a value of 1.000 indicating the absence of any complexation between EGFP and mRFP.

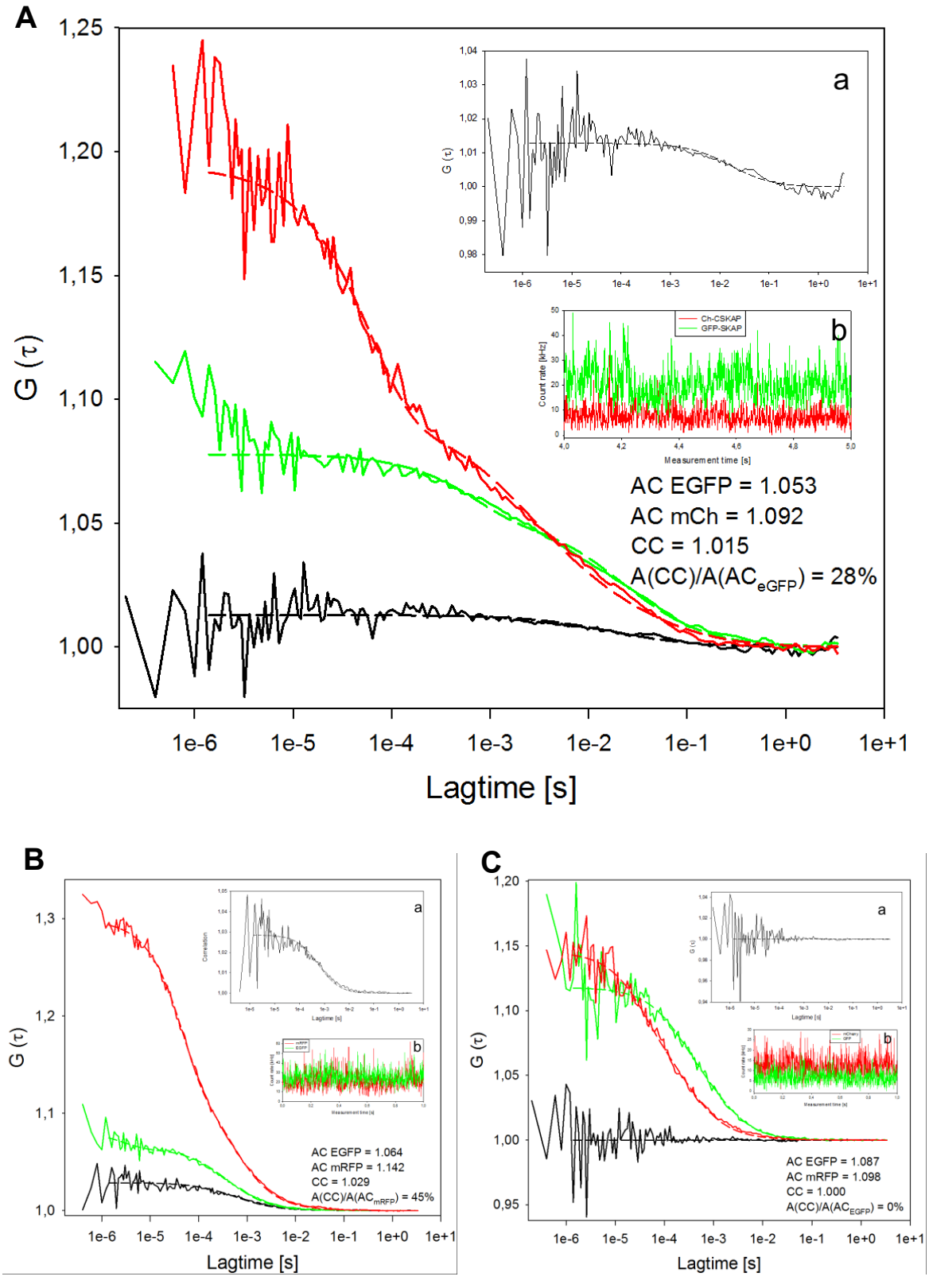

Figure 22. SKAP1 forms complexes with itself in mitotic cells. (A) HEp-2 cells were double-transfected with vectors for the simultaneous expression of EGFP- and mCherry-SKAP1 fusion proteins. FCCS analyses were done at 37°C on an LSM 710 Confocor3 microscope 48 h after transfection. Obtained measurement data were fitted with the Fit-3Dfree-1C-1Tnw model of the ZENsoftware. The cross-correlation analysis (with a magnified scale of G(Ţ); insert a) resulted in a correlation of 1.015 indicating that 28% of the molecules are co-

migrating in the cytoplasm of mitotic cells. The count rate in a 1 sec resolution time scale is shown in insert b. (B) As positive control, HEp-2 cells were transfected with pH-mR-G-C expressing an RFP-EGFP fusion protein. Cross-correlating the two channels against each other, a value of 1.029 was obtained, indicating that about 45% of the molecules form a complex. (C) As negative control, HEp-2 cells were transfected with vector plRES2, separately expressing EGFP and mRFP as single molecules. The cross-correlation curve resulted in a value of 1.000, indicating the absence of any complexation between EGFP and mRFP.

4.4.2 SKAP16 forms homomeric complexes

After showing that SKAP1 forms complexes with itself, in order to examine whether SKAP16 subunits are also able to bind to each other, pull-down experiments were performed. In pull-down assays with several truncated recombinant SKAP16 proteins it was found that SKAP16 molecules indeed directly associate with each other. In contrast to SKAP1, the SKAP16-SKAP16 interaction occurs through the second coiled-coil domain (Fig. 23A). Co-immunoprecipitation experiments showed that SKAP16 self-association also occurs within cells (Fig. 23B).

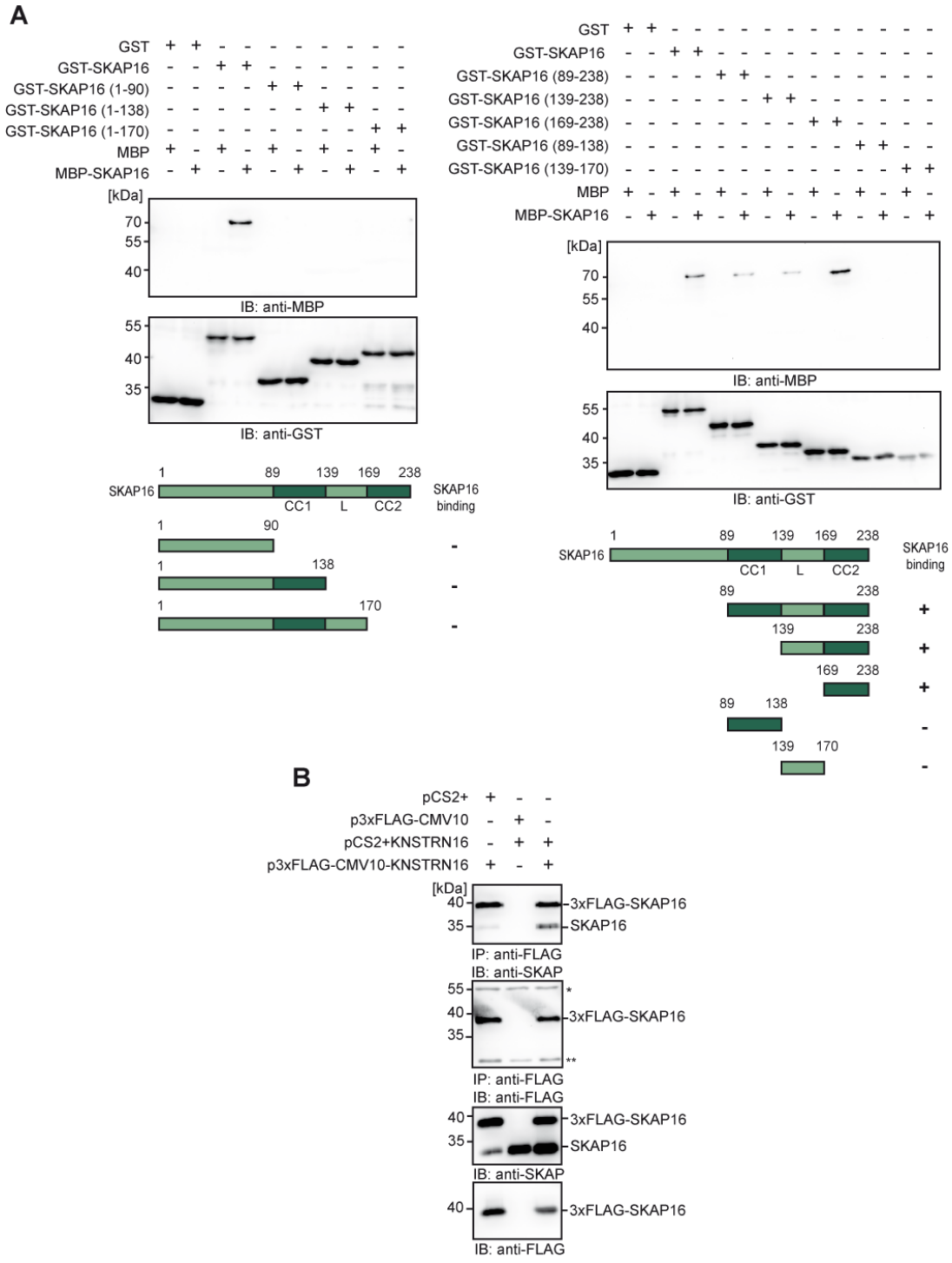

Figure 23. SKAP16 forms homomeric complexes. (A) To test the direct interaction of SKAP16 subunits, purified MBP-SKAP16, GST-SKAP16 and deletion constructs thereof were used in a GST-pull-down assay. The interaction region between SKAP16 molecules is mapped to the second coiled-coil domain. CC1 and CC2 represent two predicted coiled-coil domains. L represents the linker region between CC1 and CC2. Representatives of two independent experiments are shown. (B) For co-immunoprecipitation experiments, HEK-293 cells were transiently transfected as indicated. Protein complexes were immunoprecipitated from the cell lysates using anti-FLAG M2 antibody and Western blotting was performed with polyclonal anti-SKAP and anti-FLAG M2 antibodies. Lower panels represent lysate controls. *Heavy chain of the precipitating antibody, **Light chain of the precipitating antibody. Representative blots of at least three independent experiments are shown (from (Cindric Vranesic et al. 2016)).

FRET experiments were performed to confirm that at least two SKAP16 molecules are a part of one and the same complex in the cells (Fig. 24). For these experiments, HeLa cells were double-transfected with SKAP16-Clover and SKAP16-mRuby2. Individually, both fusion proteins co-localized to spindles in human cells (data not shown). FRET analyses were performed the same way as for SKAP1. In mitosis (43 analyzed spindles in 22 cells) a mean E_{FRET} of 2.1% and a mean E_{VAR} of -1.4% were obtained, resulting in a statistically significant difference between the two distributions with a considerable FRET-value of 3.5% ($p < 0.001$).

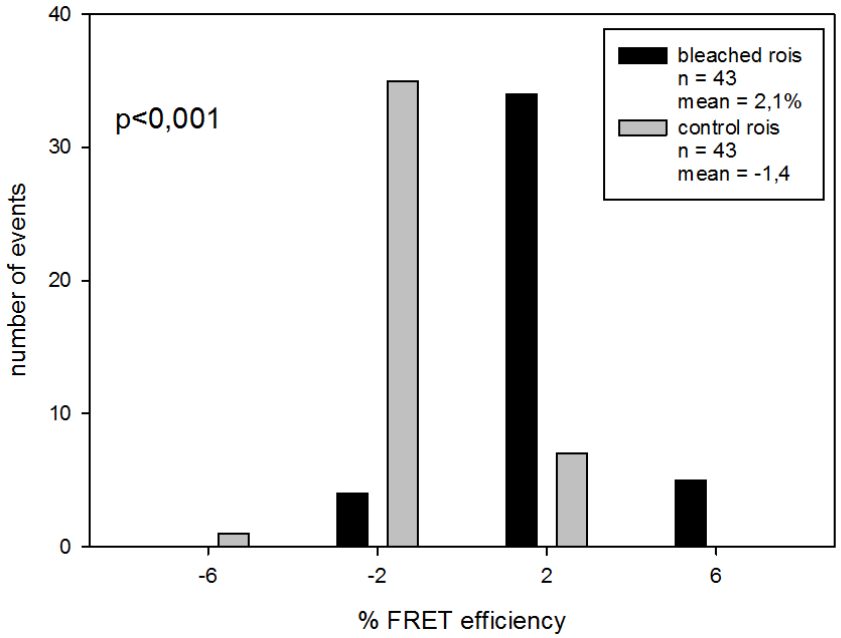

Figure 24. Acceptor-bleaching FRET between SKAP16-Clover and SKAP16- mRuby2. The low *p*-value ($p<0.001$) indicates a strong FRET signal.

Like for SKAP1, by FCCS it was finally examined whether SKAP16 forms complexes with itself in the cytoplasm of living mitotic cells. In double-transfected HEp-2 cells, the protein pair EGFP-SKAP16/mCherry-SKAP16 was analyzed. For this protein pair clear cross-correlation was observed (Fig. 25). From 16 FCCS experiments performed in 8 mitotic cells, all 16 showed obvious cross-correlation indicating that at least two SKAP16 molecules move together, i.e. SKAP forms complexes with itself in the cytoplasm of mitotic cells. The autocorrelations yielded 1.059 and 1.100 for EGFP-SKAP16 and mCherry-SKAP16, respectively. The cross-correlation analysis (with a magnified scale of G(Ƭ); insert a of Fig. 25) resulted in a correlation of 1.013 indicating that 22% of the molecules are co-migrating in the cytoplasm of mitotic cells. The percentage of co-migrating SKAP16 molecules varied from 10% to 25%,

comparable to SKAP1. In interphase cells an indication for SKAP16-SKAP16 complexation was observed too (18 experiments in 10 cells).

Same as for SKAP1, all experiments testing SKAP16 self-association showed that SKAP16 molecules are able to directly bind to each other and that in living cells there are at least two SKAP16 molecules within one and the same complex.

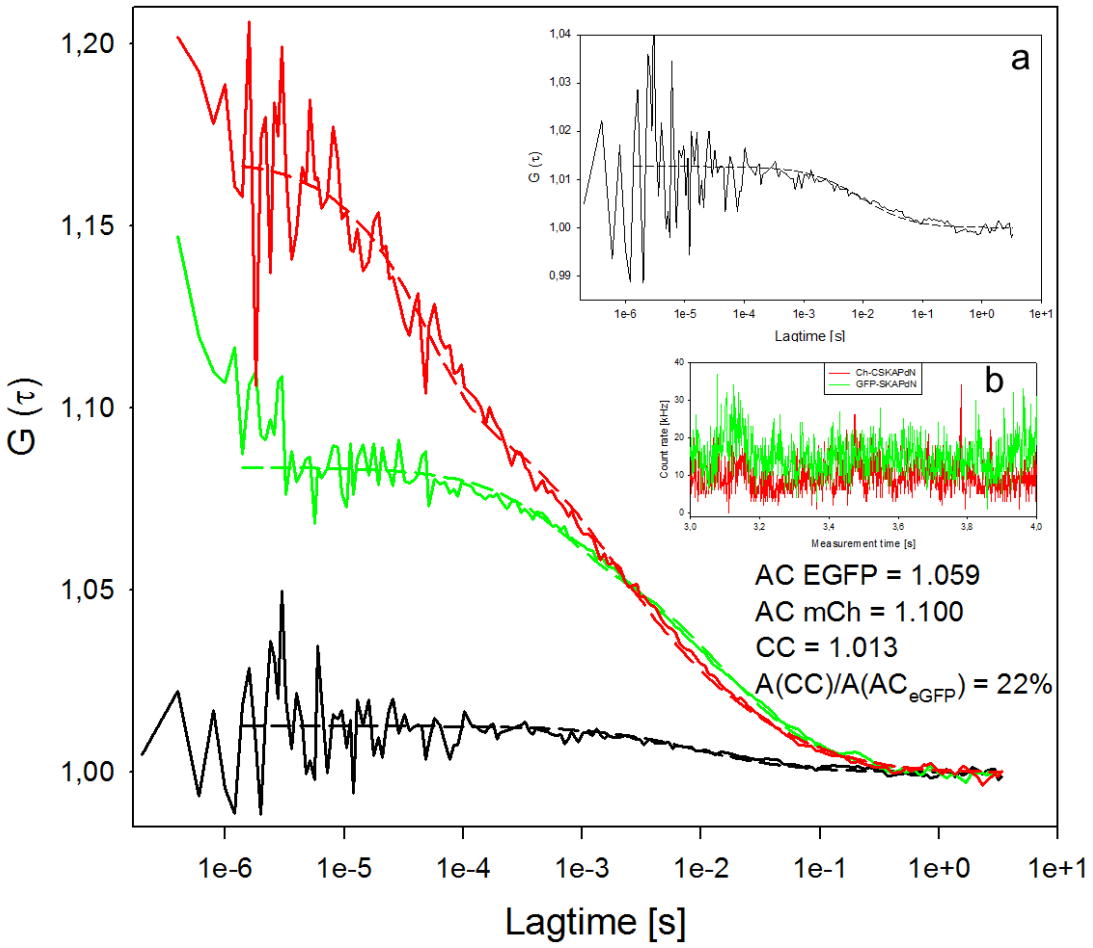

Figure 25. SKAP16 forms complexes with itself in mitotic cells. HEp-2 cells were double-transfected with vectors for the simultaneous expression of EGFP- and mCherry-SKAP16 fusion proteins. FCCS analyses were performed and data were fitted the same way as for SKAP1. The cross-correlation analysis (with a magnified scale of G(Ţ); insert a) resulted in a correlation of 1.013 indicating that 22% of the molecules are co-migrating in the cytoplasm of mitotic cells. The count rate in a 1 sec resolution time scale is shown insert b. Positive and negative controls are shown in Fig. 22B and 22C, respectively.

4.5 Identification of novel SKAP1 interaction partners

4.5.1 SKAP1 interacts with Pontin and Reptin

Since in this work SKAP1 was found to be a sperm-specific protein, in order to get insight into its function, it was aimed at identifying SKAP1-specific interaction partners. In this respect, previous yeast-two-hybrid screen data were revisited where Pontin was used as a bait (Bauer et al. 2000, Weiske and Huber 2005) and SKAP was identified as a potential Pontin interaction partner. To verify binding of Pontin to SKAP, pull-down assays with recombinant GST-Pontin and MBP-SKAP1 or -SKAP16 fusion proteins were performed (Fig. 26A). Intriguingly, in these experiments GST-Pontin associated with MBP-SKAP1 but not with MBP-SKAP16. This was confirmed by co-immunoprecipitation experiments using cell lysates of transiently transfected HEK-293 cells, where SKAP1-myc_6 co-precipitated with Pontin-FLAG, while SKAP16-myc_6 did not (Fig. 26B).

Given the fact that Pontin and Reptin are closely related proteins that are often found within the same macromolecular complexes, it was reasonable to test whether SKAP interacts with Reptin. Same as Pontin, in pull-down experiments, Reptin directly interacted with SKAP1 but not with SKAP16 (Fig. 26C). Additionally, in co-immunoprecipitation experiments with lysates of transfected HEK-293 cells, Reptin-FLAG co-immunoprecipitated with SKAP1-myc_6 (Fig. 26D). However, considering the lower intensity of the Western blot signals it seems that the interaction of SKAP1 with Reptin is weaker than that with Pontin. Therefore, Pontin appears to be a preferential SKAP1 interaction partner in a complex that most likely contains Pontin, Reptin and SKAP1.

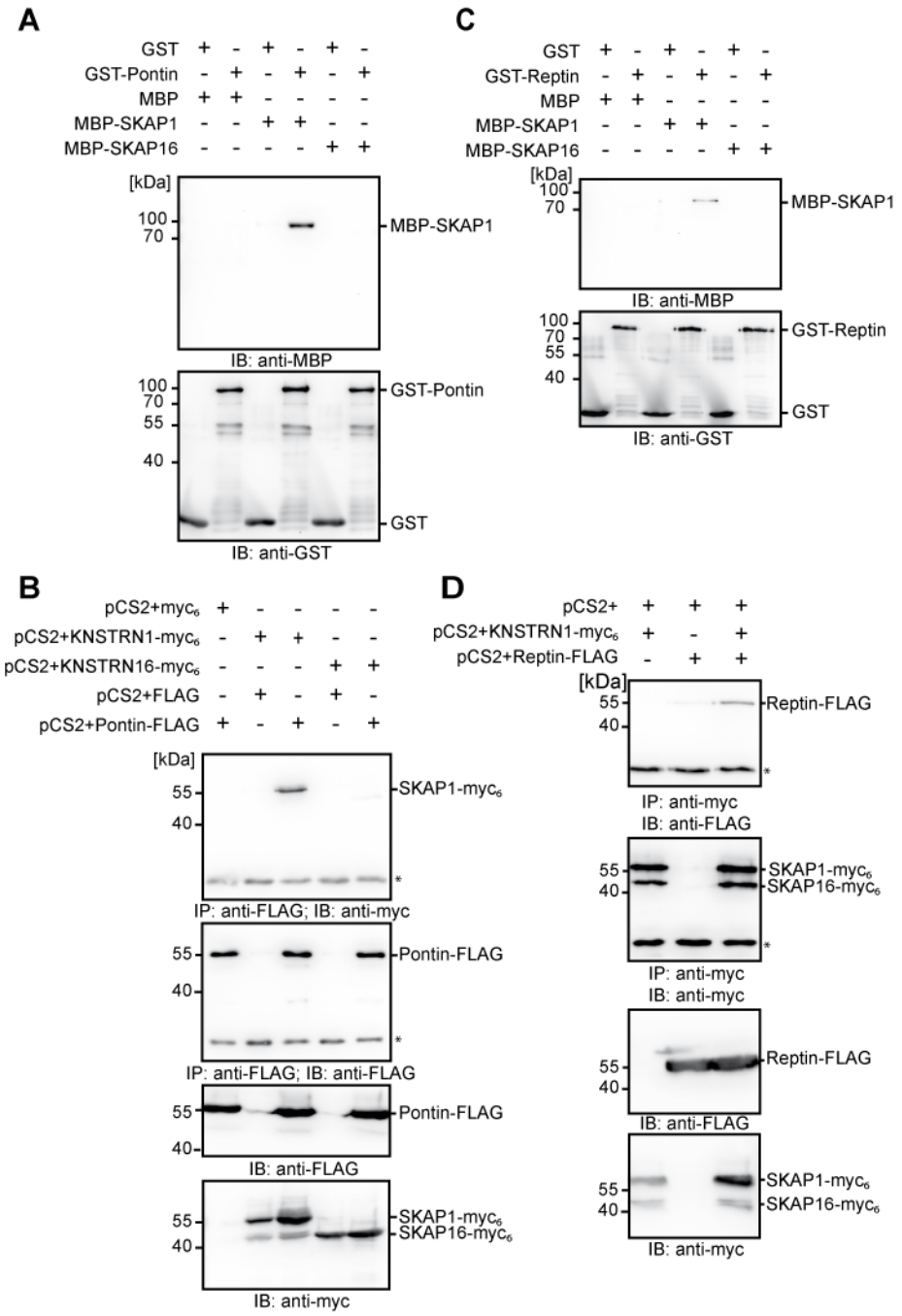

Figure 26. SKAP1 directly associates with Pontin and Reptin. (A) GST-pull-down assay was performed with purified recombinant GST-Pontin and MBP-SKAP1 or MBP-SKAP16 to test the direct interaction of SKAP and Pontin. (B) In co-immunoprecipitation experiments myc_6-tagged SKAP1 forms a complex with FLAG-tagged Pontin. Co-transfection of empty pCS2+myc_6 and pCS2+FLAG vector was used as a control. *Light chain of the precipitating antibody. In the case of SKAP1-myc_6 overexpression, there is always a minor fraction of SKAP16-myc_6 co-expressed from the downstream in-frame SKAP16 start codon. The blots are representatives of at least three independent experiments. (C) Purified GST-Reptin and MBP-SKAP1 or MBP-SKAP16 were used in GST-pull-down assays. (D) Myc_6-tagged SKAP1 forms a complex with FLAG-tagged Reptin in co-immunoprecipitation experiments performed with anti-myc antibody. *Light chain of the precipitating antibody. Representatives of at least two independent experiments are shown (from (Cindric Vranesic et al. 2016)).

As SKAP1 is expressed exclusively in testis, SKAP1-Pontin/Reptin interactions are probably testis-specific. Interestingly, Pontin and Reptin show highest expression in testis, which indicates that these interactions are functionally relevant. Based on the interaction studies, following investigations focused on Pontin as a major SKAP1 binding partner. On Western blots it was shown that Pontin protein is present in lysates of isolated human spermatozoa (Fig. 27A). Furthermore, in immunofluorescence stainings of spermatozoa using a polyclonal antibody against Pontin, it was obvious that Pontin, like SKAP1, localizes to the sperm flagellum (Fig. 27B).

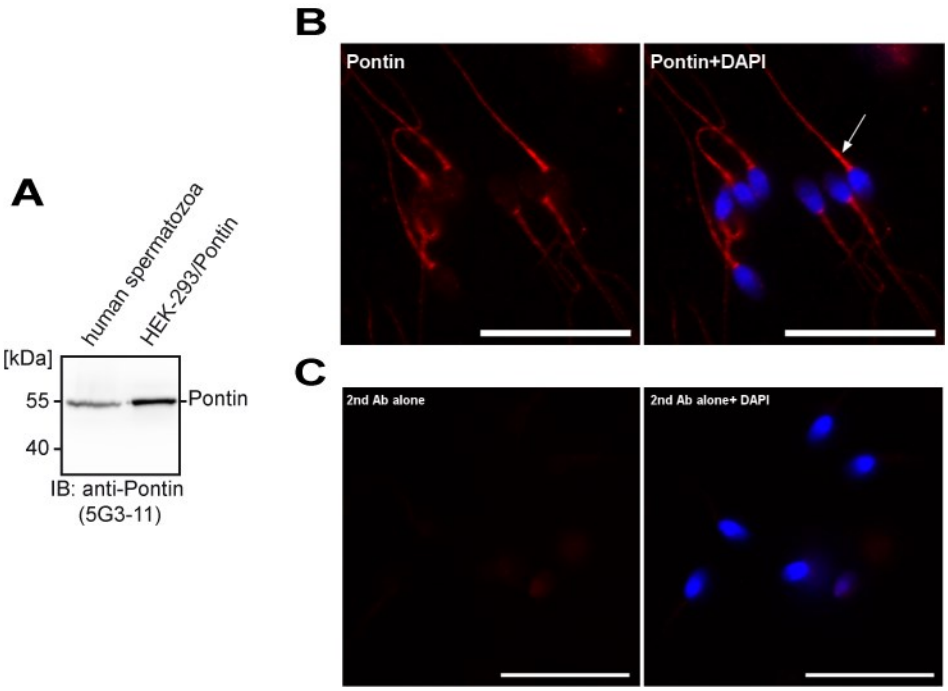

Figure 27. Pontin localizes to the flagellum of human spermatozoa. (A) Pontin expression in human sperm was analyzed by Western blotting using anti-Pontin (5G3-11) antibody. Lysate of HEK-293 cells overexpressing Pontin was used as a positive control. (B) Immunofluorescence staining of Pontin in human spermatozoa using polyclonal anti-Pontin (E12TC) antibody. Pontin localizes predominantly to the connecting piece and midpiece of the sperm flagellum (arrow). Scale bars 20 µm. Representatives of at least two experiments are shown (from (Cindric Vranesic et al. 2016)).

4.5.1.1 Cancer-associated SKAP1 mutations do not influence interaction with Pontin

Lee at al. reported cancer-associated mutations in the N-terminal domain of SKAP, whereby the most frequent ones are the S24F and A40E substitutions (Lee et al. 2014). In order to investigate whether these mutations have an impact on binding of SKAP1 to Pontin, SKAP1 S24F and A40E mutants were generated and used together with the wild-type SKAP1 in co-immunoprecipitation experiments to test binding to Pontin (Fig. 28). Three independent experiments have shown that the S24F and A40E mutations have only minor, non-significant influence on binding of SKAP1 to Pontin.

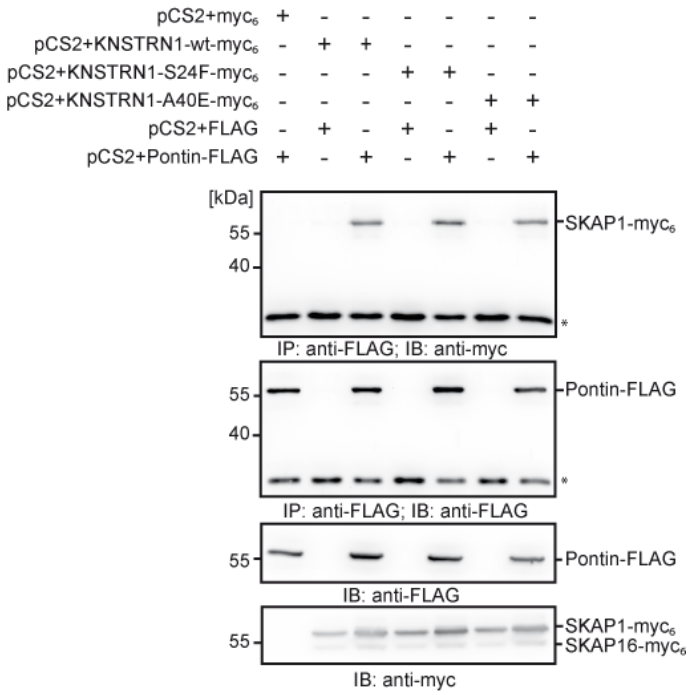

Figure 28. SKAP1 mutations do not influence SKAP1-Pontin interaction. Co-immunoprecipitation experiments were performed with Pontin-FLAG, myc_6-tagged SKAP1-wt and its mutants, SKAP1-S24F and SKAP1-A40E. *Light chain of the precipitating antibody. In the case of SKAP1-myc_6 overexpression, there is always a minor fraction of SKAP16-myc_6 co-expressed from the downstream in-frame SKAP16 start codon. Representative blots of three experiments are shown (from (Cindric Vranesic et al. 2016)).

4.5.2 SKAP1 directly binds to β-catenin

Considering that Pontin and Reptin are known to interact with β-catenin (Bauer et al. 2000) and SKAP1 is also binding to Pontin and Reptin, it was interesting to test whether SKAP1 binds to β-catenin. Pull-down assays performed with recombinant SKAP1 and β-catenin revealed that SKAP1 and β-catenin indeed directly bind to each other. In β-catenin this interaction is mediated by the core-region containing armadillo repeats (Fig. 29). Until now, SKAP1-β-catenin interaction could not be confirmed by co-immunoprecipitation using the lysates of cells overexpressing SKAP1 and β-catenin.

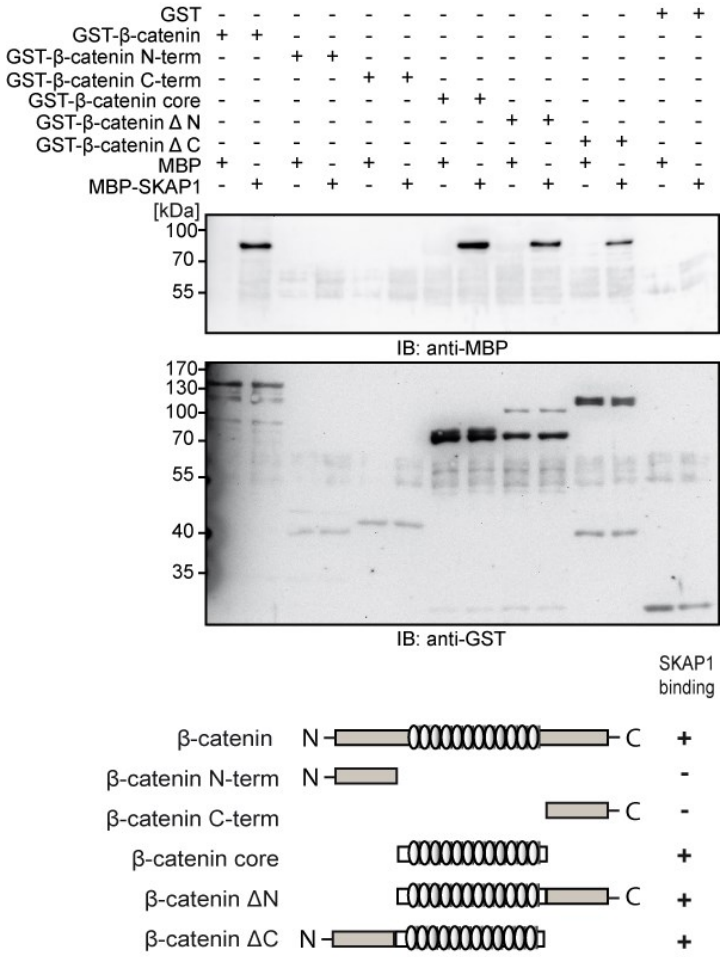

Figure 29. SKAP1 directly interacts with the core-region of β-catenin. Purified recombinant MBP-SKAP1, GST-β-catenin and its deletion constructs were used in a GST-pull-down assay to test the direct interaction of SKAP1 and β-catenin. The interaction between SKAP1 and β-catenin molecules occurs through the core-region of β-catenin. In control experiments, MBP and MBP-SKAP1 proteins do not unspecifically bind to GST or GST-fusion proteins. Representative blots of at least three experiments are shown.

4.5.3 SKAP1 forms a complex with TIP60

Another well-known fact is that Pontin and Reptin are components of the TIP60 histone acetyltransferase complex (Jha et al. 2013). In order to examine if SKAP1 is also found within the TIP60 complex, co-immunoprecipitation experiments were performed. The results of such experiments showed that SKAP1 forms a complex with TIP60 in HEK-293 cells overexpressing SKAP1-myc$_6$ and 3xFLAG-TIP60 (Fig. 30).

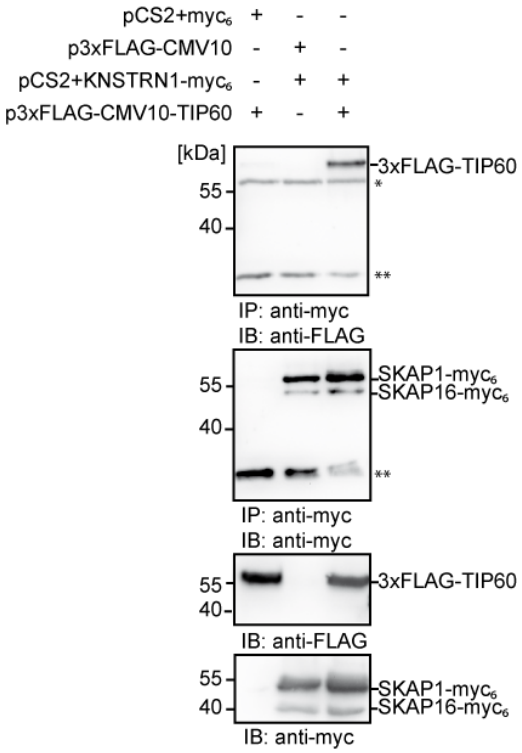

Figure 30. SKAP1 forms a complex with TIP60. Myc$_6$-tagged SKAP1 forms a complex with 3xFLAG-tagged TIP60 in co-immunoprecipitation experiments performed with anti-myc antibody. Co-transfections of empty pCS2+myc$_6$ and p3xFLAG-CMV10 vectors were used as controls. *Heavy chain of the precipitating antibody, **Light chain of the precipitating antibody. In the case of SKAP1-myc$_6$ overexpression, there is always a minor fraction of SKAP16-myc$_6$ co-expressed from the downstream in-frame SKAP16 start codon. Representative blots of at least three experiments are shown.

4.6 SKAP is overexpressed in colon cancer

With the aim to investigate whether SKAP is indeed a potential oncogene, SKAP mRNA expression levels were investigated by qPCR on colon samples obtained from healthy individuals and colon cancer patients. Analyses of 7 independent samples from each group (healthy and colon cancer patients) showed that SKAP is significantly overexpressed in the colon of cancer patients when compared to normal colon (Fig. 31). This finding still needs to be confirmed on larger sample numbers.

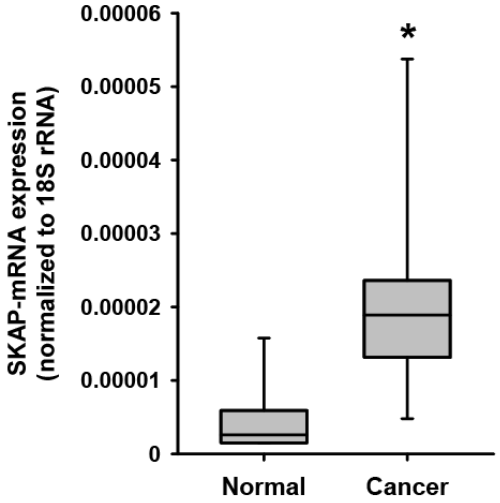

Figure 31. Relative SKAP mRNA expression in normal human colon and colon cancer. For visualization of data sets box plots were used, where boxes represent 25th and 75th percentiles, respectively. Medians are indicated by a horizontal line. Whiskers indicate 10th and 90th percentiles, respectively. Differences between normal colon and cancerous colon were identified with the Mann-Whitney rank sum test; * p=0.004.

5 Discussion

SKAP was originally described as a mitotic protein with a critical role in regulation of chromosome segregation (Fang et al. 2009, Dunsch et al. 2011, Huang et al. 2012, Wang et al. 2012). Further studies have shown that SKAP also functions in processes that are not directly related to mitosis, like apoptosis (Lu et al. 2014) and cell migration (Cao et al. 2015). Moreover, SKAP is suggested to act as an oncogene in human skin cancers (Lee et al. 2014, Jaju et al. 2015, Bonilla et al. 2016, Helbig et al. 2016). Despite the obvious importance of SKAP, no studies addressing the roles of different SKAP isoforms in these vital processes have been performed to date. In this work, the expression profile of different SKAP isoforms was examined, as well as their oligomerization state. Additionally, this work describes novel SKAP isoform-specific interaction partners and shows that SKAP indeed might be an oncogene.

5.1 SKAP16 is the major SKAP isoform expressed in human cells

According to online databases, SKAP encoding gene exists in 16 different transcript variants, 4 of which are predicted to be protein-coding. The new set of monoclonal antibodies against SKAP generated during this study made it possible to differentiate between all of the predicted protein isoforms. In the many human cell lines that were examined, SKAP16 was the only detectable isoform. Previous studies of the function of SKAP, however, have been carried out in experimental settings employing overexpressed SKAP1. Strikingly, SKAP1 is not detectably translated in any of the cells analyzed in this study. Such finding certainly challenges the relevance of previous studies that examined the function of SKAP using SKAP1 or SKAP3 isoforms.

Compared to the commonly used SKAP1, SKAP16 lacks a stretch of 78 amino acids in the N-terminal part. SKAP interaction partners critical for its role in mitosis have been demonstrated to bind to the C-terminal region of SKAP1 (Dunsch et al. 2011, Wang et al. 2012, Cao et al. 2015), which is also present in SKAP16. Likewise, SKAP kinetochore localization is also mediated through the C-terminal part of the protein (Wang et al. 2012). A recent study addressing the SKAP-Astrin interaction, microtubule-binding and kinetochore recruitment of SKAP described amino acids 135-225 in SKAP1 as the region essential for the interaction with tubulin and for the microtubule plus-end tracking activity (Friese et al. 2016). Based on these

observations it can be assumed that the corresponding amino acids 57-147 in SKAP16 have similar microtubule-associated functions. Still, it remains possible that the N-terminal 78 amino acid extension in SKAP1 may modulate all the reported SKAP functions. Indeed, in parallel with our study, SKAP16 was identified in HeLa cells as the mitosis-specific isoform (Kern et al. 2016). This is the first study that addressed the role of SKAP16 in mitosis. Unlike SKAP1, SKAP16 was able to rescue the phenotype caused by SKAP depletion in mitosis. Interestingly, SKAP16 was assigned a novel role in regulation of mitotic spindle positioning, which was previously unappreciated, possibly due to studying the wrong SKAP isoform. Therefore, considering these new data, future studies on the function of SKAP in human somatic cells should focus on SKAP16 as the universally present isoform.

5.2 SKAP1 expression is testis/sperm-restricted

In order to get further insight into the expression profile of human SKAP, presence of different KNSTRN transcript variants was analyzed in various human tissues. Consistent with the data obtained on human cells, KNSTRN16 was detectable in all tissues tested. Interestingly, only in testis another KNSTRN transcript was observed, KNSTRN1. Additional investigation of samples with normal testicular morphology versus defined testicular pathology revealed that two KNSTRN variants exist in testis, KNSTRN1 and KNSTRN16. KNSTRN16 is expressed throughout testicular cell populations, while KNSTRN1/SKAP1 is specifically expressed in spermatids and mature sperm, as confirmed by analyses of ejaculated sperm. In mice, SKAP expression seems to be restricted to testes and ovaries. Similar to human, in mouse testes two transcript variants of murine Knstrn are detectable: Knstrn1 and Knstrn4. Knstrn4 (comparable to human KNSTRN16) appeared in testis early after birth, whereas Knstrn1 expression starts when spermatogenesis is complete and all testicular cell populations are present in the testis. Interestingly, even though Knstrn4 expression is detectable already at the age of 1 week, it seems to be downregulated at 2 weeks and again upregulated at 4 weeks of age. This indicates that the oscillation in Knstrn4 expression might have a physiological relevance during testis development in the period between week 1 and 4. A study by Grey et al. described an important function of murine SKAP in male gametogenesis (Grey et al. 2016). SKAP knockout mice had spermatogenesis defects that showed SKAP4 is crucial for normal fertility. The authors of the study concluded that SKAP4 is essential for proper

germ cell division, but the role of SKAP1 was not further investigated. In testis, similar to SKAP4 in mice, human SKAP16 might be indispensable for early cell divisions to ensure faithful chromosome segregation during spermatogenesis. On the other hand, SKAP1 likely has a different, mitosis-unrelated function in spermatids and mature sperm. Obviously, the first 78 N-terminal amino acids are responsible for spermatid/sperm-specific localization and function of SKAP1. In this study, SKAP was observed to localize mainly to the midpiece region of the flagellum of human spermatozoa. There are several possible explanations for SKAP1 localization to the flagellum. One of the likely explanations lies in the fact that SKAP is potentially able to bind to axonemal microtubules. Namely, SKAP1 was found to associate with microtubular structures through its N-terminal half (Schmidt et al. 2010, Huang et al. 2012, Wang et al. 2012). In addition, SKAP1 was shown to interact with cytoplasmic dynein light chain DYNLL1 and DYNLL2 and cytoplasmic dynein heavy chain (Schmidt et al. 2010), both of which are parts of the axoneme-associated dynein arms in the sperm flagellum (Inaba 2011). Since the flagellum is critical for sperm motility, SKAP1 is likely to play a role in assuring proper sperm motility. Furthermore, SKAP1 directly binds to Astrin (SPAG5; Sperm-associated antigen 5) in mitotic HeLa cells (Schmidt et al. 2010, Dunsch et al. 2011, Friese et al. 2016). Spag5 was reported to associate with outer dense fibers (ODFs) in rat spermatids (Shao et al. 2001, Fitzgerald et al. 2006). Putative SKAP1-Astrin interaction in human spermatids and mature spermatozoa provides another possible explanation for SKAP localization to the flagellum.

In sum, the analyses of KNSTRN/SKAP expression in different human cells and tissues resulted unexpectedly in discovery of SKAP16 as a ubiquitously expressed isoform, while SKAP1 expression is restricted to testis/sperm. This is a novel finding with critical importance for all future studies, since most investigations on SKAP in somatic cells were done by overexpressing isoforms that could not be detected in any of the human cells analyzed here.

Additionally, data from a study by Lee et al. (Lee et al. 2014) should be revised. These authors reported mutations in the KNSTRN gene in skin cancers based on whole exome sequencing. The observed mutations were postulated to result in missense mutations in the N-terminal region of the putative SKAP3 isoform. SKAP3 contains the N-terminus of SKAP1, but it differs in the C-terminal part due to

alternative splicing, resulting in a protein with a molecular weight similar to SKAP16. However, in the described study, the specific expression of SKAP3 was not proven, neither on mRNA nor on protein level. Thus, it remains to be discussed whether the proposed effects of these mutations can actually be correlated to alterations in the SKAP3 protein. However, it can not be excluded that other isoforms might be expressed under specific stress or pathological conditions, e.g. cancer.

5.3 SKAP1 and SKAP16 form homomeric complexes

Defining protein stoichiometry is crucial to understand its molecular function. COILS server (Lupas et al. 1991) predicts that both SKAP1 and SKAP16 contain two coiled-coiled domains in the C-terminal region. Coiled-coils are protein structural motifs that consist of two to five α-helices wrapped around each other to form a supercoil. They are known to often mediate protein oligomerization and protein-protein interactions (Mason and Arndt 2004). Based on the COILS server predictions, this study tested the ability of SKAP1 and SKAP16 to self-associate. Biochemical analyses have shown that indeed both of the proteins form homomeric complexes, both i*n vitro* and within the cells. Thereby, SKAP16 self-associated via the second coiled-coil domain, while SKAP1 oligomerization domains were not studied in detail. However, some experiments gave a hint that N-terminal domains of SKAP1 might also be involved in its self-association. Consistent with this, data from Cao et al. show that SKAP1 seems to form dimers partly through the N-terminus (Cao et al. 2015). This provides another proof that differences between these two proteins clearly have an impact on their behavior. Further studies of SKAP oligomerization by FCCS experiments have clearly shown that self-association of SKAP proteins occurs within the living cells. Hence, SKAP oligomerization is undoubtedly important for its functions *in vivo*.

In the frame of this study, it was not determined whether SKAP proteins form dimers, trimers or higher-order oligomers. Cao et al. reported that SKAP1 builds dimers (Cao et al. 2015). Interestingly, in another study, the SKAP1 135-225 construct behaved as a trimer (Friese et al. 2016). MultiCoil software (Wolf et al. 1997) predicts that both SKAP1 and SKAP16 are more likely to form dimers than trimers. This aspect remains to be clarified experimentally.

5.4 Newly identified SKAP1-specific interaction partners

5.4.1 Pontin and Reptin

The search for SKAP1-specific interaction partners resulted in the detection of a previously unknown interaction of SKAP1 with Pontin and Reptin. Both proteins are AAA+ ATPase superfamily members and essential components of several multi-protein complexes (Huber et al. 2008, Jha and Dutta 2009, Nano and Houry 2013). They are also known to associate with microtubular structures during mitosis where they are necessary for proper spindle assembly (Gartner et al. 2003, Sigala et al. 2005, Ducat et al. 2008). Additionally, Pontin and Reptin are important for cilia formation (Stolc et al. 2005) and were reported to be highly expressed in testis. This work shows that SKAP1, but not SKAP16, directly interacts with Pontin and Reptin, whereby Pontin seems to be the preferential SKAP1 binding partner. The SKAP1-Pontin interaction was not significantly influenced by the previously published SKAP mutations in the N-terminal region of the protein (Lee et al. 2014). Proteomic analyses that found both Pontin/Reptin and SKAP1 to be present in human sperm proteome (Wang et al. 2013) support the exsistence of a SKAP1-Pontin/Reptin interaction. These interaction studies suggest a SKAP1-Pontin/Reptin sperm-specific function and represent the first visualization of SKAP and Pontin in spermatozoa. Expectedly, SKAP1 and Pontin both localized to the same region of the sperm flagellum. As Pontin/Reptin are assigned a chaperone function in many macromolecular complexes (Nano and Houry 2013), one logical explanation for SKAP1-Pontin/Reptin interaction in sperm could be that Pontin/Reptin serve as a chaperone bringing SKAP1 to its site of action. Consistent with this idea, Pontin/Reptin were reported to participate in the R2TP complex which forms a chaperone complex with Hsp90 in somatic cells (Boulon et al. 2012). Hsp90 is one of the chaperones crucial for male fertility and it localizes mainly to the sperm flagellum (connecting and midpiece regions) where it plays key roles in controlling the morphological transformation of germ cells during spermatogenesis and their post-testicular maturation (Dun et al. 2012, Li et al. 2014). Since all the components of R2TP/Hsp90 complex are present in the sperm proteome (Wang et al. 2013), it is conceivable that a similar chaperone complex is formed in sperm. Such a complex could play a role in biogenesis of multi-molecular protein complexes and assure the proper maturation of the sperm cell. These findings do not provide the full picture yet,

however, they suggest a role for SKAP and Pontin/Reptin as factors important for sperm motility.

5.4.2 β-catenin

Pontin and Reptin are well-known to interact with β-catenin (Bauer et al. 1998, Bauer et al. 2000). Since in this work it was found that Pontin is a SKAP1-specific binding partner, it was tested whether SKAP1 is also able to bind to β-catenin. In pull-down assays using recombinant proteins, SKAP1 directly binds to the core-region of β-catenin. Until now, this interaction could not be confirmed in co-immunoprecipitation assays with lysates from the cells overexpressing SKAP and β-catenin. Nevertheless, the discovery of a putative SKAP1-β-catenin interaction suggested it possibly has a spermatid/sperm specific function, perhaps together with Pontin and Reptin. β-catenin is the main player of the evolutionarily conserved canonical Wnt signaling and as such it is essential for development and adult tissue homeostasis (Clevers and Nusse 2012). Precise control of Wnt signaling was found to be crucial for the Sertoli cells support of spermatogenesis (Chang et al. 2008). Some studies also showed that the germ-cell-specific deletion of β-catenin causes spermatogenesis failure and subsequently impaired fertility (Chang et al. 2011, Kerr et al. 2014). This is inconsistent with the data from Rivas et al., who found that β-catenin is completely nonessential in germ cells (Rivas et al. 2014). Most of these studies reported nuclear localization of β-catenin in sperm cells, which does not agree with the SKAP staining pattern in sperm cells. Thus, data available on the role and localization of β-catenin in spermatozoa are rather contradictory and do not really support a potential sperm-specific SKAP1-β-catenin interaction.

Since the β-catenin interaction site in SKAP1 was not mapped and SKAP16 differs from SKAP1 only in that it lacks the 78 N-terminal amino acids, it is possible that the signal for interaction with β-catenin comes from the region of SKAP1 which is also present in SKAP16. The interaction of SKAP16 with β-catenin was not tested here, but indeed, according to literature, it seems to be more likely than the sperm-specific interaction of SKAP1 with β-catenin. Namely, besides the role in canonical Wnt signaling, β-catenin is an important player in cell-cell adhesion. There it links E-cadherin to α-catenin and cytoskeleton (Kemler 1993). Direct interaction of β-catenin with IQGAP1 is also important in the context of cell adhesion (Kuroda et al. 1998). IQGAP1 is a scaffold protein involved in organization of the actin cytoskeleton and

directional cell movement, cellular adhesion and regulation of transcription. Recently, SKAP was found to associate with IQGAP1 and to regulate the directional cell movement (Cao et al. 2015). It remains to be investigated whether SKAP16 binds to β-catenin/IQGAP1 in somatic cells and whether the potential interaction could contribute to understanding of the proposed role of SKAP in directional cell movement.

5.4.3 TIP60

TIP60 complex is one of the many protein complexes that contain Pontin and Reptin. TIP60 is a histone acetyltransferase complex involved in a variety of cellular processes including transcriptional regulation, cellular signaling, DNA damage repair, cell cycle control and apoptosis (Sapountzi et al. 2006). Again, as Pontin and Reptin are required for assembling a functional TIP60 complex (Jha et al. 2013), it was interesting to check if SKAP1 also interacts with TIP60, presumably in a sperm-specific manner. In co-immunoprecipitation assays, SKAP1 was found to form a complex with TIP60 in the lysates of cells overexpressing these proteins. In the same type of experiments, TIP60 did not co-precipitate with SKAP16. This indicated that there indeed might be a sperm-specific SKAP1-TIP60 interaction. Interestingly, TIP60 in mice is found to have the strongest expression in testis, where the expression substantially increases with the emergence of meiotic and post-meiotic germ cells (Thomas et al. 2007). Still, the fact that TIP60 was not found to be present in the proteome of human sperm (Wang et al. 2013), the localization of TIP60 in the nucleus of round spermatids (Reynard et al. 2009) and its described roles in mainly nucleus-related processes do not support the existence of a sperm-specific SKAP1-TIP60 complex. At the moment there seems to be no alternative explanation for the existence of such a complex.

5.5 SKAP is a potential oncogene

Several studies have found a mutation in the human KNSTRN gene (S24F) associated with skin cancers (Lee et al. 2014, Jaju et al. 2015, Bonilla et al. 2016, Helbig et al. 2016). A study by Lee et al. explained the functional relevance of this mutation using the SKAP3 mutant overexpression in human keratinocytes and concluded that SKAP3 mutagenesis correlates with increased aneuploidy and probably plays a role in SCC development (Lee et al. 2014). While it is obvious that the described KNSTRN mutation is connected to SCC, according to data on the

expression profile of SKAP isoforms obtained in this work, a mutant SKAP3 protein is not likely to be responsible for SKAPs oncogenic function. Alternatively, it is possible that the observed mutation deregulates the expression of SKAP and results in increased expression of SKAP16 in cancers. While studying the expression of SKAP in human cells, it became obvious that SKAP expression is higher in cancer cell lines in comparison to fibroblasts. This suggested that SKAP indeed might be an oncogene overexpressed in human cancers. Analyses of SKAP expression levels in colon cancer showed that SKAP mRNA levels are significantly higher in samples obtained from colon cancer patients compared to the healthy controls. However, due to the small number of samples analyzed, this finding has to be taken with caution and needs to be confirmed on a larger sample.

6 Conclusions

This work represents a detailed characterization of SKAP isoforms and of their tissue localization, both in human and mouse. It demonstrates for the first time that SKAP16 is the major isoform expressed in human cells and tissues, while SKAP1 expression is restricted to testis/sperm. As most investigations of SKAP in somatic cells were performed with SKAP1, this work provides a new basis for future studies on the role of SKAP in both human somatic cells and male germ cells.

Additionally, this study shows that SKAP1 and SKAP16 form homomeric complexes in living cells, which is certainly a feature essential for their functions *in vivo*.

Furthermore, identification of previously unknown SKAP1 interaction partners provides a valuable base for future work on understanding of SKAP biology. For instance, the very specific interaction of SKAP1 with Pontin/Reptin in human sperm suggests a sperm-specialized function of this protein interaction. A critical challenge for the future work is to uncover the mechanistic explanation for SKAP1-Pontin/Reptin function in human sperm. Also, it will be very interesting to investigate whether SKAP1 and Pontin/Reptin are useful candidates to be screened for abnormalities causing male fertility problems.

Finally, the overexpression of SKAP in colon cancer suggests it is a potential oncogene. Further studies on SKAP in different cancers will lead to better understanding of its oncogenic nature and eventually to therapeutic implications.

References

Aberle H, Butz S, Stappert J, Weissig H, Kemler R, Hoschuetzky H. 1994. Assembly of the cadherin-catenin complex in vitro with recombinant proteins. J Cell Sci, 107 (Pt 12):3655-3663.

Amann RP. 2008. The cycle of the seminiferous epithelium in humans: a need to revisit? J Androl, 29 (5):469-487.

Bacia K, Schwille P. 2007. Practical guidelines for dual-color fluorescence cross-correlation spectroscopy. Nat Protoc, 2 (11):2842-2856.

Bacia K, Kim SA, Schwille P. 2006. Fluorescence cross-correlation spectroscopy in living cells. Nat Methods, 3 (2):83-89.

Bastiaens PI, Majoul IV, Verveer PJ, Soling HD, Jovin TM. 1996. Imaging the intracellular trafficking and state of the AB5 quaternary structure of cholera toxin. EMBO J, 15 (16):4246-4253.

Bauer A, Huber O, Kemler R. 1998. Pontin52, an interaction partner of β-catenin, binds to the TATA box binding protein. Proc Natl Acad Sci USA, 95:14787-14792.

Bauer A, Chauvet S, Huber O, Usseglio F, Rothbacher U, Aragnol D, Kemler R, Pradel J. 2000. Pontin52 and Reptin52 function as antagonistic regulators of β-catenin signalling activity. EMBO J, 19 (22):6121-6130.

Bonilla X, Parmentier L, King B, Bezrukov F, Kaya G, Zoete V, Seplyarskiy VB, Sharpe HJ, McKee T, Letourneau A, Ribaux PG, Popadin K, Basset-Seguin N, Chaabene RB, Santoni FA, Andrianova MA, Guipponi M, Garieri M, Verdan C, Grosdemange K, Sumara O, Eilers M, Aifantis I, Michielin O, de Sauvage FJ, Antonarakis SE, Nikolaev SI. 2016. Genomic analysis identifies new drivers and progression pathways in skin basal cell carcinoma. Nat Genet, 48 (4):398-406.

Boulon S, Bertrand E, Pradet-Balade B. 2012. HSP90 and the R2TP co-chaperone complex: building multi-protein machineries essential for cell growth and gene expression. RNA Biol, 9 (2):148-154.

Cao D, Su Z, Wang W, Wu H, Liu X, Akram S, Qin B, Zhou J, Zhuang X, Adams G, Jin C, Wang X, Liu L, Hill DL, Wang D, Ding X, Yao X. 2015. Signaling scaffold protein IQGAP1 interacts with microtubule plus-end tracking protein SKAP and

links dynamic microtubule plus-end to steer cell migration. J Biol Chem, 290 (39):23766-23780.

Chang H, Gao F, Guillou F, Taketo MM, Huff V, Behringer RR. 2008. Wt1 negatively regulates beta-catenin signaling during testis development. Development, 135 (10):1875-1885.

Chang MS, Huang CJ, Chen ML, Chen ST, Fan CC, Chu JM, Lin WC, Yang YC. 2001. Cloning and characterization of hMAP126, a new member of mitotic spindle-associated proteins. Biochem Biophys Res Commun, 287 (1):116-121.

Chang YF, Lee-Chang JS, Harris KY, Sinha-Hikim AP, Rao MK. 2011. Role of beta-catenin in post-meiotic male germ cell differentiation. PLoS One, 6 (11):e28039.

Cheeseman IM. 2014. The kinetochore. Cold Spring Harb Perspect Biol, 6 (7):a015826.

Cheeseman IM, Desai A. 2008. Molecular architecture of the kinetochore-microtubule interface. Nat Rev Mol Cell Biol, 9 (1):33-46.

Cindric Vranesic A, Reiche J, Hoischen C, Wohlmann A, Bratsch J, Friedrich K, Gunes B, Cappallo-Obermann H, Kirchhoff C, Diekmann S, Gunes C, Huber O. 2016. Characterization of SKAP/Kinastrin isoforms - The N-terminus defines tissue specificity and Pontin binding. Hum Mol Genet.

Clevers H, Nusse R. 2012. Wnt/beta-catenin signaling and disease. Cell, 149 (6):1192-1205.

Cvackova Z, Albring KF, Koberna K, Ligasova A, Huber O, Raska I, Stanek D. 2008. Pontin is localized in nucleolar fibrillar centers. Chromosoma, 117 (5):487-497.

Diekmann S, Hoischen C. 2014. Biomolecular dynamics and binding studies in the living cell. Phys Life Rev, 11 (1):1-30.

Dornblut C, Quinn N, Monajambashi S, Prendergast L, van Vuuren C, Munch S, Deng W, Leonhardt H, Cardoso MC, Hoischen C, Diekmann S, Sullivan KF. 2014. A CENP-S/X complex assembles at the centromere in S and G2 phases of the human cell cycle. Open Biol, 4:130229.

Ducat D, Kawaguchi S, Liu H, Yates JR, 3rd, Zheng Y. 2008. Regulation of microtubule assembly and organization in mitosis by the AAA+ ATPase Pontin. Mol Biol Cell, 19 (7):3097-3110.

Dun MD, Aitken RJ, Nixon B. 2012. The role of molecular chaperones in spermatogenesis and the post-testicular maturation of mammalian spermatozoa. Hum Reprod Update, 18 (4):420-435.

Dunsch AK, Linnane E, Barr FA, Gruneberg U. 2011. The astrin-kinastrin/SKAP complex localizes to microtubule plus ends and facilitates chromosome alignment. J Cell Biol, 192 (6):959-968.

Fang L, Seki A, Fang G. 2009. SKAP associates with kinetochores and promotes the metaphase-to-anaphase transition. Cell Cycle, 8 (17):2819-2827.

Feig C, Kirchhoff C, Ivell R, Naether O, Schulze W, Spiess AN. 2007. A new paradigm for profiling testicular gene expression during normal and disturbed human spermatogenesis. Mol Hum Reprod, 13 (1):33-43.

Fitzgerald CJ, Oko RJ, van der Hoorn FA. 2006. Rat Spag5 associates in somatic cells with endoplasmic reticulum and microtubules but in spermatozoa with outer dense fibers. Mol Reprod Dev, 73 (1):92-100.

Foo Y, Korzh, V, Wohland, T. 2011. Fluorescence correlation and cross-correlation spectroscopy using fluorescent proteins for measurements of biomolecular processes in living organisms. In: Jung G, Hrsg. Fluorescent proteins II. Springer Verlag Berlin Heidelberg, 213-248.

Friese A, Faesen AC, Huis In 't Veld PJ, Fischbock J, Prumbaum D, Petrovic A, Raunser S, Herzog F, Musacchio A. 2016. Molecular requirements for the inter-subunit interaction and kinetochore recruitment of SKAP and Astrin. Nat Commun, 7:11407.

Gartner W, Rossbacher J, Zierhut B, Daneva T, Base W, Weissel M, Waldhausl W, Pasternack MS, Wagner L. 2003. The ATP-dependent helicase RUVBL1/TIP49a associates with tubulin during mitosis. Cell Motil Cytoskeleton, 56 (2):79-93.

Grey C, Espeut J, Ametsitsi R, Kumar R, Luksza M, Brun C, Verlhac MH, Suja JA, de Massy B. 2016. SKAP, an outer kinetochore protein, is required for mouse germ cell development. Reproduction, 151 (3):239-251.

Grzanka D, Gagat M, Izdebska M. 2014. Involvement of the SATB1/F-actin complex in chromatin reorganization during active cell death. Int J Mol Med, 33 (6):1441-1450.

Hartley JL, Temple GF, Brasch MA. 2000. DNA cloning using in vitro site-specific recombination. Genome Res, 10 (11):1788-1795.

Helbig D, Ihle MA, Putz K, Tantcheva-Poor I, Mauch C, Buttner R, Quaas A. 2016. Oncogene and therapeutic target analyses in Atypical fibroxanthomas and pleomorphic dermal sarcomas. Oncotarget.

Hellwig D, Emmerth S, Ulbricht T, Doring V, Hoischen C, Martin R, Samora CP, McAinsh AD, Carroll CW, Straight AF, Meraldi P, Diekmann S. 2011. Dynamics of CENP-N kinetochore binding during the cell cycle. J Cell Sci, 124 (Pt 22):3871-3883.

Hess R. Spermatogenesis, overview. In: Knobil E, Neil JD (eds.), Encyclopedia of Reproduction. New York: Academic Press, 1999. 539–545.

Huang Y, Wang W, Yao P, Wang X, Liu X, Zhuang X, Yan F, Zhou J, Du J, Ward T, Zou H, Zhang J, Fang G, Ding X, Dou Z, Yao X. 2012. CENP-E kinesin interacts with SKAP protein to orchestrate accurate chromosome segregation in mitosis. J Biol Chem, 287 (2):1500-1509.

Huber O, Weiske J. 2008. Beta-catenin takes a HIT. Cell Cycle, 7 (10):1326-1331.

Huber O, Menard L, Haurie V, Nicou A, Taras D, Rosenbaum J. 2008. Pontin and Reptin, two related ATPases with multiple roles in cancer. Cancer Res, 68 (17):6873-6876.

Inaba K. 2011. Sperm flagella: comparative and phylogenetic perspectives of protein components. Mol Hum Reprod, 17 (8):524-538.

Jaju PD, Nguyen CB, Mah AM, Atwood SX, Li J, Zia A, Chang AL, Oro AE, Tang JY, Lee CS, Sarin KY. 2015. Mutations in the kinetochore gene KNSTRN in basal cell carcinoma. J Invest Dermatol, 135 (12):3197-3200.

Jha S, Dutta A. 2009. RVB1/RVB2: running rings around molecular biology. Mol Cell, 34 (5):521-533.

Jha S, Gupta A, Dar A, Dutta A. 2013. RVBs are required for assembling a functional TIP60 complex. Mol Cell Biol, 33 (6):1164-1174.

Jonsson ZO, Jha S, Wohlschlegel JA, Dutta A. 2004. Rvb1p/Rvb2p recruit Arp5p and assemble a functional Ino80 chromatin remodeling complex. Mol Cell, 16 (3):465-477.

Kemler R. 1993. From cadherins to catenins: cytoplasmic protein interactions and regulation of cell adhesion. Trends Genet, 9 (9):317-321.

Kern DM, Nicholls PK, Page DC, Cheeseman IM. 2016. A mitotic SKAP isoform regulates spindle positioning at astral microtubule plus ends. J Cell Biol.

Kerr GE, Young JC, Horvay K, Abud HE, Loveland KL. 2014. Regulated Wnt/beta-catenin signaling sustains adult spermatogenesis in mice. Biol Reprod, 90 (1):3.

Kohl T, Haustein E, Schwille P. 2005. Determining protease activity in vivo by fluorescence cross-correlation analysis. Biophys J, 89 (4):2770-2782.

Kuroda S, Fukata M, Nakagawa M, Fujii K, Nakamura T, Ookubo T, Izawa I, Nagase T, Nomura N, Tani H, Shoji I, Matsuura Y, Yonehara S, Kaibuchi K. 1998. Role of IQGAP1, a target of the small GTPases Cdc42 and Rac1, in regulation of E-cadherin- mediated cell-cell adhesion. Science, 281 (5378):832-835.

Lee CS, Bhaduri A, Mah A, Johnson WL, Ungewickell A, Aros CJ, Nguyen CB, Rios EJ, Siprashvili Z, Straight A, Kim J, Aasi SZ, Khavari PA. 2014. Recurrent point mutations in the kinetochore gene KNSTRN in cutaneous squamous cell carcinoma. Nat Genet, 46 (10):1060-1062.

Lee JH, Kim MS, Yoo NJ, Lee SH. 2016. Absence of KNSTRN Mutation, a Cutaneous Squamous Carcinoma-Specific Mutation, in Other Solid Tumors and Leukemias. Pathol Oncol Res, 22 (1):227-228.

Li K, Xue Y, Chen A, Jiang Y, Xie H, Shi Q, Zhang S, Ni Y. 2014. Heat shock protein 90 has roles in intracellular calcium homeostasis, protein tyrosine phosphorylation regulation, and progesterone-responsive sperm function in human sperm. PLoS One, 9 (12):e115841.

Lu S, Wang R, Cai C, Liang J, Xu L, Miao S, Wang L, Song W. 2014. Small kinetochore associated protein (SKAP) promotes UV-induced cell apoptosis through negatively regulating pre-mRNA processing factor 19 (Prp19). PLoS One, 9 (4):e92712.

Lupas A, Van Dyke M, Stock J. 1991. Predicting coiled coils from protein sequences. Science, 252 (5009):1162-1164.

Mack GJ, Compton DA. 2001. Analysis of mitotic microtubule-associated proteins using mass spectrometry identifies astrin, a spindle-associated protein. Proc Natl Acad Sci U S A, 98 (25):14434-14439.

Mason JM, Arndt KM. 2004. Coiled coil domains: stability, specificity, and biological implications. Chembiochem, 5 (2):170-176.

Nano N, Houry WA. 2013. Chaperone-like activity of the AAA+ proteins Rvb1 and Rvb2 in the assembly of various complexes. Philosophical Transactions of the Royal Society B-Biological Sciences, 368 (1617).

Nguyen VQ, Ranjan A, Stengel F, Wei D, Aebersold R, Wu C, Leschziner AE. 2013. Molecular architecture of the ATP-dependent chromatin-remodeling complex SWR1. Cell, 154 (6):1220-1231.

Orthaus S, Klement K, Happel N, Hoischen C, Diekmann S. 2009. Linker histone H1 is present in centromeric chromatin of living human cells next to inner kinetochore proteins. Nucleic Acids Res, 37 (10):3391-3406.

Orthaus S, Biskup C, Hoffmann B, Hoischen C, Ohndorf S, Benndorf K, Diekmann S. 2008. Assembly of the inner kinetochore proteins CENP-A and CENP-B in living human cells. Chembiochem, 9 (1):77-92.

Pesenti ME, Weir JR, Musacchio A. 2016. Progress in the structural and functional characterization of kinetochores. Curr Opin Struct Biol, 37:152-163.

Reynard LN, Cocquet J, Burgoyne PS. 2009. The multi-copy mouse gene Sycp3-like Y-linked (Sly) encodes an abundant spermatid protein that interacts with a histone acetyltransferase and an acrosomal protein. Biol Reprod, 81 (2):250-257.

Rivas B, Huang Z, Agoulnik AI. 2014. Normal fertility in male mice with deletion of beta-catenin gene in germ cells. Genesis, 52 (4):328-332.

Sapountzi V, Logan IR, Robson CN. 2006. Cellular functions of TIP60. Int J Biochem Cell Biol, 38 (9):1496-1509.

Schmidt JC, Kiyomitsu T, Hori T, Backer CB, Fukagawa T, Cheeseman IM. 2010. Aurora B kinase controls the targeting of the Astrin-SKAP complex to bioriented kinetochores. J Cell Biol, 191 (2):269-280.

Shao X, Xue J, van der Hoorn FA. 2001. Testicular protein Spag5 has similarity to mitotic spindle protein Deepest and binds outer dense fiber protein Odf1. Mol Reprod Dev, 59 (4):410-416.

Sigala B, Edwards M, Puri T, Tsaneva IR. 2005. Relocalization of human chromatin remodeling cofactor TIP48 in mitosis. Exp Cell Res, 310 (2):357-369.

Stolc V, Samanta MP, Tongprasit W, Marshall WF. 2005. Genome-wide transcriptional analysis of flagellar regeneration in Chlamydomonas reinhardtii identifies orthologs of ciliary disease genes. Proc Natl Acad Sci U S A, 102 (10):3703-3707.

Takeuchi K, Fukagawa T. 2012. Molecular architecture of vertebrate kinetochores. Exp Cell Res, 318 (12):1367-1374.

Tanaka K. 2013. Regulatory mechanisms of kinetochore-microtubule interaction in mitosis. Cell Mol Life Sci, 70 (4):559-579.

Thein KH, Kleylein-Sohn J, Nigg EA, Gruneberg U. 2007. Astrin is required for the maintenance of sister chromatid cohesion and centrosome integrity. J Cell Biol, 178 (3):345-354.

Thomas T, Loveland KL, Voss AK. 2007. The genes coding for the MYST family histone acetyltransferases, Tip60 and Mof, are expressed at high levels during sperm development. Gene Expr Patterns, 7 (6):657-665.

Tosi A, Haas C, Herzog F, Gilmozzi A, Berninghausen O, Ungewickell C, Gerhold CB, Lakomek K, Aebersold R, Beckmann R, Hopfner KP. 2013. Structure and subunit topology of the INO80 chromatin remodeler and its nucleosome complex. Cell, 154 (6):1207-1219.

Vergouwen RP, Huiskamp R, Bas RJ, Roepers-Gajadien HL, Davids JA, de Rooij DG. 1993. Postnatal development of testicular cell populations in mice. J Reprod Fertil, 99 (2):479-485.

Wang G, Guo Y, Zhou T, Shi X, Yu J, Yang Y, Wu Y, Wang J, Liu M, Chen X, Tu W, Zeng Y, Jiang M, Li S, Zhang P, Zhou Q, Zheng B, Yu C, Zhou Z, Guo X, Sha J. 2013. In-depth proteomic analysis of the human sperm reveals complex protein compositions. J Proteomics, 79:114-122.

Wang X, Zhuang X, Cao D, Chu Y, Yao P, Liu W, Liu L, Adams G, Fang G, Dou Z, Ding X, Huang Y, Wang D, Yao X. 2012. Mitotic regulator SKAP forms a link between kinetochore core complex KMN and dynamic spindle microtubules. J Biol Chem, 287 (47):39380-39390.

Weise JM, Günes C. 2009. Differential regulation of human and mouse telomerase reverse transcriptase (TERT) promoter activity during testis development. Mol Reprod Dev, 76 (3):309-317.

Weiske J, Huber O. 2005. The histidine triad protein Hint1 interacts with Pontin and Reptin and inhibits TCF-β-catenin-mediated transcription. J Cell Sci, 118 (Pt 14):3117-3129.

Wolf E, Kim PS, Berger B. 1997. MultiCoil: a program for predicting two- and three-stranded coiled coils. Protein Sci, 6 (6):1179-1189.

Appendix

List of figures:

List of tables:

Acknowledgements

Firstly, I would like to express my sincere gratitude to my supervisor Prof. Dr. Otmar Huber for giving me the opportunity to work in his group. His guidance and continuous support during my PhD studies, his patience, motivation and immense knowledge helped me during all phases of research and writing. Thank you.

I would also like to thank the rest of my thesis committee, Prof. Dr. Regine Heller and Prof. Dr. Karlheinz Friedrich for their insightful comments and encouragement.

I am grateful to all my lab colleagues for technical and moral support and their friendship throughout the years. Especially Kai, Sonni, Juliane and Franzi, who have served as great role models. I thank the group of Prof. Friedrich for all the help with the antibodies and for their enjoyable company during daily lunch times. I sincerely thank Dr. Martin Schmidt for numerous introductions and his help with statistics. All in all, I am truly grateful to all the members of the Institute of Biochemistry II for their expert help with scientific questions, the wonderful working atmosphere and for making me feel at home there.

Further, I would like to express my great appreciation to Dr. Cagatay Günes for his constructive suggestions and enthusiastic encouragement during the planning of my research work. All of the generously provided samples and the invested time and support are very much appreciated. Also, I thank Sabrina Eichwald for the excellent technical help.

My special thanks go to Dr. Christian Hoischen for the expert help with the FRET and FCCS experiments. I highly appreciate his patience, time, commitment and humor that lightened up the dark microscopy lab. My gratitude is extended to Sylke Pfeifer and Sabine Gallert for their great technical assistance.

Dr. Yuan Chen provided me with valuable samples for my research and I sincerely thank her for that.

To Prof. Dr. Regine Heller I am grateful for her immense effort in organization of the Summer School. A big thanks goes to all the summer school and other friends who supported me and made the time out of the lab enjoyable.

I thank IZKF for financing my PhD studies, as well as all organizations providing me with funding to attend courses and conferences that have contributed to my scientific growth and served as platform for meeting wonderful people from all over the world.

Finally, I am very thankful to my family, especially my loving parents for giving me the chance for education, for always believing in me and encouraging me throughout this time and my life in general.

At last, the biggest "Thank you!" I owe to Anton, my strength, for his unconditional support and for always being there for me. This is for you, I couldn´t have done it without you!

Hvala!
Anita

Ehrenwörtliche Erklärung

Hiermit erkläre ich, dass mir die Promotionsordnung der Medizinischen Fakultät der Friedrich-Schiller-Universität bekannt ist,

ich die Dissertation selbst angefertigt habe und alle von mir benutzten Hilfsmittel, persönlichen Mitteilungen und Quellen in meiner Arbeit angegeben sind,

dass die Personen, die mich bei der Auswahl und Auswertung des Materials sowie bei der Herstellung des Manuskripts unterstützt haben, vollständig genannt sind,

die Hilfe eines Promotionsberaters nicht in Anspruch genommen wurde und dass Dritte weder unmittelbar noch mittelbar geldwerte Leistungen von mir für Arbeiten erhalten haben, die im Zusammenhang mit dem Inhalt der vorgelegten Dissertation stehen,

dass ich die Dissertation noch nicht als Prüfungsarbeit für eine staatliche oder andere wissenschaftliche Prüfung eingereicht habe und dass ich die gleiche, eine in wesentlichen Teilen ähnliche oder eine andere Abhandlung nicht bei einer anderen Hochschule als Dissertation eingereicht habe.

Teile dieser Dissertation wurden bereits in Human Molecular Genetics publiziert (Cindric Vranesic, A., Reiche, J., Hoischen, C., Wohlmann, A., Bratsch, J., Friedrich, K., Günes, B., Cappallo-Obermann, H., Kirchhoff, C., Diekmann, S., Günes, C. and Huber O. Characterization of SKAP/Kinastrin isoforms - The N-terminus defines tissue specificity and Pontin binding. Hum. Mol. Genet. first published online May 11, 2016, doi:10.1093/hmg/ddw140) und wurden hier mit Erlaubnis des Verlags benutzt (Zulassung Nummer 3896941406164 und 3896950055308).

Jena, 29.06.2016

Anita Cindrić Vranešić